MCR-70-171 (Vol II) Copy No.

INVESTIGATION OF SPACE STORABLE PROPELLANT ACQUISITION DEVICES

FINAL REPORT

VOLUME II - DESIGN AND ANALYSIS

DECEMBER 1970

This work was performed for the Jet Propulsion Laboratory, California Institute of Technology, as sponsored by the National Aeronautics and Space Administration under Contract NAS7-754.

MARTIN MARIETTA
DENVER DIVISION

MCR-70-171 (Vol II)

INVESTIGATION OF SPACE STORABLE PROPELLANT ACQUISITION DEVICES

FINAL REPORT

VOLUME II
DESIGN AND ANALYSIS

December 1970

Approved

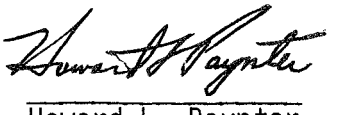

Howard L. Paynter
Program Manager

This work was performed for the Jet Propulsion Laboratory, California Institute of Technology, as sponsored by the National Aeronautics and Space Administration under Contract NAS7-754.

MARTIN MARIETTA CORPORATION
P.O. Box 179
Denver, Colorado 80201

FOREWORD

This report is submitted in accordance with Article II, Paragraph D, of Contract NAS7-754 dated July 24, 1969. The report consists of two volumes. Volume I covers Phase I of the investigation. This volume (Vol II) covers Phase II, which was conducted during the period from April to August 1970.

The following Martin Marietta personnel made technical contributions to this portion (second phase) of the program. Dr. Ralph E. Hise, James R. Tegart, G. Robert Page, Thomas J. Cassidy, and Preston E. Uney. Mr. Dale A. Fester directed the technical effort.

The work was administered under the technical direction of Mr. Robert Lem of the Jet Propulsion Laboratory. Mr. Howard L. Paynter, Subsystems Technology Section Chief, Propulsion Research Department, served as the Martin Marietta Program Manager.

An experimental assessment of the Martin Marietta "Fruhof" propellant acquisition concept for low-gravity environment applications was conducted to support the design of this system. A color-film summary of the experimental results can be obtained from Mr. Lem.

CONTENTS

Figure

SYMBOLS

a	acceleration, ft/sec^2
Bo	Bond number, dimensionless
BP	bubble point, psf
d	pore diameter, ft
d_s	settling distance, ft
D	diameter, ft
Ga	Galileo number, dimensionless
h	liquid height, ft
H	post height, ft
L	tank length or characteristic dimension, ft
P	pressure, psfa
ΔP_c	capillary retention pressure differential, psf
ΔP_h	hydrostatic pressure differential, psf
$\Sigma \Delta P_a$	summation of adverse pressure differentials, psf
r	tank radius, ft
r´	standpipe radius, ft
R	pore radius, ft
R_s	radius of curvature of spherical interface, ft
R_1, R_2	principal radii of curvature, ft
t	settling time, sec
v_c	liquid impingement velocity, fps
V	volume, ft^3

We	Weber number, dimensionless
β	kinematic surface tension (σ/ρ), ft^3/sec^2
γ	radius ratio, dimensionless
θ	liquid-to-solid contact angle, deg
λ_N	natural frequency parameter, dimensionless
ν	kinematic viscosity, ft^2/sec
ξ	open-to-total area ratio, dimensionless
ρ	density, lb_m/ft^3
σ	liquid/gas surface tension, lb_f/ft
τ	settling factor, dimensionless
ϕ	acceleration to capillary force ratio, dimensionless
ω_N	natural frequency, $1/sec^2$

Subscripts

g	gas
ℓ	liquid
$t\ell$	test liquid

SUMMARY

A two-phase program was conducted to investigate space storable propellant acquisition devices for three baseline missions, including two 1-year Mars Orbiter missions and a 10-year Grand Tour mission to the outer planets. The spacecraft for the latter mission uses a nitrated hydrazine monopropellant while one Mars orbiter uses the OF_2/B_2H_6 space storable combination and the other uses N_2O_4 and MMH Earth storables.

During Phase I, current propellant acquisition techniques, possible propellant tank configurations, and helium versus nitrogen stored-gas pressurization were evaluated for each mission. The preferred combination of subsystems was then selected and recommended. Surface tension devices were clearly shown to be the best propellant acquisition method for all three missions. Results of the Phase I subsystem evaluation and selection are presented in Volume I of this report.

Detailed analyses and designs of the recommended and approved surface tension propellant acquisition systems were made for the three baseline missions during Phase II. Two basic approaches were used in making the designs. The first approach required that the surface tension system be testable under minus 1 g, i.e., gas-free liquid expelled from the inverted, full-scale propellant tank against the gravity vector. Under the second approach, the surface tension system was designed to perform reliably under the low-g operational environment only. Various surface tension concepts were considered in order to provide the best concept for each mission.

Results of the Phase II design and analysis are presented in this volume. Based on the surface tension designs, the Fruhof low-gravity propellant acquisition concept is preferred for each baseline mission. The inherent simplicity, reliability, temperature insensitivity, and attractive compatibility characteristics make this system preferable to fine-mesh screen trap designs if testing under minus 1 g is not a requirement.

I. INTRODUCTION

This investigation of space storable propellant acquisition devices was conducted by Martin Marietta Corporation under the direction of the Jet Propulsion Laboratory as part of the NASA's Advanced Technology Program to provide propulsion systems for post-1975 unmanned missions to Mars, Jupiter, and the outer planets. Program objectives were to:

- Investigate the utility of current (developed or under development) propellant acquisition devices for use in advanced spacecraft applications;
- Recommend acquisition modes, pressurization subsystems, and propellant tank subsystems for three specific baseline missions;
- Complete detailed designs of the selected propellant acquisition devices for each baseline mission.

Two general mission requirements were considered: flights to Mars that include midcourse, orbit insertion, and orbit trim maneuvers; and a multiple planet fly-by, or Grand Tour mission, including a number of midcourse maneuvers.

The problems associated with propellant orientation and control during zero g (well publicized in the literature) were the primary concern of this study. As a result, the investigation, selection, analysis, and design of the propellant acquisition devices received the major emphasis. The acquisition subsystem was the determining factor in selecting the preferred propulsion system (which also included pressurization and tankage subsystems) for each of the three missions.

The program was conducted in two separate phases (Fig. I-1). During Phase I, the mission criteria and study guidelines were established and the Project Work Plan (Ref I-1) was prepared. An extensive survey was conducted to collect background information and data on each of the three propulsion subsystems. This survey included literature searches and personal contact with government agencies, aerospace companies, and vendors. No new propellant acquisition methods were found except for the capillary/bellows concept devised under Contract NAS9-8939 (Ref I-2). The capillary/bellows device was evaluated further during this program under Task VIII. Information on material compatibility with the baseline propellants was also compiled (Ref I-3 and I-4).

Phase I system evaluation and selection consisted of five major tasks (Fig. I-1), in addition to the separate capillary/bellows evaluation previously mentioned. During Task I, a preliminary rating system was formulated for a comparative evaluation of propellant acquisition concepts. During Task II, background information, design criteria, and operational characteristics of propellant acquisition, pressurization, and propellant tank subsystems were compiled and analyzed. The resulting information and data, together with the preliminary rating technique (Task I), were used in the comparative evaluation conducted during Task III. Based on these comparisons, the best propulsion subsystems were selected. The pressurization and tankage subsystems were selected from weight, efficiency, and reliability comparisons and their effect, if any, on the propellant acquisition subsystem. The latter was selected by using the rating system. The preferred subsystems were then subjected to further evaluation (Task IV) where possible changes to the baseline Mars and Grand Tour missions were considered. The selected propulsion systems were recommended to JPL for approval (Task V) in April, 1970, to conclude Phase I. A brief summary of the results of Phase I [as presented in Volume I of this report (Ref I-5)] follows.

The propellant acquisition concepts that were evaluated included surface tension devices, polymeric and metallic bladders and diaphragms, bellows, dielectrophoretic systems, main engine start tanks, external propellant settling systems, and the capillary/bellows device. Surface tension devices clearly rated best and were recommended to JPL as the preferred acquisition method for each mission. In evaluating the propellant tank subsystems, the number of tanks, size, geometry, materials, and type of construction were considered. For the two bipropellant (N_2O_4/MMH and OF_2/B_2H_6) Mars orbiters evaluated, two spherical, all-metal, propellant tanks were selected. For the monopropellant (nitrated hydrazine) Grand Tour spacecraft, the single tank recommended was metal and spherical. Type of pressurant (helium or nitrogen) and storage and operating conditions were considered in evaluating the pressurization subsystem. The assessment showed that helium pressurant provided advantages over nitrogen for both of the separately-stored Mars orbiter subsystems and for the Grand Tour blowdown pressurization mode. A single-pressurant storage sphere was recommended for the Mars missions with helium stored at the nominal propellant temperature under an initial pressure of 4000 psia.

During Phase II (Fig. I-1), detailed analyses and designs were made of the recommended and approved surface tension propellant acquisition systems for the three reference missions (Task VI).

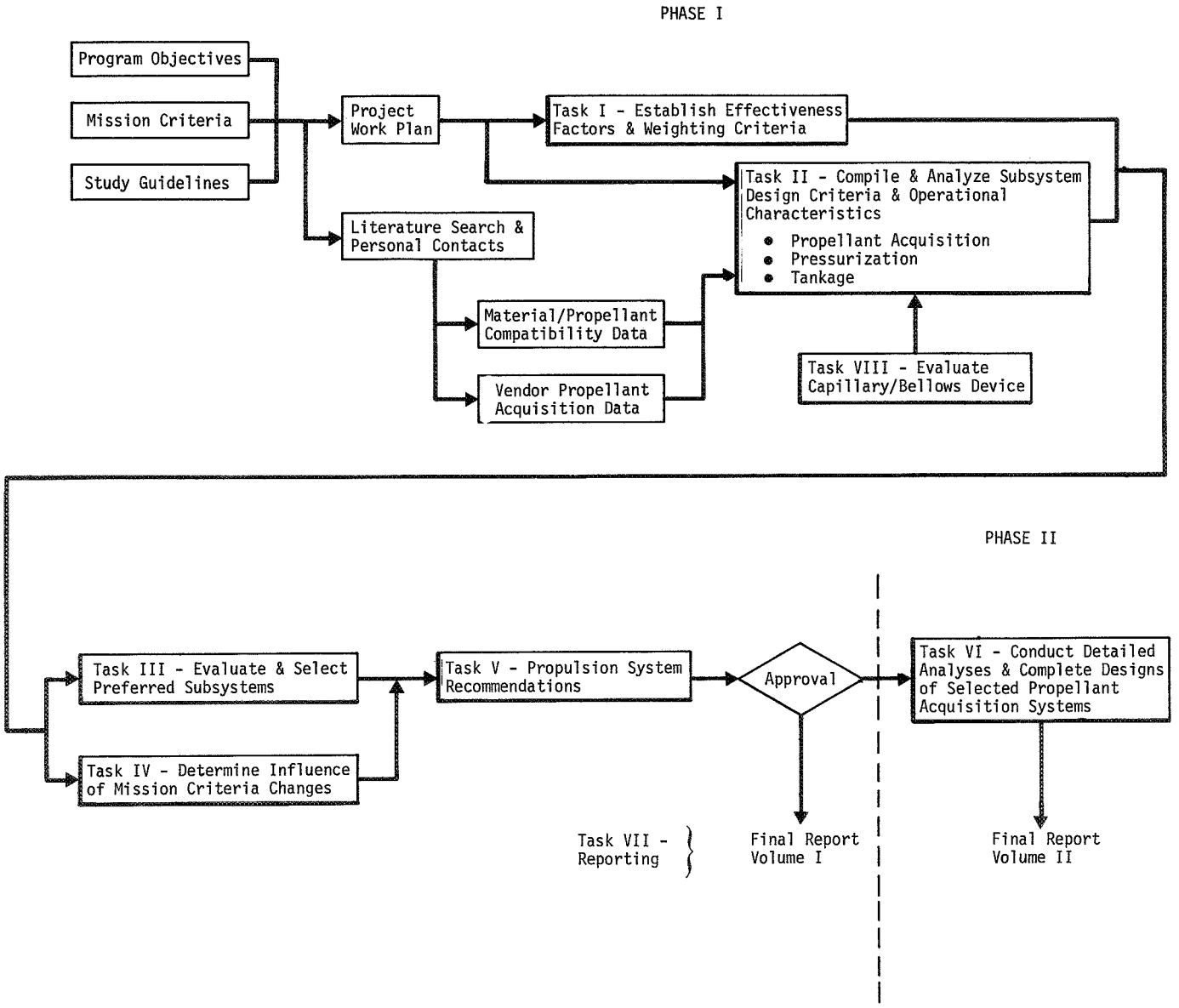

Figure I-1 Program Study Approach

The Phase II objectives, mission criteria, and study guidelines are outlined in Chapter II. A brief discussion and state-of-the-art review of surface tension propellant control devices is presented in Chapter III. The design and analysis for each of the fine-mesh propellant acquisition systems are included in Chapter IV; the so-called "Fruhof" systems that do not use fine-mesh foraminous material are detailed in Chapter V. Conclusions and recommendations are discussed in Chapter VI; references are listed in Chapter VII.

II. OBJECTIVES, MISSION CRITERIA, AND STUDY GUIDELINES

A. PROGRAM OBJECTIVES

The objectives of Phase II were to make detailed designs of the selected surface tension propellant acquisition systems for each of the three spacecraft missions and to conduct supporting analyses.

B. MISSION CRITERIA

The three baseline planetary missions are designated as Missions A_1, A_2, and B. Missions A_1 and A_2 are Mars missions with a baseline spacecraft of the advanced Viking-type orbiter, launched by a Titan IIID/Centaur. A typical spacecraft configuration is shown in Figure II-1. Mission A_1 uses space storable propellants, oxygen difluoride (OF_2) and diborane (B_2H_6), and Mission A_2 uses Earth storables, nitrogen tetroxide (N_2O_4) and monomethylhydrazine ($CH_3N_2H_3$ or MMH). The more energetic space storables provide an increase in specific impulse over the Earth storables, and appear to be the logical choice for the next generation of unmanned, planetary, spacecraft propulsion systems since increased payload capability can be realized from the lower propellant requirement.

Mission B is the Grand Tour multiple planet mission to Jupiter, Saturn, Uranus, and Neptune. The baseline spacecraft configuration (Fig. II-2) uses the monopropellant 75/25 (wt %) hydrazine/hydrazine nitrate ($N_2H_4/N_2H_5NO_3$) and is launched by a Titan IIID/Centaur/Burner II (1440).

The basic mission and propulsion system criteria are presented in Volume I; however, additional criteria were defined at the start of Phase II design effort. The selected and approved propulsion subsystems were used as the baseline configurations. The design criteria and propulsion systems are discussed in the following paragraphs.

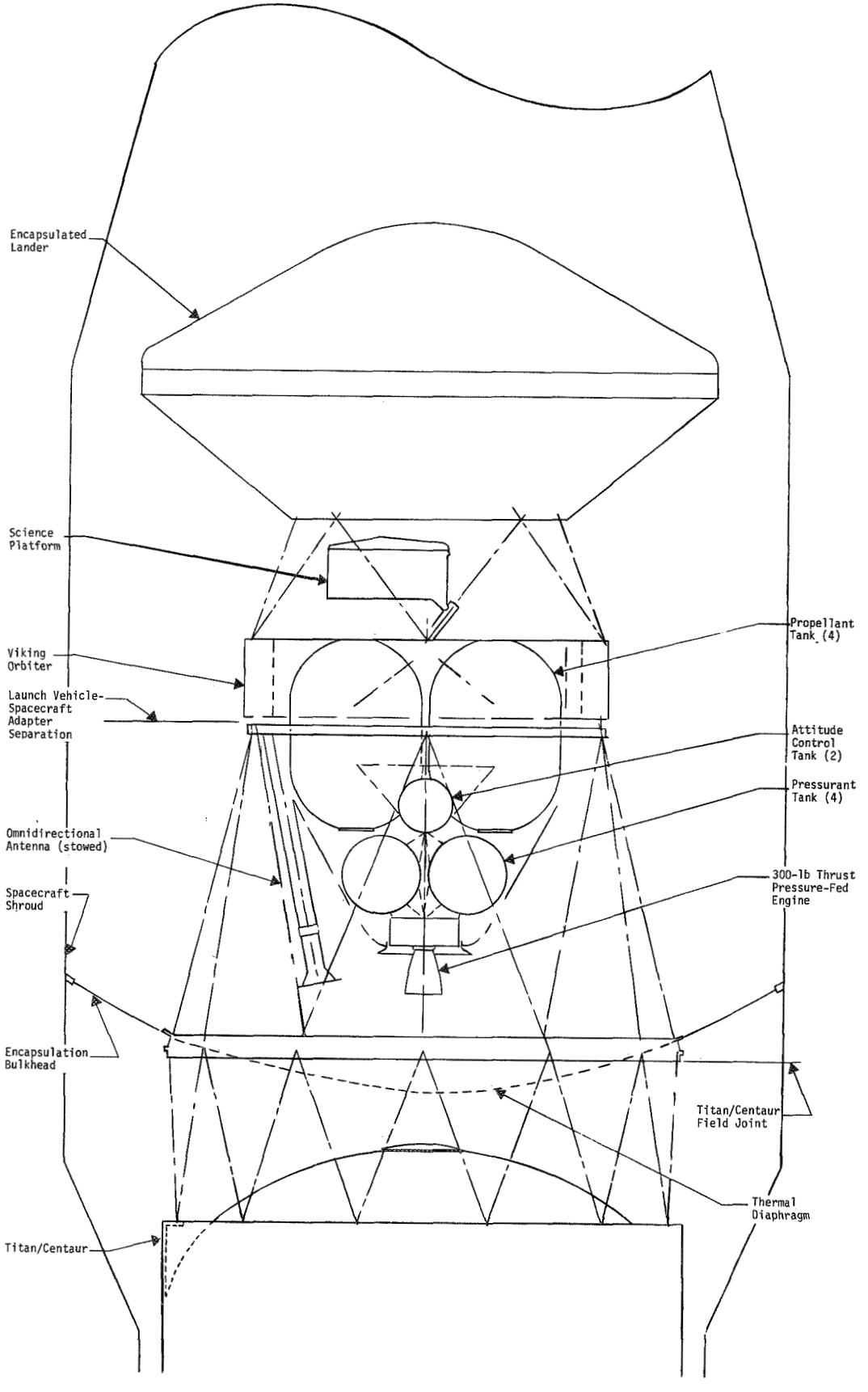

Figure II-1 Viking Spacecraft Configuration (Typical)

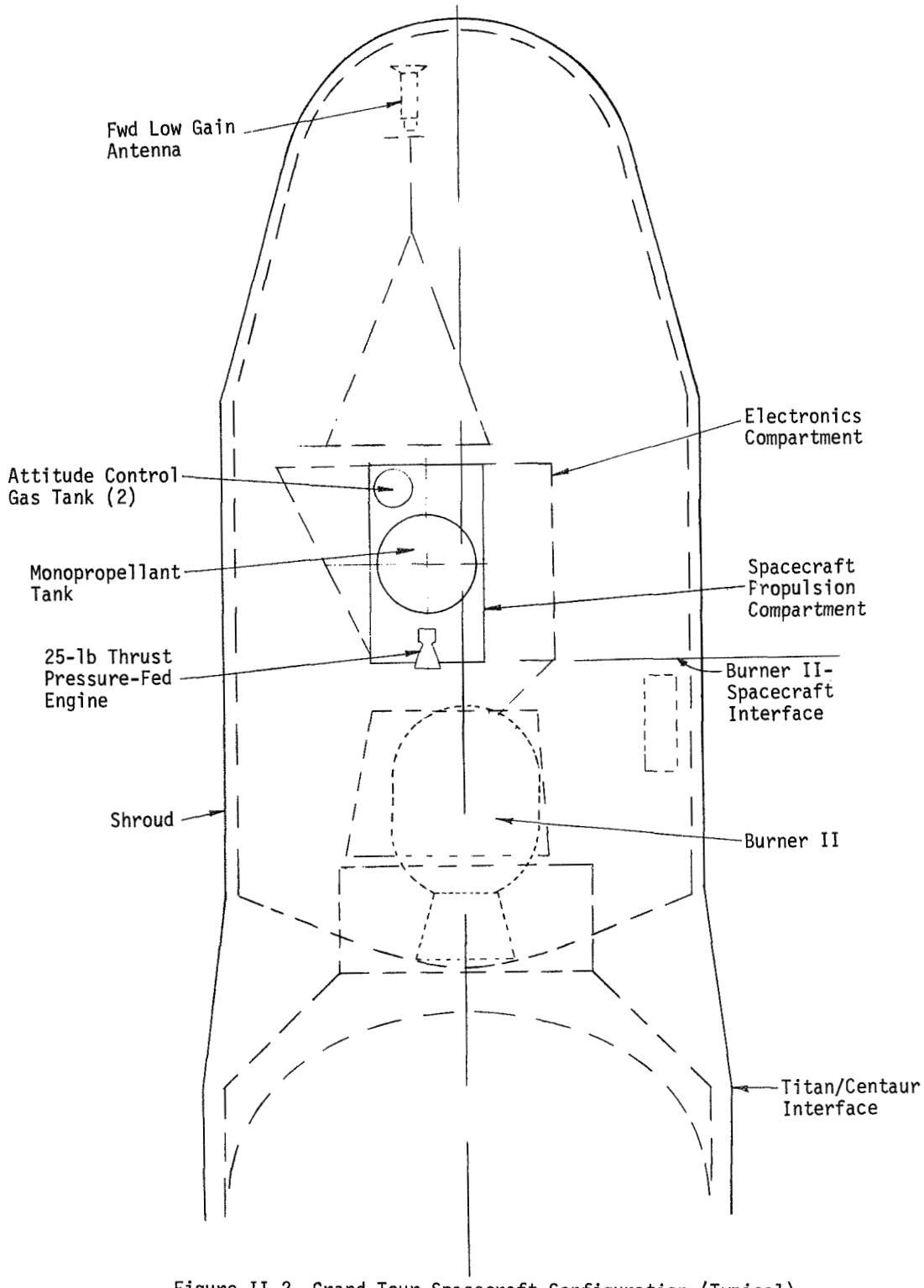

Figure II-2 Grand Tour Spacecraft Configuration (Typical)

1. Mission Description

a. Missions A_1 and A_2 - The Mars Orbiter Mission includes a groundhold period of up to 30 days prior to launch aboard the Titan IIID/Centaur. Transit time to Mars is 180 days, followed by insertion into a 24-hour elliptical Mars orbit. The maximum Mars orbiting requirement is 90 days. The baseline mission propulsion events (Table II-1) include two midcourse corrections, orbit insertion, and three orbit trims. The possibility of additional orbit trim burns was also considered in the design of the acquisition subsystems.

During coast periods, the reaction jet attitude control system (ACS) maintains the spacecraft on celestial references with the sun on the roll axis, and a star aligned on the star-sensor boresight axis. Prior to each main engine burn, the spacecraft is maneuvered by the ACS to provide the desired thrust axis orientation. This is accomplished by switching from celestial to inertial reference and performing a roll maneuver to align the pitch thrusters. Next, a pitch maneuver is used to align the thrust axis and another roll is conducted to point the maneuver antenna toward Earth. These attitude changes are executed in reverse order after each main engine burn to reacquire the celestial reference. The mission acceleration environment, associated with the various maneuvers, coast periods, and propulsion events, is summarized in Table II-2.

b. Mission B - The multiple planet Grand Tour Mission may include flybys of Jupiter, Saturn, Uranus, and Neptune. Total mission time is approximately 3500 days. The nine midcourse propulsion events are presented in Table II-3. The first course correction maneuver occurs 10 days after launch; the last engine burn occurs 3272 days after launch. Expected nominal plus three-sigma velocity increments for the propulsion events are shown in the table. The total (nominal plus 3σ) velocity requirement is approximately 320 meters per second.

The ACS for the spacecraft performs the same functions as those described earlier for the Mars orbiter ACS; however, attitude control for this mission is provided by a reaction jet system in combination with a momentum wheel. The mission acceleration environment is presented in Table II-4.

Table II-1 Propulsion Event Sequence for Missions A_1 and A_2

Event	Event Time [days from launch (L)]	Propellant Load Expended (%)	Mission A_1			Mission A_2		
			Burn Time (sec)	OF_2 (lb_m)	B_2H_6 (lb_m)	Burn Time (sec)	N_2O_4 (lb_m)	MMH (lb_m)
First Midcourse	L + 5	0.6	2.5	4.86	1.62	8.3	5.2	3.35
Second Midcourse	L + 160	0.6	2.5	4.86	1.62	8.3	5.2	3.35
Orbit Insertion	L + 180	95.0	395.0	769.5	256.5	1317.0	828.5	534.0
First Orbit Trim	L + 181	1.3	5.4	10.53	3.51	18.0	11.3	7.3
Second Orbit Trim	L + 225	1.2	5.0	9.72	3.24	16.6	10.5	6.7
Third Orbit Trim	L + 270	1.3	5.4	10.53	3.51	18.0	11.3	7.3

Table II-2 Acceleration Environment for Missions A_1 and A_2

Mission Phase	Acceleration (g)	Duration (sec)
Boost	3.8	-
Main Engine Burns		
Mission A_1		
Initial	0.133	-
Final	0.156	-
Mission A_2		
Initial	0.0400	-
Final	0.0495	-
Deep Space and Mars Orbit	10^{-7}	-
Celestial/Inertial Attitude Control		
Deadband Thrust		
Before Orbit Insertion		
Pitch/Yaw	5.6×10^{-5}	0.53
Roll	2.6×10^{-5}	1.14
After Orbit Insertion		
Pitch/Yaw	6.5×10^{-5}	0.46
Roll	2.7×10^{-5}	1.09
Deadband Coast		
Celestial	$<10^{-8}$	$\leq$960
Inertial	$<10^{-8}$	$\leq$330
Maneuvers before and after Main Engine Burns		
Attitude Control Thrust		
Before Orbit Insertion		
Pitch/Yaw	5.6×10^{-5}	7
Roll	2.6×10^{-5}	15
After Orbit Insertion		
Pitch/Yaw	6.5×10^{-5}	6
Roll	2.7×10^{-5}	14
Rotation Coast at Constant Angular Velocity	10^{-6}	<500 (first roll) <800 (pitch) <250 (second roll)

Table II-3 Propulsion Event Sequence for Mission B

Event	Event Time [days after launch (L)]	Propellant Load Expended (%)	Maximum Burn Time (sec)	Maximum Propellant Mass (lb_m)
Post-Launch	L + 10	10.00	138	13.5
Pre-Jupiter	L + 493	2.22	31	3.0
Post-Jupiter	L + 531	5.49	75	7.4
Pre-Saturn	L + 1087	3.93	54	5.3
Post-Saturn	L + 1116	34.15	468	46.1
Pre-Uranus	L + 2310	10.89	150	14.7
Pre-Uranus	L + 2331	4.15	57	5.6
Post-Uranus	L + 2360	20.73	285	28.0
Pre-Neptune	L + 3272	8.44	115	11.4

Table II-4 Acceleration Environment for Mission B

Mission Phase	Acceleration (g)	Duration (sec)
Boost	3.8	-
Main Engine Burns		
Initial Level	0.022	-
Final Level	0.025	-
Deep Space	10^{-7}	-
Celestial/Inertial Attitude Control		
Deadband Thrust		
Momentum Wheel		
Pitch	3×10^{-5}	0.06
Yaw/Roll	15×10^{-7}	1.33
Reaction Jet		
Pitch	3×10^{-4}	0.006
Yaw/Roll	15×10^{-6}	0.133
Deadband Coast		
Momentum Wheel	$<10^{-10}$	$\leq$ 2,000
Reaction Jet	$<10^{-10}$	$\leq$ 10,000
Maneuvers before and after Main Engine Burns		
Attitude Control Thrust		
Momentum Wheel		
Pitch	3×10^{-5}	6
Yaw/Roll	15×10^{-7}	117
Reaction Jet		
Pitch	3×10^{-4}	0.6
Yaw/Roll	15×10^{-6}	12
Rotation Coast at Constant Angular Velocity	2.5×10^{-7}	<500 (first roll) <800 (pitch) <250 (second roll)

2. Propulsion System Description

The propulsion systems for the three missions (used as reference configurations in the design of the surface tension propellant acquisition subsystems) reflect the selections made as a result of the Phase I evaluation. The system criteria are summarized in Table II-5. The variation in density and surface tension of the propellants over the temperature range of interest, together with the change in propellant tank initial ullage over the same range of temperature, are presented in Table II-6. The propulsion systems are discussed by mission in the following paragraphs.

a. Mission A_1 - The propulsion system schematic for the space-storable Mars Orbiter is presented in Figure II-3. The system includes helium pressurant stored at the nominal propellant temperature of 250°R with an initial pressure of 4000 psia in a single, metal sphere constructed of 6Aℓ-4V titanium; two 2219 aluminum spherical propellant tanks (one for OF_2 oxidizer and one for B_2H_6 fuel); and an aluminum surface tension propellant acquisition system in each propellant tank. The propulsion system is oriented with tank outlets pointed toward Earth during launch. The probable packaging arrangement for the Viking Orbiter propulsion system envelope is shown in Figure II-4.

Because of the low storage temperature, a thermal protection system is required for the propellant and pressurant tanks to offset environmental heating and to maintain these commodities between 210 and 280°R. An insulation shroud with louvers on both the sun and shade sides was assumed. If required, solar heating could be used to raise the temperature with heat radiated to space to lower propellant and pressurant temperature. Thermal criteria are presented in Table II-7.

b. Mission A_2 - The propulsion system schematic for the Earth-storable Mars Orbiter is presented in Figure II-5. The system employs helium pressurant stored at the nominal propellant temperature of 500°R with an initial pressure of 4000 psia in a single, 6Aℓ-4V titanium sphere; two spherical 6Aℓ-4V titanium propellant tanks (one for N_2O_4 oxidizer and one for $CH_3N_2H_3$ fuel); and a titanium surface tension propellant acquisition system in each propellant tank. The propulsion system is oriented with tank outlets pointed toward Earth during launch. Packaging in the Viking Orbiter propulsion system envelope would be similar to the Mission A_1 system shown in Figure II-4.

Table II-5 Propulsion System Criteria

	Mission		
	A_1	A_2	B
Propellants	OF_2/B_2H_6	N_2O_4/MMH	75/25-$N_2H_4/N_2H_5NO_3$
Propellant Temperature (°R)			
Range	210-280	500-580	475-575
Nominal	250	500	500
Mixture Ratio	3.0	1.55	-
Isp(vac) $(lb_f\text{-sec}/lb_m)$	385	290	255
Thrust (lb_f)	1000	300	25
Chamber Pressure (psia)	100	100	100
Propellant Tank Pressure (psia)	∿350	∿350	∿350 (initial)
Thrust Vector Control	Gimbals	Gimbals	Gimbals
Number of Burns	6	6	9
Total Impulse $(lb_f\text{-sec})$	400,000	400,000	33,000
Minimum Impulse Bit $(lb_f\text{-sec})$	400	400	1.0
Spacecraft Mass (lb_m)			
Wet	7500	7500	1124
Dry	6420	6066	989
Propellant Mass (lb_m)	810/270	872/562	135
Propulsion Envelope (ft^3)	198	198	22
Propellant Tanks			
Number	2	2	1
Geometry	Spherical	Spherical	Spherical
Material	2219 Aℓ	6Aℓ-4V Ti	6Aℓ-4V Ti
Initial Ullage (%)	∿10	∿10	∿50
Propellant Margin	4%	4%	3σ
Volume (ft^3)	9.92	11.25	3.86
Diameter (in.)	32.0	33.33	23.35
Pressurant	Helium	Helium	Helium
Pressurant Temperature (°R)	Same as Propellants		
Initial Storage Pressure (psia)	∿4000	∿4000	∿350
Pressurant Tanks			
Number	1	1	-
Geometry	Spherical	Spherical	-
Material	6Aℓ-4V Ti	6Aℓ-4V Ti	-
Volume (ft^3)	2.68	2.38	
Diameter (in.)	20.7	19.9	
Propellant Acquisition	Surface Tension System		

Table II-6 Variation of Propellant Properties and Propellant Tank Initial Ullage with Temperature

Temperature (°R)	Density (lb_m/ft^3)		Surface Tension (lb_f/ft)		Initial Ullage (%)	
	Ox	Fuel	Ox	Fuel	Ox	Fuel
Mission A_1 OF_2 Oxidizer & B_2H_6 Fuel						
210	98.0	32.2	1.29×10^{-3}	1.73×10^{-3}	16.7	15.7
250 (nominal)	92.3	30.3	0.92×10^{-3}	1.43×10^{-3}	11.5	10.0
280	87.0	29.1	0.67×10^{-3}	1.21×10^{-3}	6.2	6.5
Mission A_2 N_2O_4 Oxidizer & MMH Fuel						
500 (nominal)	92.5	55.6	2.02×10^{-3}	2.46×10^{-3}	16.2	10.0
525	90.5	54.8	1.85×10^{-3}	2.37×10^{-3}	14.3	8.9
580	85.6	53.0	1.78×10^{-3}	2.22×10^{-3}	9.5	5.8
Mission B 75/25-$N_2H_4/N_2H_5NO_3$ Monopropellant						
475		70.5		4.05×10^{-3}		50.3
500 (nominal)		69.8		3.84×10^{-3}		50.0
575		67.8		3.30×10^{-3}		48.5

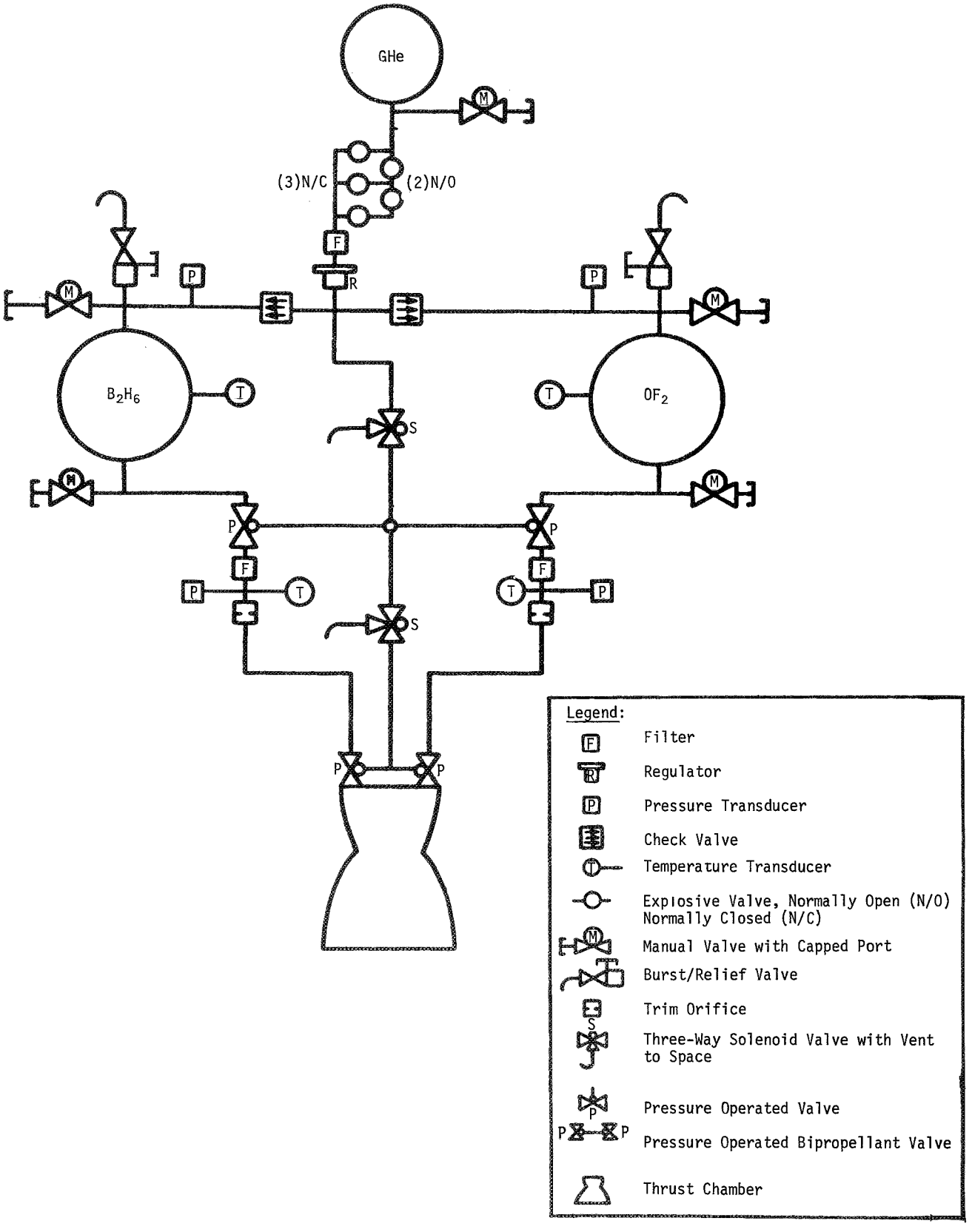

Figure II-3 Propulsion System Schematic for Mission A_1

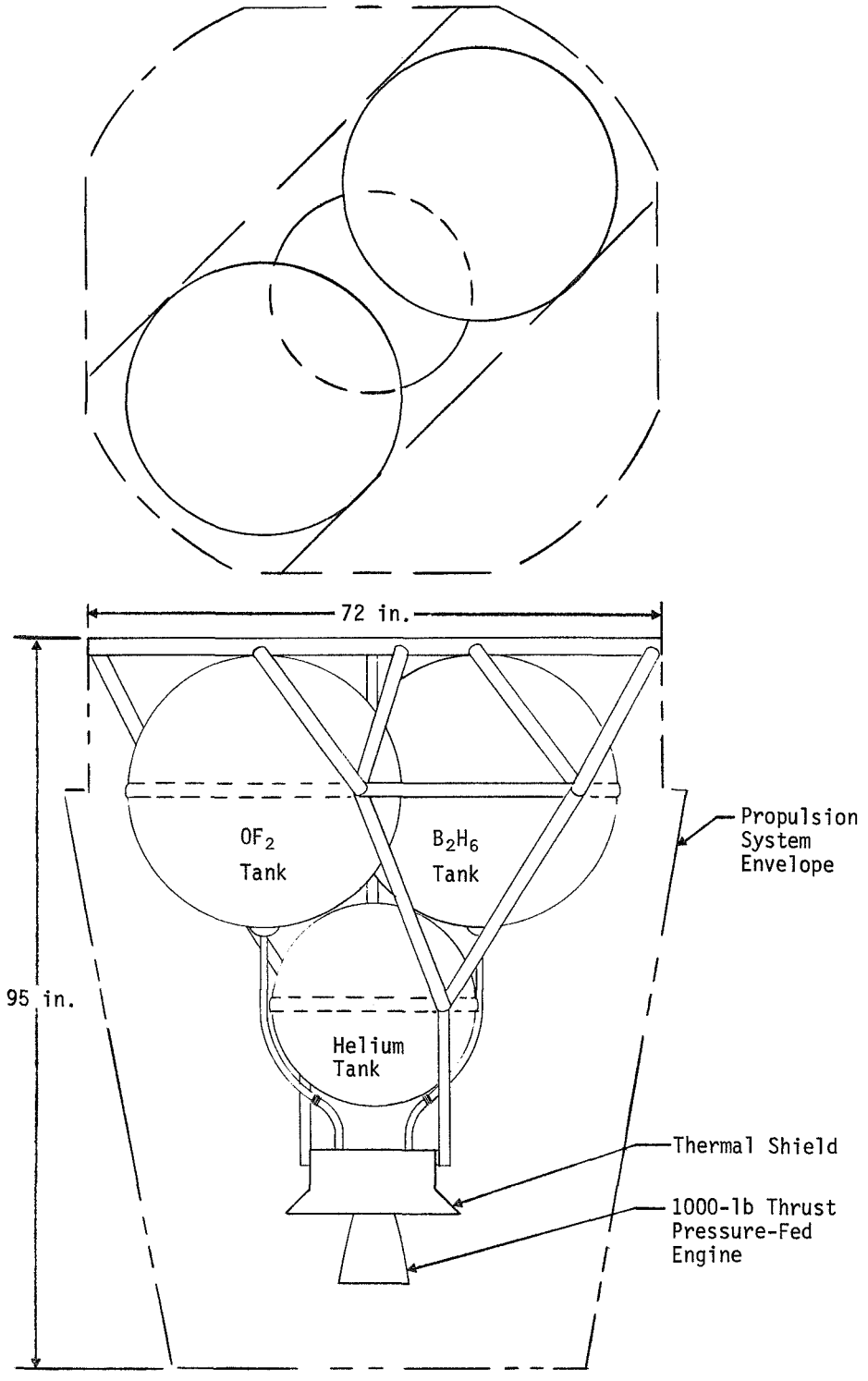

Figure II-4 Propulsion System Arrangement (Typical) for Mission A_1

Table II-7 Mission A_1 Environmental Heating Criteria

	Earth Orbit		Mars Orbit	
	OF_2	B_2H_6	OF_2	B_2H_6
Insulation Outer Surface Temperature (°R)	282	282	258	258
Nominal Propellant Temperature (°R)	250	250	250	250
Heat Flux (Btu/hr ft^2)	0.032	0.032	0.008	0.008
Thermal Conductance (Btu/hr ft^2 °R)	0.001	0.001	0.001	0.001

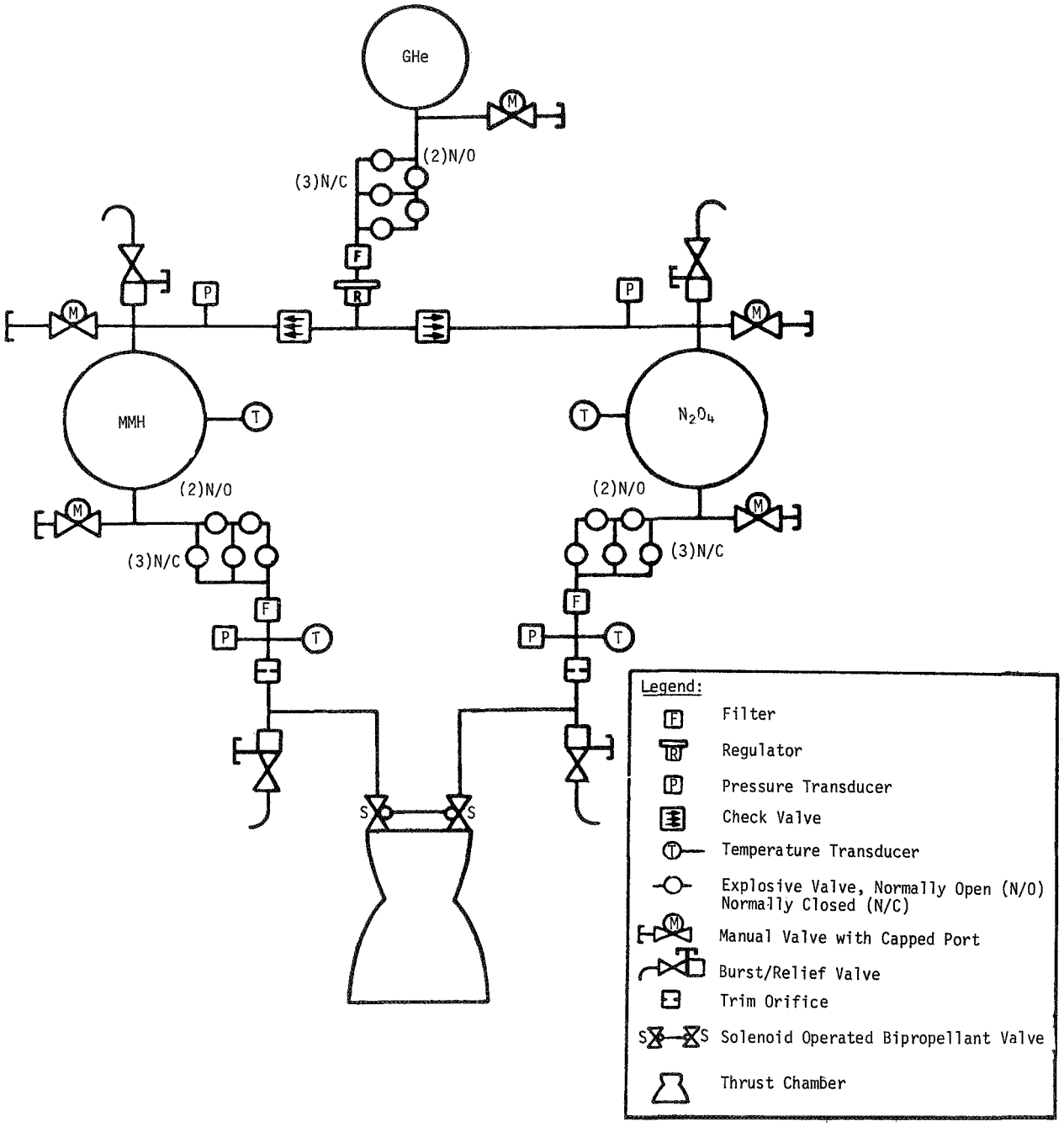

Figure II-5 Propulsion System Schematic for Mission A_2

Heating is required to prevent freezing of N_2O_4. A combination of thermal coatings and heaters may be employed to reduce temperature gradients and maintain propellant temperatures between 500 and 580°R.

c. Mission B - Helium pressurant is used in the single-tank, monopropellant propulsion system. Propellant expulsion is accomplished by blowdown of tank-top pressure. A titanium surface tension propellant acquisition system is contained in the spherical, 6Aℓ-4V titanium tank. Nominal pressurant and propellant temperature is 500°R and the initial system pressure is 350 psia. The propulsion system is oriented with the tank outlet pointed toward Earth during launch. The propulsion system schematic for the Grand Tour spacecraft is presented in Figure II-6. The probable packaging arrangement within the propulsion system envelope is shown in Figure II-7.

Heating of the propellant tank is required during the mission to prevent freezing of the nitrated hydrazine propellant. Use of a radioisotope heat source in conjunction with an external heat exchanger on the tank is one possibility. Environmental cooling, rather than heating, is the primary concern.

C. STUDY GUIDELINES

Two basic approaches were to be used in designing the surface tension systems to meet the requirements for each mission. The first approach required that the surface tension device be testable under minus 1 g so that the full-scale propellant tank may be inverted and gas-free liquid expelled from the top of the tank against the gravity vector. Under the second approach, the surface tension system was to be designed to perform reliably under the low-g operational environment only. Various surface tension concepts were to be considered in order to obtain the best concept for each mission.

Detailed prototype designs were defined as engineering drawings which were to include overall dimensions, tolerances, materials of construction, and general fabrication requirements. Fabrication and assembly, cleaning and passivation, and prelaunch operations (including loading and ground hold) were considered in the design along with the actual launch and postlaunch flight periods. Handling, checkout, and maintenance requirements were also considered.

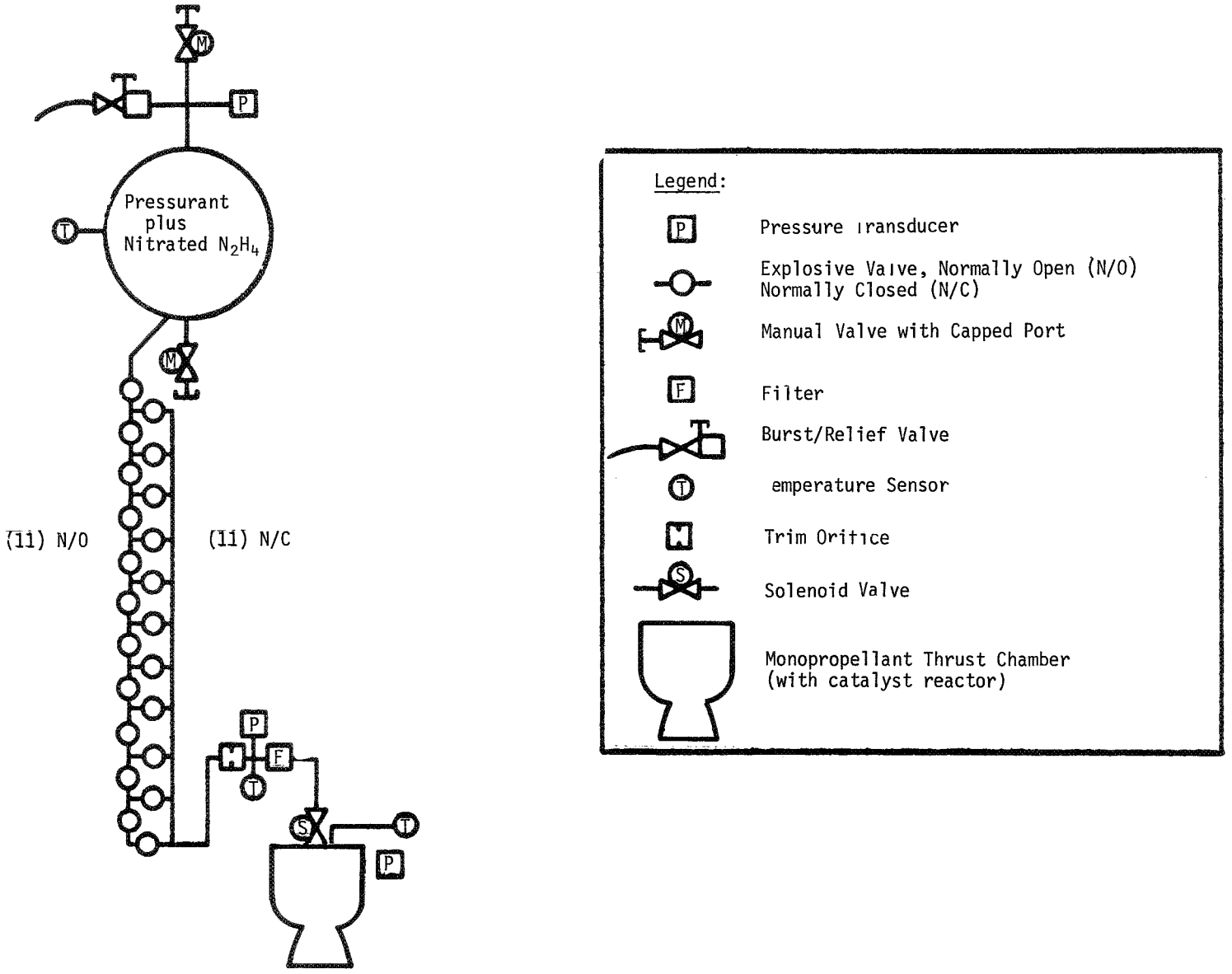

Figure II-6 Propulsion System Schematic for Mission B

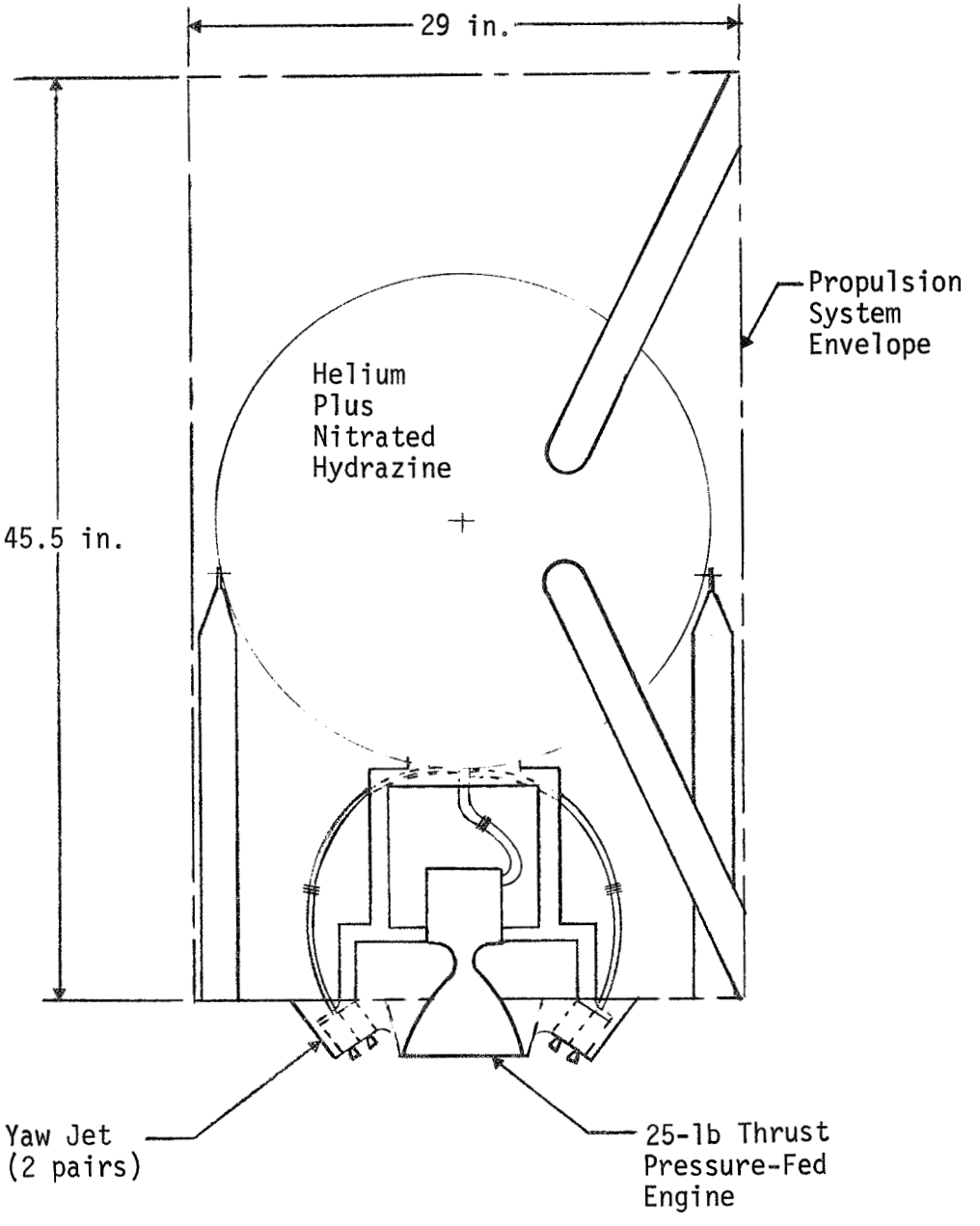

Figure II-7 Propulsion System Arrangement (Typical) for Mission B

The refined propulsion system schematics (Fig. II-3, II-5, and II-6) were reviewed and modified, as required, to furnish a reliable and operational system. Considerations included the need for additional valving to accomplish tank loading or draining.

III. SURFACE TENSION PROPELLANT CONTROL DEVICES

A discussion of passive devices that use surface tension forces to provide propellant orientation and control is presented in Volume I, Chapter III. Several different capillary concepts applicable to planetary missions are described. The more attractive features of these devices, when compared to other propellant acquisition techniques developed, or under development, are that they are completely passive (no moving parts), simple in design and operation, and low in weight. As the results of the Phase I comparative evaluation show, their simplicity and passive operation make them most reliable for the three baseline planetary missions. Also, the small quantity of material used for these devices placed them lowest in weight for each mission.

Two different capillary concepts were designed to satisfy the three baseline mission requirements during the second phase of the program. They are: fine-mesh screen traps, and the so-called "Fruhof" devices. The fine-mesh trap systems are testable under minus 1 g, i.e., gas-free propellant expulsion can be demonstrated using the full-scale tank. The tank is inverted (propellant outlet pointed away from Earth) so that the gravitational acceleration tends to position propellant away from the outlet. The Fruhof concept is not testable under minus 1 g.

A. DESIGN CRITERIA

A general discussion of capillary system design criteria is presented in this section. Each criterion is treated separately for the specific designs, and is presented in more detail in Chapters IV and V.

1. Pressure Retention

The different capillary designs presented in Chapters IV and V rely upon the relatively small pressure difference that exists across a curved liquid/gas interface, due to intermolecular forces, to orient liquid and stabilize the liquid/ullage interface. This capillary pressure difference, ΔP_c, may be expressed at any point across the interface as:

$$\Delta P_c = \left(\frac{1}{R_1} + \frac{1}{R_2}\right) \sigma, \qquad \text{[III-1]}$$

where σ is the liquid/gas surface tension and R_1 and R_2 are the principal radii of curvature at that point. For a spherical interface ($R_1 = R_2$), the pressure difference is

$$\Delta P_c = \frac{2\sigma}{R_s}, \qquad \text{[III-2]}$$

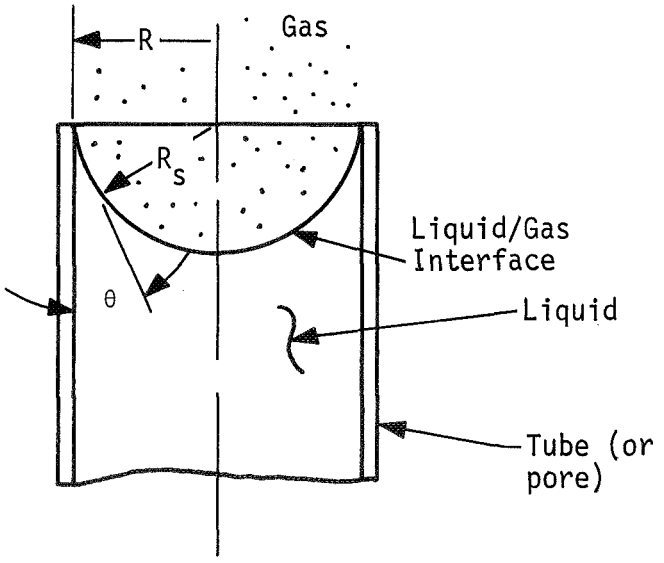

Figure III-1 Liquid/Gas Interface Shape

where R_s is the radius of curvature. The capillary pressure difference can be related to a dimension (other than the radius of curvature) such as the pore radius, R, and a second parameter, the liquid-to-solid contact angle, θ. This is done by introducing the relationship between R, θ, and R_s, as shown in Figure III-1. Then, rewriting Equation [III-2] as

$$\Delta P_c = \frac{2\sigma}{R} \cos \theta, \qquad \text{[III-3]}$$

the designer can easily calculate the capillary pressure difference from measurable parameters. Surface tension values for the propellants of interest are presented in Table II-6. Surface tension generally varies markedly with the compositions of the fluids and with temperature, while the variation with pressure is small (Ref III-1). It decreases with increased temperature, as shown in Table II-6, becoming zero at the critical temperature.

Based upon the contact angle measurements presented in Ref III-2, the liquid propellants of interest will tend to exhibit contact angles ranging from zero to two degrees when in contact with a clean, metal surface. The contact angles were measured for hydrogen peroxide (90%), nitrogen tetroxide, fuming nitric acid (Type IIIB), UDMH, hydrazine and Aerozine-50 in contact with the following metals: 6061-T6 aluminum; ASTM B348-59T (Grade 6) titanium; and 301 stainless steel. The metals were given both a polished and a randomly-roughened finish. The zero to two degree values included both advancing and receding contact angles obtained for the test liquid on the clean, dry solid. The reader is referred to Ref III-3 for a more complete discussion of contact angle.

The capillary pressure difference for a circular pore, as in a perforated plate, can be determined from Equation [III-3]. Capillary pressure retention for pore geometries other than circular is more accurately determined empirically. The accepted technique is the so-called "bubble point" method. The foraminous material is covered by a thin layer of liquid, usually alcohol, and its underside is pressurized slowly with air or gaseous nitrogen. The pressure difference at which the first bubble passes through the material is termed the bubble point (BP). The pressure retention capability for various screen mesh sizes, as determined by Martin Marietta using the BP technique, is presented in Table III-1.

Table III-1 Screen Pressure Retention Data

Screen Material	Screen Mesh	Bubble Point, BP (in. of H_2O)		
		As Received	Degreased	Ultrasonic Cleaning
Stainless Steel	30x30	(2)0.68	(3)0.68-0.69	--
Stainless Steel	50x50	(2)1.19-1.20	(6)1.22-1.23	--
Stainless Steel	80x80	(2)1.75-1.80	(6)1.80-1.85	--
Stainless Steel	100x100	(4)2.20-2.28	(5)2.20-2.22	--
Stainless Steel	150x150	(4)2.73-3.20	(5)3.10-3.12	--
Stainless Steel	200x200	(11)3.75-4.60	(12)3.89-4.40	--
Aluminum	120x120	(13)2.06-2.24	(16)2.17-2.55	--
Aluminum	30x250	(6)2.50-2.70	(7)2.63-2.71	--
Aluminum	200x1400	(2)16.30-16.40	--	--
Stainless Steel	24x110	(5)1.99-2.09	(12)1.96-2.12	--
Stainless Steel	30x250	(5)2.58-2.65	(15)2.54-3.00	--
Stainless Steel	80x700	(5)6.37-6.48	(6)6.28-6.36	--
Stainless Steel	165x800	(17)7.82-8.30	(14)7.90-8.23	(15)7.85-8.16
Stainless Steel	200x1400	(18)16.70-17.40	(15)16.70-17.04	(17)17.08-17.25
Stainless Steel	250x1370	(12)21.10-22.83	(13)20.80-22.20	(20)21.40-22.40
Stainless Steel	325x2300	(18)24.80-26.75	(16)25.15-26.40	(21)25.82-26.70

As shown in Table III-1, the flat screen samples were tested at three different conditions: as received, i.e., the sample was cut from the roll of screen and tested; degreased (vapor degreaser); and ultrasonically cleaned using a mild detergent solution. Bubble point was measured using a 1/16- to 1/8-inch thick liquid methanol cover above the screen. The data are representative of this measurement method and show the range of bubble points measured. The number in parenthesis in the BP column is the number of bubble point tests conducted.

The pressure retention for a given screen material and mesh size can be determined for other liquids from:

$$(BP)_{\ell} = \frac{\sigma_{\ell}}{\sigma_{t\ell}} (BP)_{t\ell}, \qquad [III-4]$$

where the subscripts refer to the other liquid, ℓ, and to the BP test liquid, $t\ell$.

When ordering fine-mesh screen, it is usually best to specify material, weave, mesh size, and minimum BP. The basic criterion used for selecting the capillary material is that

$$\Delta P_c \geq \Sigma \Delta P_a, \qquad [III-5]$$

where $\Sigma \Delta P_a$ is the sum of pressure differences acting at the pore tending to disrupt (break down) the liquid/gas interface. These adverse pressure differences may result from hydrostatic and hydrodynamic heads, losses due to flow (entrance and viscous contributions), etc.

2. Hydrostatic Interface Stability

Figure III-2 shows a partially filled tank. The acceleration vector, as shown, is parallel to the tank axis and acts in the direction tending to reorient the propellant to the opposite end of the tank. However, if the proper relationship between fluid properties (surface tension and density) and system geometry (tank radius) exist, the liquid/gas interface will be stable and the liquid will remain as shown. The criterion for determining hydrostatic interface stability is the Bond number (Bo), a dimensionless ratio of body forces-to-capillary forces:

$$Bo = \frac{\rho a L^2}{\sigma}. \qquad [III-6]$$

The characteristic system dimension, L, is the tank radius (r) for the system shown.

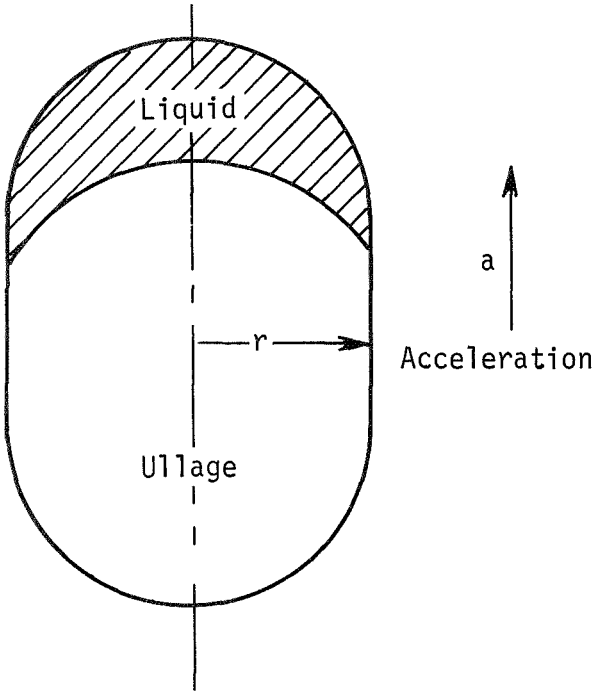

Figure III-2 Partially-Filled Propellant Tank

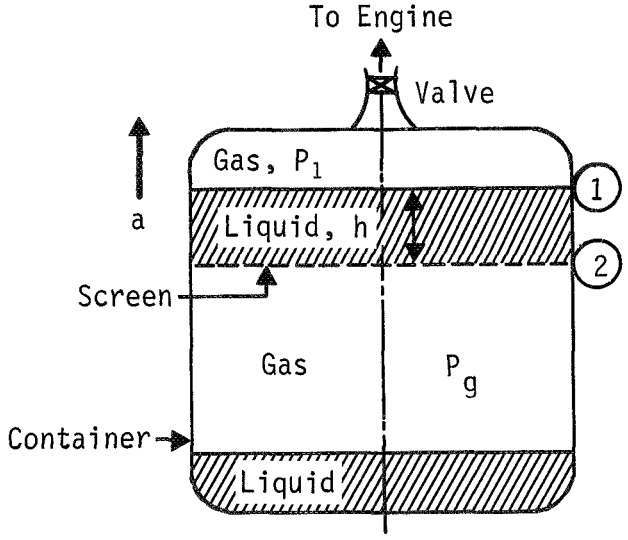

Figure III-3 Hydrostatic Retention Capability, Acceleration Normal

Under Contract NAS8-11328 (Ref III-4), the liquid/vapor interface behavior in an unbaffled, cylindrical tank during axisymmetric propellant settling was evaluated both experimentally and theoretically. Drop tests were conducted in the 2.1-sec drop tower (Ref III-5) to investigate the response of the liquid surface to sudden changes in axial acceleration. The interface was initially flat (Bo >> 1000). Good qualitative agreement between analytical results and experiments performed for settling Bo numbers to 1730 was achieved. At a Bo of 0.84, or less,* the liquid/vapor interface was observed to be stable. At higher Bo values, $0.84 < Bo < 30$, liquid flow was predominantly along the walls of the cylindrical container. At $Bo > 30$, liquid was settled both by flow along the walls and as a central liquid column.

The hydrostatic retention capability of foraminous material is considered next, first, with the acceleration acting normal to the perforated surface, and then with the acceleration vector parallel to the surface. The first case is pictured in Figure III-3. The accelerating force acts normal to the perforated material. Hydrostatic stability occurs if the pressure difference $\left(P_g - P_l\right)$ across the liquid can support the liquid weight and the surface tension force at each opening stabilizes the liquid/gas interface. The liquid height, h, that is supportable can be calculated from:

*Based upon tank radius.

$$h = \frac{\left(P_g - P_l\right)}{\rho a}. \qquad [III-7]$$

If the liquid is supported, liquid can only be lost by ullage displacing the liquid. The hydrostatic stability criterion at each opening (pore) can be determined from the Bo number. Results from Ref III-6 support a critical Bo of 0.84 (based on radius) for circular pores, while the low-g experimental data tend to support a value of 0.45 for square-weave screen (based on one-half the opening).

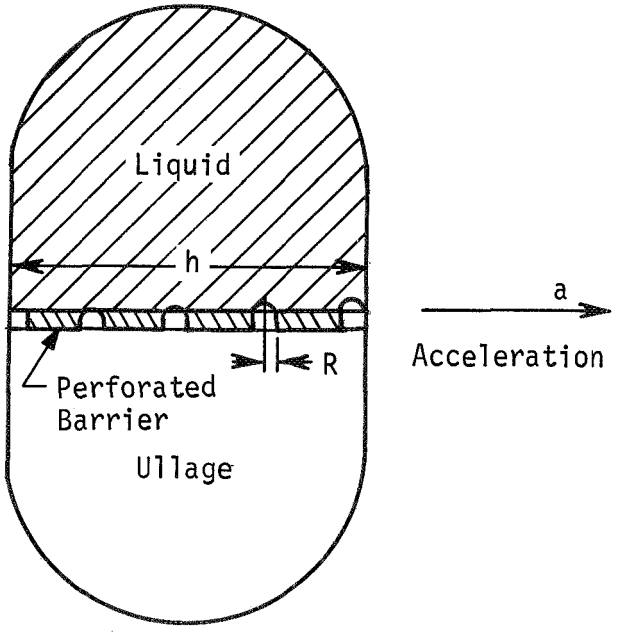

Figure III-4 Hydrostatic Retention Capability, Acceleration Parallel

Figure III-4 illustrates the case of capillary retention with the acceleration vector acting parallel to the perforated barrier. In this case, the hydrostatic pressure is such that the gas phase is attempting to enter the pores at one extremity of the barrier by displacing liquid at the opposite end. The capillary force prevents gas entry at each pore of the barrier, but only the pores at which the maximum hydrostatic pressure must be supported are of interest. For the case illustrated, the hydrostatic pressure difference across the barrier is

$$\Delta P_h = \rho a h. \qquad [III-8]$$

The capillary retention pressure and the hydrostatic pressure act in opposition to each other at the pore, and may be equated to determine the stability limit. The terms can be arranged in a dimensionless parameter, ϕ, a ratio of acceleration forces-to-capillary forces:

$$\phi = \frac{ahR}{\beta}, \qquad [III-9]$$

where β is the kinematic surface tension.* In addition to this dimensionless number, another parameter, Ga, was identified(Ref III-7):

$$Ga = \frac{ad^2h}{\nu^2} \qquad [III-10]$$

where d is pore diameter and ν is kinematic viscosity. The data show a relatively strong dependence on the ϕ number and the open-area ratio (open to total area) (ξ) and a weak dependence on the Ga number. The critical ϕ ranged from 1.2 to 1.7 (ξ = 36.2%) and 2.1 to 2.5 ($9.5 \leq \xi \leq 22.7\%$). The square-weave data ($28.1 \leq \xi \leq 34.8\%$) tend to support a critical ϕ of 0.85 to 0.95, whereas the twilled metal cloth results show the critical ϕ = 1.1. The reader is referred to Reference III-7 for a more complete discussion of these stability criteria.

3. Hydrodynamic Stability Criteria

The foraminous devices can also be designed to damp and control liquids. The experimental work performed under Contract NAS8-21259 shows that the Weber number (We) can be used to predict low-g hydrodynamic stability (Ref III-7). The critical We number, a ratio of inertia-to-capillary forces, is

$$We_c = \frac{v_c^2 L}{\beta}, \qquad [III-11]$$

where L is the characteristic dimension of the foraminous material (pore radius, for example), v_c is the liquid impingement velocity, and β is the kinematic surface tension. To a lesser extent, the effect of open-area ratio (ξ) was also assessed.

The tests were conducted over a range of settling Bo numbers from 30.4 to 135.0, based upon the radius of the cylindrical tanks. Liquid was settled against different perforated barrier configurations and containment was observed. For example, complete damping (containment) was verified experimentally at $We \leq 0.02$ for Dutch-twill cloth and to $We \leq 3.0$ for double, perforated plate. The latter configuration consisted of two plates separated by a small gap (0.032 in.) with the plates skewed so that $\xi = 0$.

*Kinematic surface tension is the ratio of surface tension-to-liquid density.

Formulas for liquid impingement velocity and liquid wall flow, presented in Ref III-7, can be used to determine v_c. These data are directly applicable to the coverplates for the trap designs presented in Chapter IV.

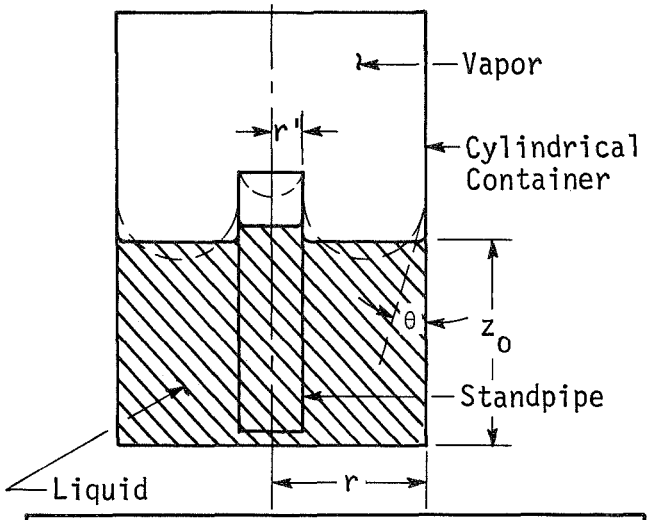

Note: Dashed lines are zero-g interface conditions; solid interface lines are gravity-dominated.

Figure III-5 Capillary Standpipe Concept

4. Capillary Pumping

Referring to Figure III-5, the capillary pressure difference acting on the liquid in the annular region is:

$$P_g - P_\ell = \frac{2\sigma(\cos\theta)}{r - r'}, \qquad \text{[III-12]}$$

where P_ℓ is the liquid pressure at the liquid/vapor interface, P_g is ullage pressure, and r and r' are the tube radii. The pressure difference causing liquid in the standpipe to rise or fall due to surface tension alone is:

$$P_\ell - P'_\ell\left(\frac{r}{\sigma}\right) = 2\left(\frac{1}{\gamma} - \frac{1}{1-\gamma}\right)\cos\theta, \qquad \text{[III-13]}$$

where P'_ℓ is the liquid pressure at the liquid/vapor interface of the standpipe, and $\gamma = r'/r$. It is seen that no capillary pumping results when $\gamma = 0.50$; liquid will rise in the annulus when $\gamma > 0.50$. Liquid will be pumped from the annulus to the standpipe when $\gamma < 0.50$.

This capillary pumping phenomenon, i.e., liquid will be pumped from a region with a large interface curvature to a region of lesser curvature, is used in the Fruhof design to ensure propellant over the tank outlet. Open capillary channels are used to provide physical communication between the outlet and other regions in the tank where propellant may come to rest. Liquid will tend to flow from these regions to the outlet due to capillary pumping. The capillary channels are an open design so that ullage is not trapped during

filling. If the channel is in the form of a V-shape, entrained ullage bubbles will be moved outward by capillary action to the point where the channel width is equal to the bubble diameter. Coalescence of bubbles will result in larger bubbles, which will be moved further out in the channel. Analytical tools and experimental data are available to estimate capillary pumping rates (Ref III-7, III-8, and III-9).

5. Propellant Settling

The fine-mesh screen designs rely upon thrusting periods to settle propellant (away from the trap prior to engine start) over the trap. Settling is a lesser consideration for the Fruhof design.

Settling was discussed earlier under Subsection 2, Hydrostatic Interface Stability. These works (Ref III-4 and III-7) considered the case where the liquid/ullage interface was initially flat. Flow characteristics for initially curved interfaces have also been studied (Ref III-9, III-10, and III-11). Liquid velocities, volumetric flowrates, and settling times, can be estimated using these results. McCarthy (Ref III-11) suggests a dimensionless time parameter (τ) defined as the number of free-fall periods (t) required to obtain bubble-free, settled liquid:

$$\tau = \frac{t}{\sqrt{\frac{2d_s}{a}}}, \qquad \text{[III-14]}$$

where d_s is the liquid free-fall height and a is the axial acceleration. At $\tau = 10$, bubble-free liquid is settled (Ref III-11). Bubble-free propellant is not required at the coverplate, however, because the capillary pressure difference at each pore of the wetted, foraminous material will permit liquid to enter the trap while excluding ullage gas. Based on the McCarthy data, $\tau = 3.0$ is considered conservative for estimating settling times in designing trap devices. Ullage will be ingested during engine burns until the propellant is settled over the coverplate and the trap is sized to accommodate this ingestion.

B. DEVELOPMENT STATUS

The development of surface tension systems for subcritical fluid storage during low-g operation has progressed rapidly over the past decade. The literature reviews presented in Ref III-12 and III-13 summarize this work. The recent survey paper (Ref III-14) summarizes various flight applications for surface tension propellant acquisition systems. This flight experience includes successful performance for systems used in the Agena, Apollo Service Module, and the Transtage. The Apollo Service Module and Transtage use ullage rockets in conjunction with capillary devices to ensure liquid feed to the engine during the start sequence. The Agena relies solely on capillary sump designs to acquire sufficient liquid prior to and during the low-g restart to supply gas-free propellant until the remaining propellant in the tank is reoriented.

The flight experience to date has been for Earth-storable propellants; therefore, the surface tension systems presented in Chapters IV and V for Missions A_2 and B are considered state-of-the-art. The designs presented for the space storables (Mission A_1) are also considered to be within the state-of-the-art, since tank venting is not a design requirement. If tank venting is a requirement, as in cryogenic storage, more development work (Ref III-15, III-16, and III-17) is needed.

IV. PROPELLANT ACQUISITION SYSTEM - ONE-G TESTABLE DESIGN

This chapter presents analyses and designs of various surface tension devices that can demonstrate gas-free liquid expulsion in a 1-g environment. The expulsion is performed with the full-scale capillary design inverted, i.e., the liquid drain port is at the highest station. This testing is commonly referred to as "minus 1 g" since Earth's gravitation tends to position liquid away from the drain port.

A. ONE-G TEST CRITERIA

The surface tension device must have the pressure retention capability required to expel single-phase liquid in minus 1 g, under which the hydrostatic differential pressures are usually much larger than the sum of other upsetting pressure differences that may be experienced during the actual mission. Therefore, minus 1 g tends to impose a worst-case expulsion condition on the device. However, if the device can retain liquid and function properly under this worst-case condition, there is ample assurance that it will operate satisfactorily during the mission.* Since the objective was to design the surface tension device to satisfy the minus 1-g expulsion requirement, the approach was to make the design/test as meaningful and comprehensive as possible. The preferred test is one in which the actual propellant is completely expelled from the full-scale device using the design flowrates.

---

* Martin Marietta has demonstrated gas-free liquid expulsion under minus 1 g with various capillary devices, including fine-mesh traps. The liquid reservoir in the trap is expelled ... not the total loadable propellant. The reservoir and flow annulus in the trap were filled with liquid during tank loading. The minus 1-g tests, therefore, did not demonstrate refill capability of the trap nor the ability of the trap to retain sufficient liquid under the low-g acceleration environment ... merely gas-free liquid expulsion. Additional tests, including subscale models with referee liquids (not propellants) tested in a drop tower, are needed to demonstrate the required liquid retention in the trap.

Availability of material for use in the device is important in establishing criteria for 1-g testing. Aluminum was selected for constructing the Mission A_1 tank; titanium was selected for Missions A_2 and B. These materials provide the best mechanical properties and are most compatible with the propellants (Ref IV-1). It is desirable that the surface tension device and the tank be constructed of the same materials, so that problems associated with the use of dissimilar materials are avoided, and compatibility is not compromised.

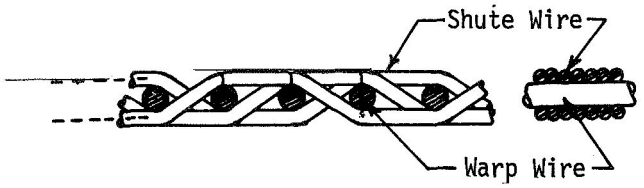

Figure IV-1 Dutch Twill Weave (Ref J. C. Armour and J. N. Cannon: Fluid Flow through Woven Screens," *AICHE Journal*, May 1968

The finest aluminum screen material commercially available is 200 x 1400 mesh Dutch twill weave, which has two hundred 0.0028-in. diameter warp wires and fourteen hundred 0.0016-in. diameter shute wires, per inch. This type of weave (Fig. IV-1) produces a close overlapping of the shute wires, which presents a tortuous flow path through the screen.

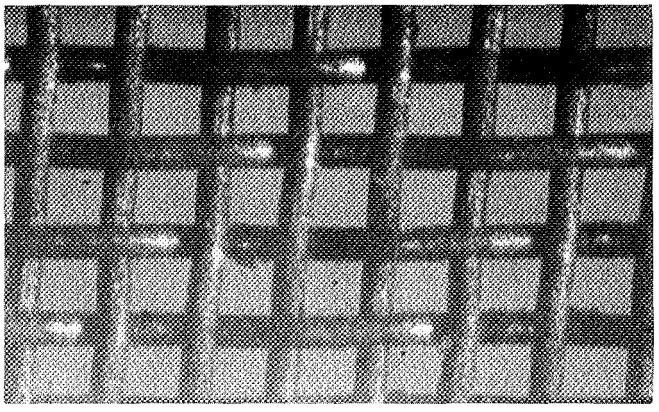

Figure IV-2 180 x 180 Mesh Twill Weave Titanium Screen

The finest titanium screen material (Fig. IV-2) available is 180 x 180 mesh twill weave, which has 180 wires (0.0021-in. diameter) per inch for both the warp and shute wires. The form of the mesh twill weave is considerably more open and loose than the Dutch twill weave.

The retention capability of screen is best determined by the bubble point method (Chapter III). Under 1-g static conditions, the retention capability of the foraminous material must exceed the maximum hydrostatic pressure. Based on the bubble point* for the finest aluminum and titanium screen, and the properties of the propellants, the maximum heights of liquid that can be supported under 1 g are presented in Table IV-1.

---

* The BP data presented in Table III-1 were used. A safety factor of two (normal design practice) was used for the aluminum 200 x 1400 screen. A BP = 8.2 in. H_2O was used in place of the measured 16.3 to 16.4 in. H_2O. This approach was not possible with the coarser titanium screen. Since BP data were not available for the titanium screen, the stainless steel data (Table III-1) were used. Also, the 180 x 180 mesh BP range of 3.27 to 4.00 in. H_2O was determined by interpolation. The upper limits for the BP range were used with no safety factor: 100 x 100 mesh - 2.28 in. H_2O; and 180 x 180 mesh - 4.00 in. H_2O.

Table IV-1 Maximum Hydrostatic Head

Mission	Propellant	Mesh Size	Bubble Point (with propellant, psi)	Maximum Head, 1 g (in. prop)
A_1	B_2H_6	200 x 1400	0.280*	16.01
	OF_2	200 x 1400	0.180*	3.37
A_2	MMH	180 x 180	0.217	6.75
	N_2O_4	180 x 180	0.163	3.05
B	Nitrated Hydrazine	180 x 180	0.339	8.39
		100 x 100	0.204	5.05

*Safety Factor of two.

The supportable heads listed for OF_2 and N_2O_4 are smallest because the oxidizers have relatively low surface tensions and high densities in comparison to the fuels (Table II-6). The heads listed in Table IV-1 are the limiting heights of liquid that can be supported by the screen mesh sizes under the static (no flow) 1-g condition. The surface tension device that best satisfies these relatively small hydrostatic head requirements is a propellant trap (Fig. IV-3). The trap consists of a perforated coverplate and screen annulus. The coverplate provides a barrier that holds the propellant within the reservoir, while the annulus provides a preferential path for liquid (in the trap reservoir) to flow out of the tank outlet. For this type of device, the maximum height of liquid that must be supported by the annulus screen in order to expel the trap reservoir completely is the height (h) of liquid in the annulus (Fig. IV-3).

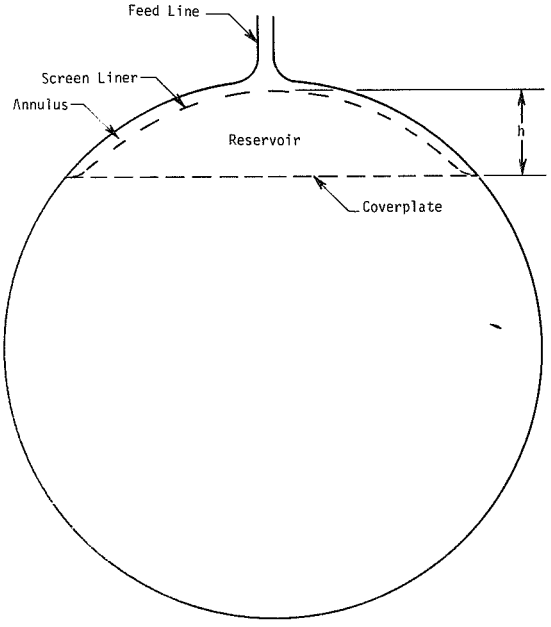

Figure IV-3 Propellant Trap

As discussed, it is desired that the height of liquid that the screen can support should be greater than the height of the trap. However, the trap volume is sized so that sufficient liquid is contained to start the engine and settle the remaining propellant in the tank, thereby providing a continuous supply of gas-free liquid to the engine. If the trap height needed to satisfy the engine demand during propellant settling is greater than that supportable by the finest mesh screens, the trap reservoir cannot be completely drained of liquid and, beyond a certain point, gas in the reservoir will be ingested into the liquid being expelled. This ingestion point can be predicted.

B. PROPELLANT TRAP DESIGN

Detailed drawings of the propellant traps designed for Missions A_1 and B are presented in Figures IV-4 and IV-5, respectively. The surface tension design for Mission A_2 is exactly the same as that of Mission B, except for its size and the screen material. A detailed drawing for A_2 is not presented; however, Figure IV-6 shows pertinent dimensions for the trap device, and Figure IV-5 shows fabrication details. The trap designs presented for Missions A_1 and A_2 would be used in both the fuel and the oxidizer tanks. The traps were designed to acquire and control the oxidizer, since oxidizers possess a lower kinematic surface tension (ratio of surface tension-to-liquid density) than fuels. As discussed in Volume I and later in this chapter, kinematic surface tension is a critical parameter in the design of surface tension control systems.

A pleated-screen liner, which offers advantages in both fabrication and operation of the trap, is used to form the annulus. A self-supporting structure is provided by pleating the screen, and no additional support is required. Since the expulsion efficiency is determined by the volume of the annulus, the pleated-liner minimizes this volume while providing a greater flow area (than flat, unpleated screen) for propellant in the reservoir to enter the annulus. The latter minimizes the pressure loss due to the flow of propellant through the screen during expulsion by reducing the flowrate per unit area.

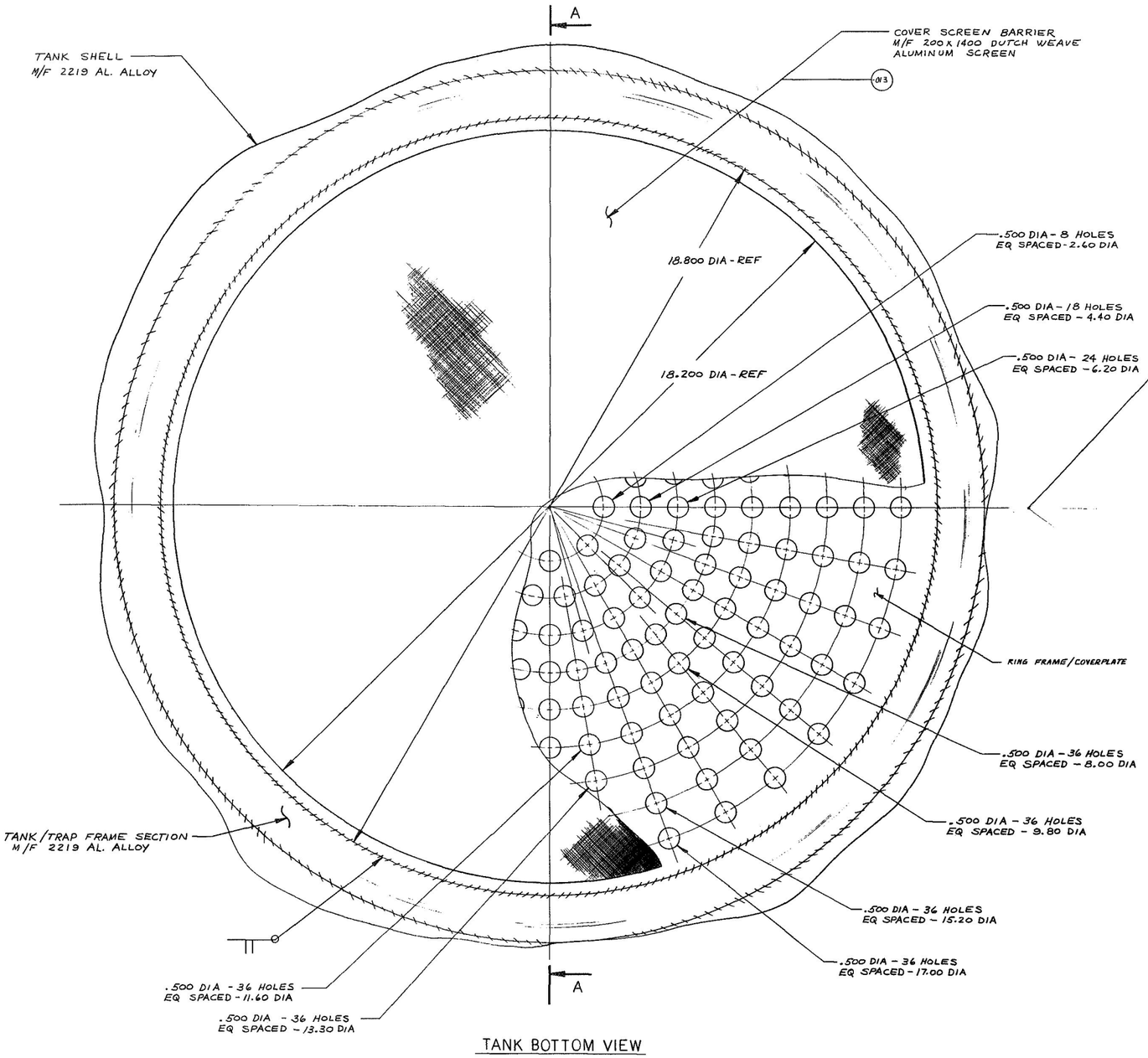

TANK BOTTOM VIEW

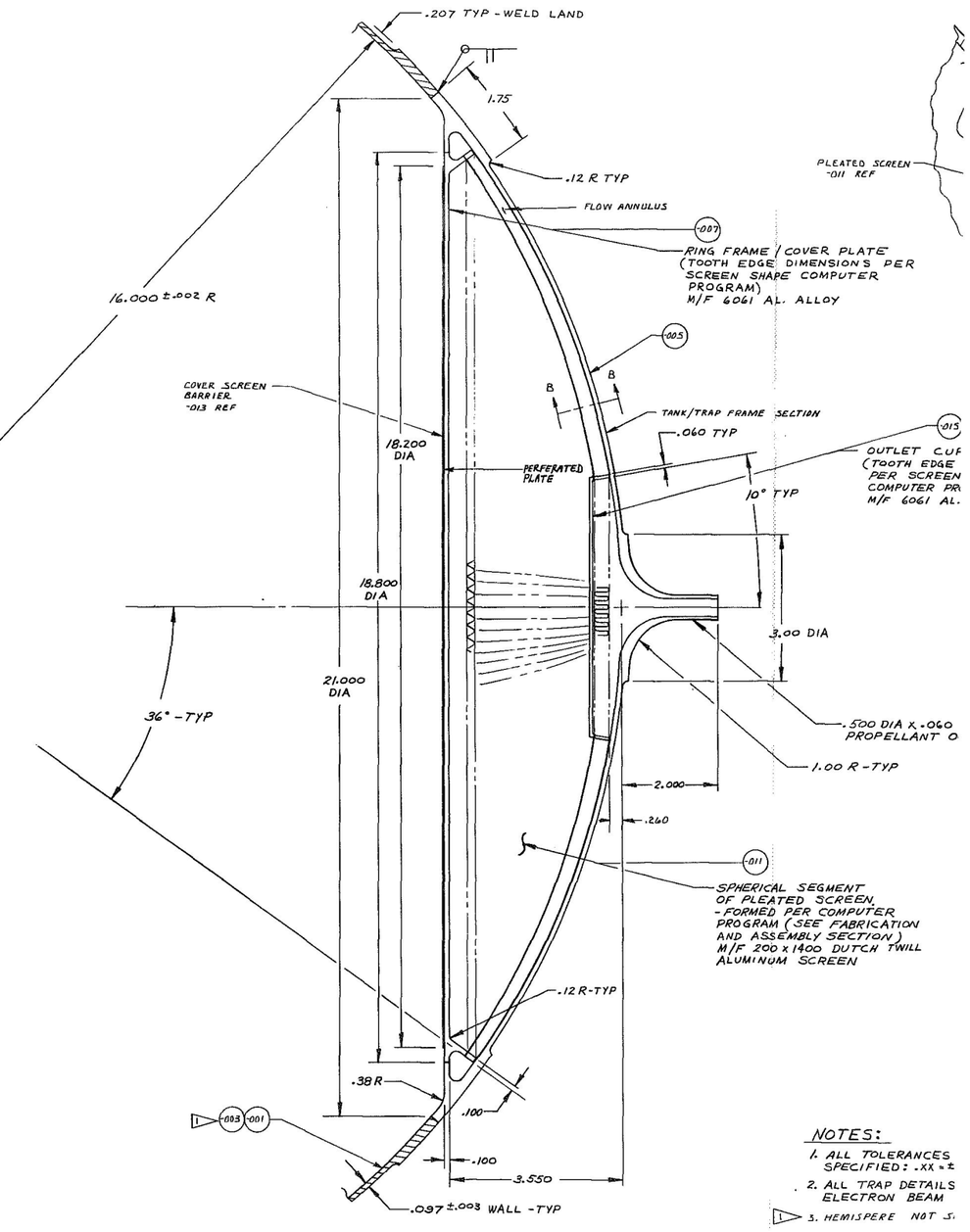

SECTION A-A

NOTES:

1. ALL TOLERANCES SPECIFIED: .XX = ±
2. ALL TRAP DETAILS ELECTRON BEAM
3. HEMISPERE NOT S.

1

2

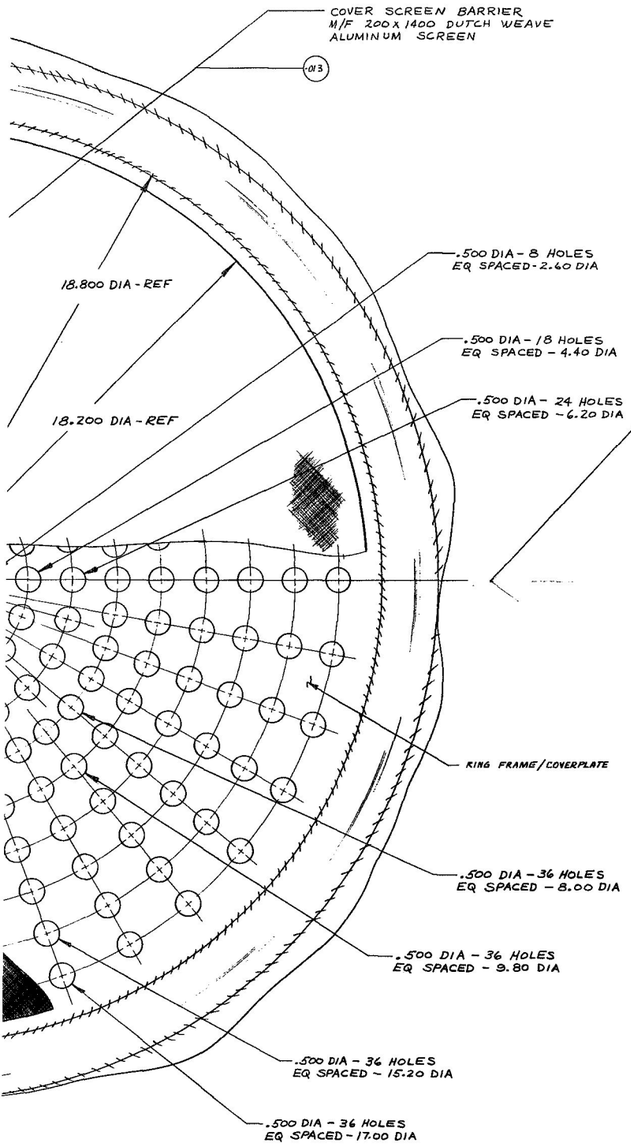

EW

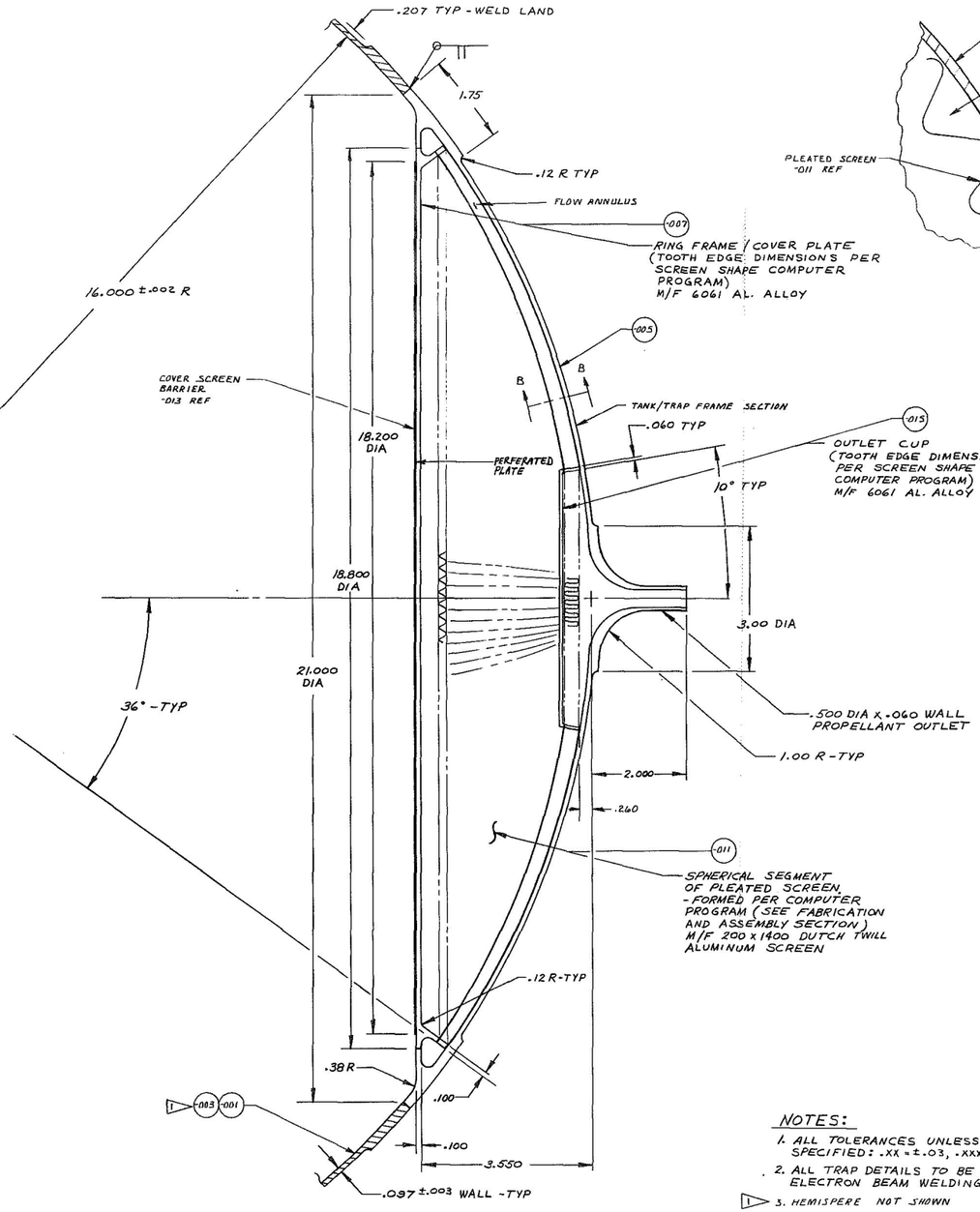

SECTION A-A

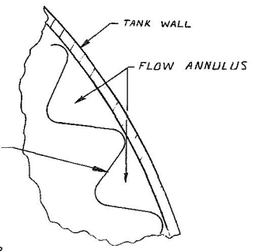

SECTION B-B
No Scale

NOTES:

1. ALL TOLERANCES UNLESS OTHERWISE SPECIFIED: .XX = ± .03, .XXX = ± .010
2. ALL TRAP DETAILS TO BE JOINED BY ELECTRON BEAM WELDING.
1 3. HEMISPERE NOT SHOWN

1

-015 OUTLET CUP ALUM 6061
-013 COVER SCREEN 200 x 1400 DUTCH TWILL ALUM
-011 PLEATED SCREEN 200x1400 DUTCH TWILL ALUM
-007 RING FRAME / COVER PLATE ALUM 6061
-005 TANK / TRAP FRAME SECTION ALUM 2219
-019 TANK / TRAP FRAME SECTION ASSEMBLY
-003 TANK HEMISPERE ALUM 2219
-001 TANK HEMISPHERE ALUM 2219

-009 TANK & EXPULSION ASSEMBLY

019 009

T. Cassidy 0434 8/17/70

Figure IV-4 Trap Device, Minus 1-g Testable Design for OF_2/B_2H_6 Mars Orbiter

2

3

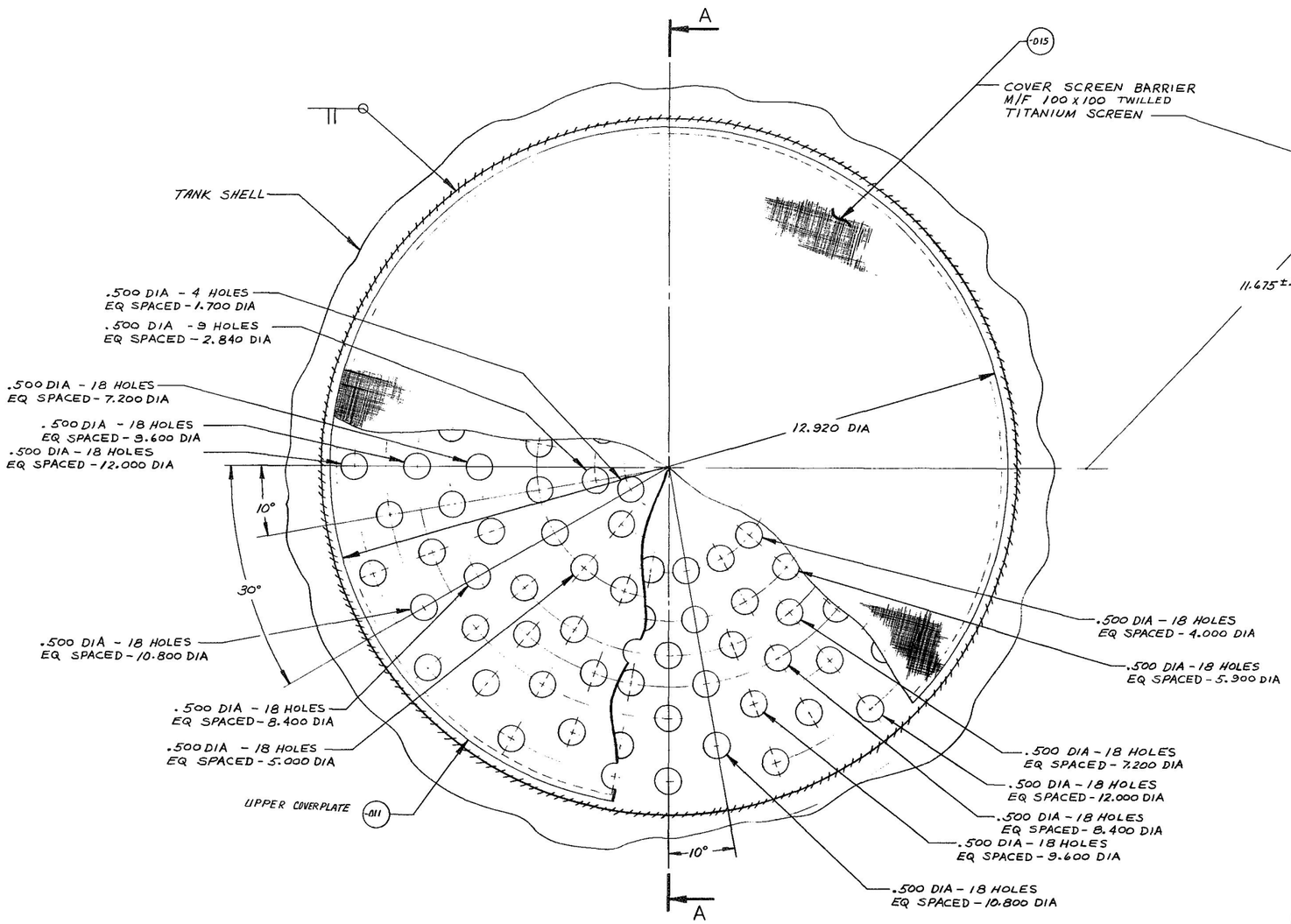

TANK BOTTOM VIEW

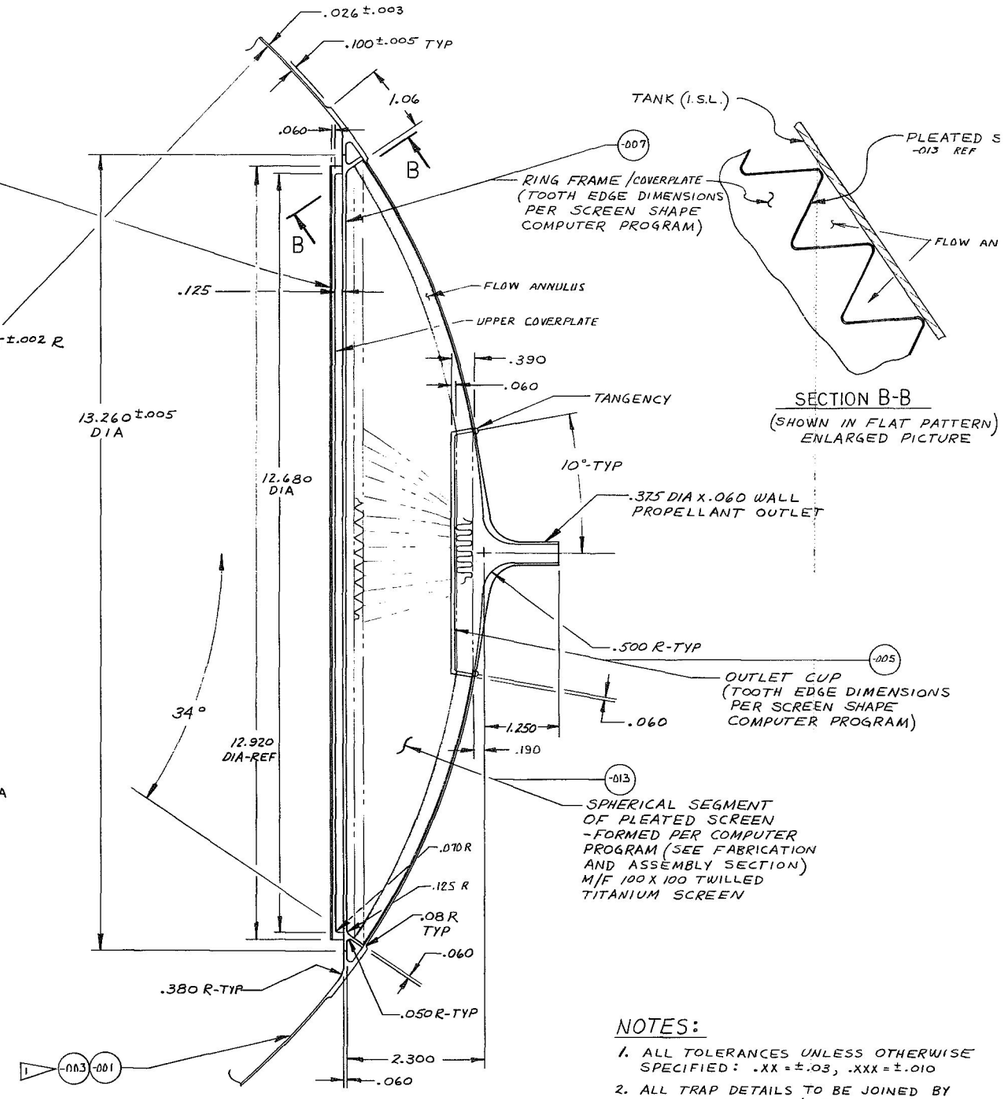

SECTION A-A

SECTION B-B
(SHOWN IN FLAT PATTERN)
ENLARGED PICTURE

NOTES:

1. ALL TOLERANCES UNLESS OTHERWISE SPECIFIED: .XX = ±.03, .XXX = ±.010
2. ALL TRAP DETAILS TO BE JOINED BY FURNACE BRAZING (SEE FABRICATION AND ASSEMBLY SECTION)

1 3 NOT SHOWN

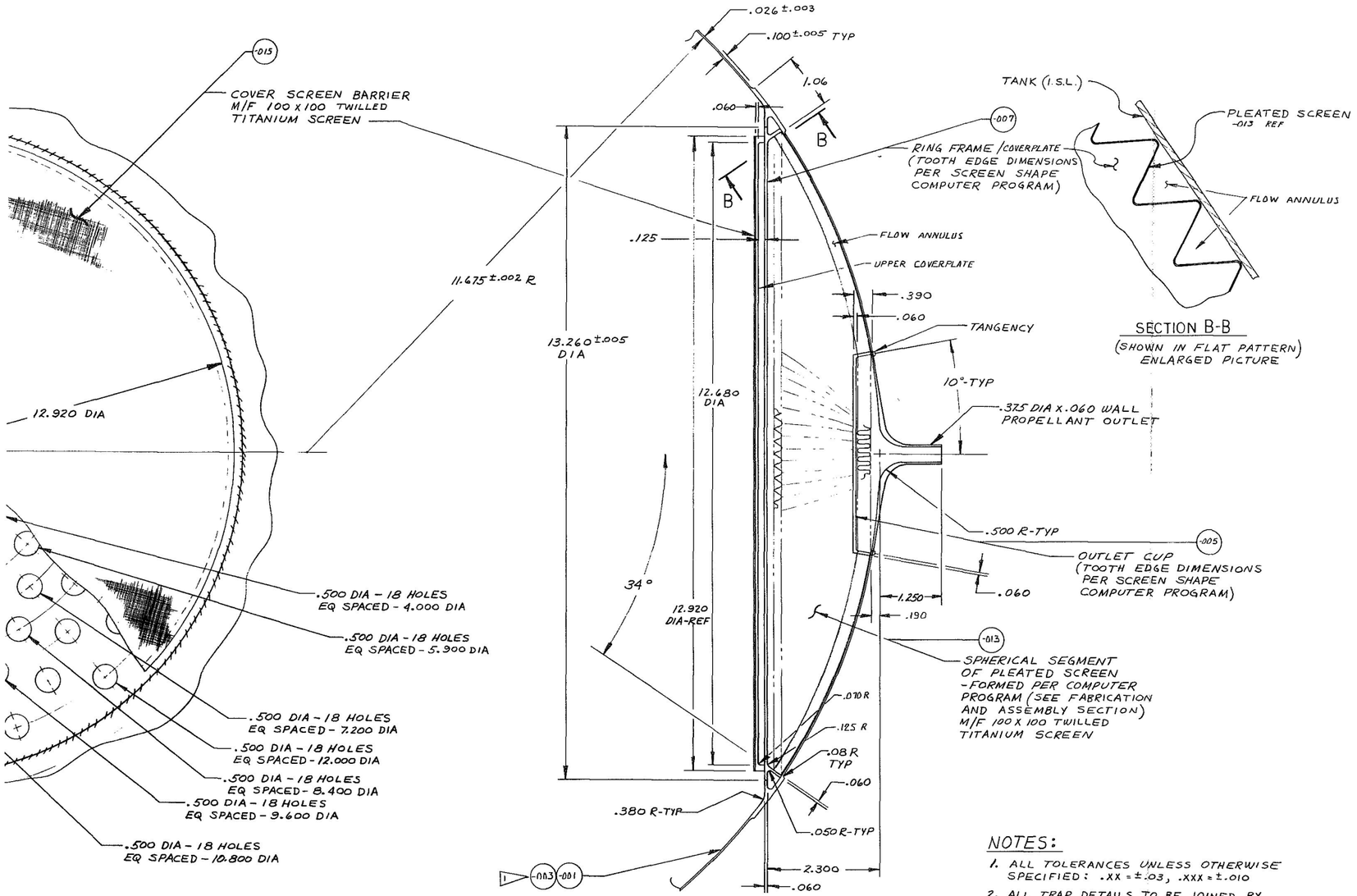

SECTION A-A

SECTION B-B
(SHOWN IN FLAT PATTERN)
ENLARGED PICTURE

NOTES:

1. ALL TOLERANCES UNLESS OTHERWISE SPECIFIED: .XX = ±.03, .XXX = ±.010
2. ALL TRAP DETAILS TO BE JOINED BY FURNACE BRAZING (SEE FABRICATION AND ASSEMBLY SECTION)
1. 3. NOT SHOWN

1		-015 COVER SCREEN 100 X 100 MESH TWILLED TITANIUM SCREEN
1		-013 PLEATED SCREEN 100 X 100 MESH TWILLED TITANIUM SCREEN
1		-011 COVERPLATE TITANIUM RMI-40 REACTIVE METALS INC
1		-007 RING FRAME COVER TITANIUM RMI-40 REACTIVE METALS INC
1		-005 OUTLET CUP TITANIUM RMI-40 REACTIVE METALS INC
	1	-019 SCREEN/TRAP FRAME SECTION ASSEMBLY
1	1	-003 TANK HEMISPHERE TITANIUM 6AL-4V
	1	-001 TANK HEMISPHERE TITANIUM 6AL-4V
		-009 TANK & EXPULSION ASSEMBLY

019 009

T. Cassidy 0930 8/14/70

Figure IV-5 Trap Device, Minus 1-g Testable Design for Grand Tour Mission

EW

2

3

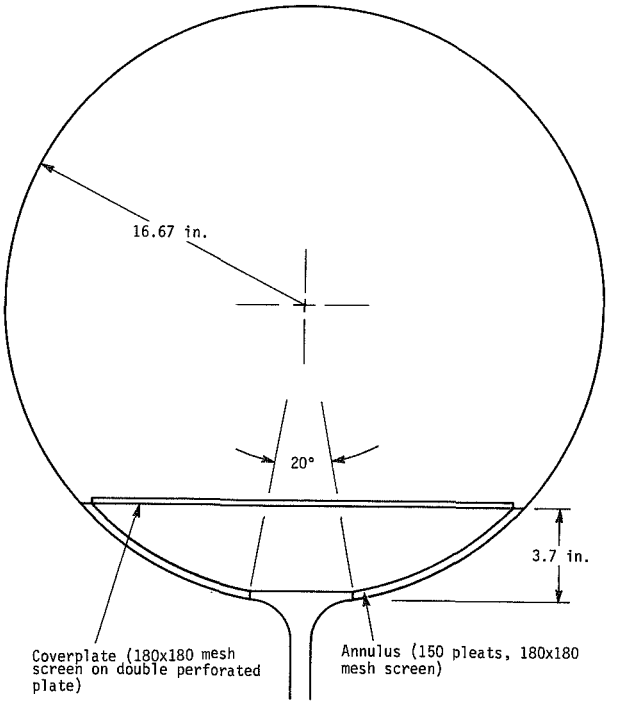

Figure IV-6 Propellant Trap for Mission A_2

The coverplate is a sandwich-type configuration that consists of sheets of screen and perforated plate, as shown in the figures. This combination provides internal capillary flow paths within the coverplate to aid wicking and maintain the desired wetted barrier, provides good damping of propellant motion (slosh) to keep liquid from leaving the trap following an engine shutdown (or under vehicle maneuvers), and also provides required structural integrity.

1. Trap Volume

The mission profile (number and duration of engine burns) determines the required size of the propellant trap. As discussed in the previous section, this trap depth is critical to the trap expulsion efficiency attainable during the minus 1-g tests. There must be enough propellant in the trap to restart the engine and to maintain gas-free propellant during the duration of the burn. From the analysis of the coverplate (Section B.3), it can be seen that the requirements of the 1-g test limit the design of the trap, in that it cannot be refilled with the settled propellant during each burn. Therefore, the trap volumes were sized to hold enough propellant in the trap to accomplish the engine start and propellant settling for all burns with no refilling (ullage purging).

Any factor that may cause loss of propellant from the trap must be considered in these designs. The primary considerations are acceleration vectors and their corresponding impulses that may tend to move the propellant away from the outlet and dislodge it from the trap. By proper selection of the coverplate pore size, as discussed later, the propellant can be completely retained under these perturbations.

Another factor is the effect of dissolved pressurant, which was discussed in detail in Volume I. The greatest effect, due to evolution of dissolved pressurant, is for the OF_2 tank. It was shown

that at most, 0.16 lb_m of OF_2 may be forced out of the trap. As will be discussed, the trap is sized to compensate for this small possible liquid loss.

Thermal effects, such as vaporization and fluid density changes, can cause a loss of propellant from the trap. The cause and the magnitude of these effects are discussed in Section D. Since these effects appear significant for Missions A_1 and A_2, a slightly different approach was used in sizing the traps for these missions. The trap volume was set equal to the volume of propellant consumed during the last three engine burns, i.e., the trims that follow orbital insertion. Since the fuel and oxidizer tanks will have the same size trap, the larger of the two volumes was used to determine the trap size for that mission. The bulk liquid above the coverplate will be in contact with the coverplate prior to each of the first three burns. When liquid is in contact with the coverplate, there will be no gas ingestion into the propellant trap during burns. At the end of the insertion burn, all of the propellant will be located within the trap.

To show that the interface of the bulk liquid would be in contact with the coverplate prior to each of the first three burns, accelerations that tend to move propellant away from the coverplate were considered. The acceleration levels included in the mission criteria were used to establish worst-case (maximum) accelerations. Firing of the ACS will produce the largest accelerations between engine burns. It was assumed that the ACS could provide simultaneous pitch, yaw, and roll maneuvers and the magnitude of the acceleration produced could equal the square root of the sum of the squares of the accelerations due to each component of the maneuver. It was further assumed that this vector could act along any axis. Using this approach, the following maximum negative-axial and lateral accelerations were calculated: Mission A_1, 9.57×10^{-5}g; Mission A_2, 8.33×10^{-5}g; and Mission B, 3.0×10^{-5}g. The free-surface interface position was calculated based on the maximum, negative-axial acceleration and the volume of propellant remaining prior to the insertion burn. Figure IV-7 shows the position of the interface under these conditions for the fuel and oxidizer tanks (Missions A_1 and A_2).

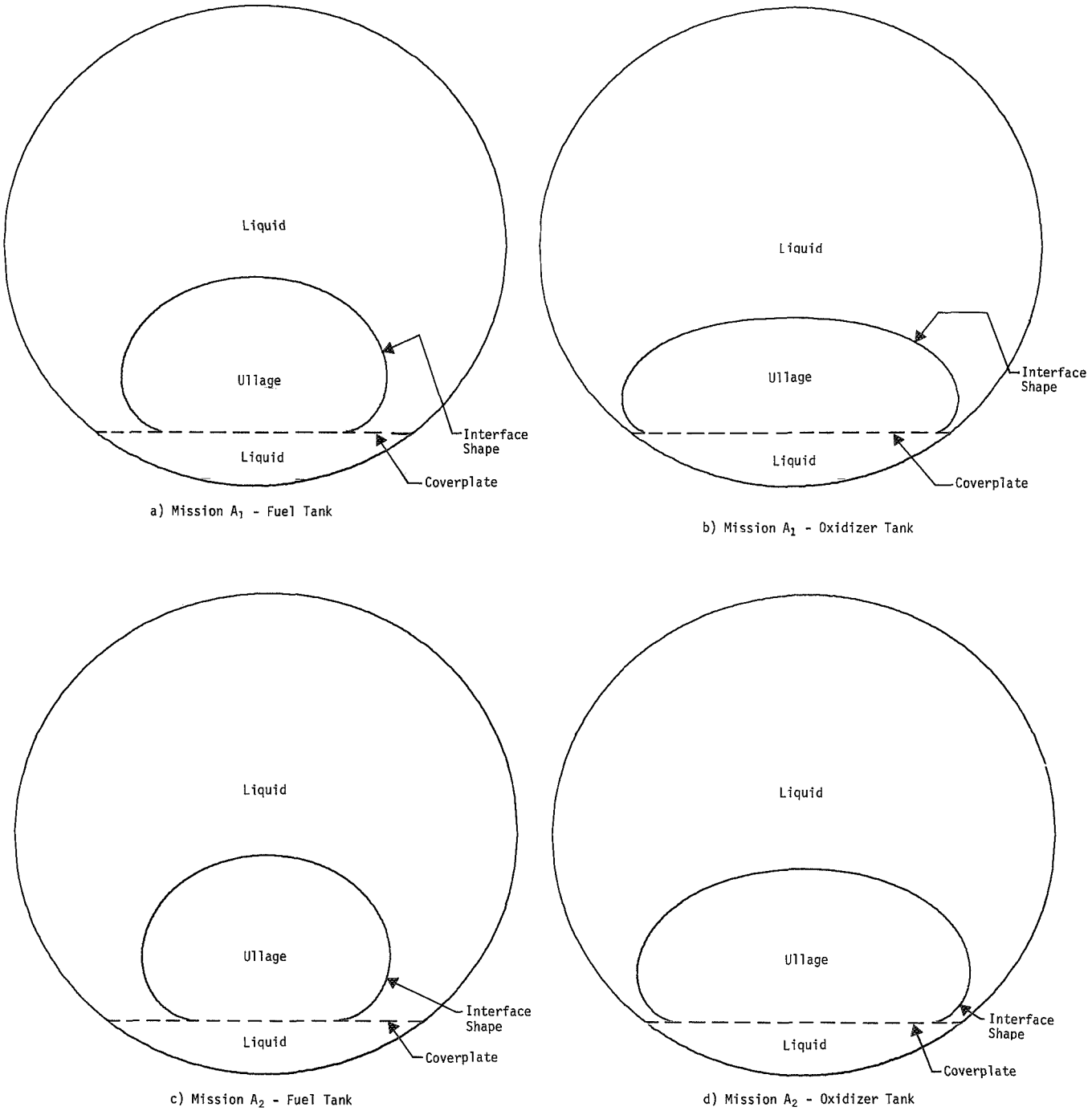

Figure IV-7 Interface Shapes Before Insertion Burn

Using this approach to size the propellant trap, all the propellant is positioned in the trap over the tank outlet following the insertion burn. The problem of heat soakback from the engine is reviewed later in this chapter. In addition to trapped propellant acting as a heat sink, there will be a surplus of propellant within the trap so that some loss due to vaporization is allowable. The amount of propellant required to start the engine and settle the propellant for each of the last three burns was calculated, and the surplus of propellant in the trap was determined (Table IV-2).

Table IV-2 Propellant Quantities Within the Trap

Mission	Propellant	Mass in Trap (lb_m)	Mass Required to Start and Settle for Last 3 Burns (lb_m)	Surplus (lb_m)
Mission A_1	B_2H_6	10.3	5.8	4.5
	OF_2	30.8	17.3	13.5
Mission A_2	MMH	21.3	7.2	14.1
	N_2O_4	33.1	11.3	21.8

For Mission B, the size of the trap was determined by the amount of propellant required to start the engine and settle the propellant for each of the nine burns. This volume was then increased by a safety factor of 1.5, to compensate for additional effects (previously identified) that may cause a loss of liquid from the trap.

As a result of this analysis, the following trap sizes were established: Mission A_1, 0.340 ft^3; Mission A_2, 0.383 ft^3; and Mission B, 0.105 ft^3. From these volumes, the height and other dimensions of the trap were calculated.

2. Annulus

a. One g - The height of the annulus and the size of the flow passages determine the magnitude of the pressure losses that will occur as the propellant flows to the tank outlet. The screen material from which the annulus is formed determines the amount of differential pressure allowable between the annulus and the

reservoir. Ingestion of gas into the annulus will occur if the differential pressure exceeds the retention capability (Bubble point) of the annulus screen material.

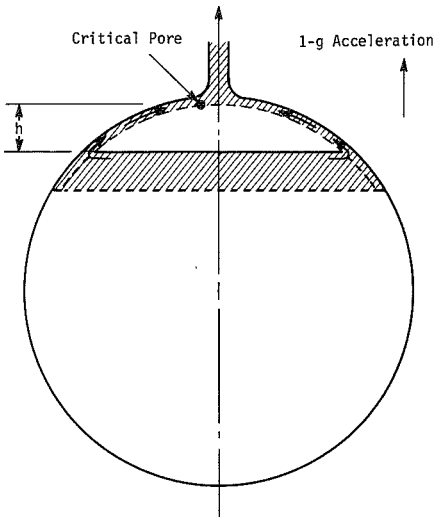

Figure IV-8 Outflow during 1-g Test

Consider the flow of propellant for a point in time during the 1-g test (Fig. IV-8). The pressure of the liquid and gas in the reservoir are equal. A pressure loss occurs as the liquid flows through the screen into the annulus. This loss is a function of the weave, mesh size, and flow area of the screen and the flowrate of the liquid. As liquid flows through the annulus, flow area decreases as the outlet is approached, so the static pressure decreases (velocity increases). In addition, friction will also cause a decrease in pressure as the liquid flows along the annulus. The height the liquid in the annulus attains (shown as h in the figure) determines how much the pressure is reduced due to the hydrostatic head. These pressure differences are additive and the point on the screen surface at which their sum is the largest is identified as the critical pore. At this point, the pressure of the liquid is reduced in comparison to the pressure of the gas on the opposite side of the screen. If the liquid pressure has been reduced such that the liquid-ullage pressure difference exceeds the retention pressure of the screen, gas will be drawn into the annulus causing interruption of the expulsion of gas-free liquid.

As liquid is expelled from the trap, the pressure difference (measured at the critical pore) increases. The height grows, increasing the head loss while reducing the flow area of liquid leaving the reservoir. The latter increases the loss due to flow through the screen. The loss due to the reduction in flow area in the annulus will tend to remain constant at the critical pore; however, since the mean length of the flow path in the annulus is

increasing, the friction loss will increase. Eventually, for any trap design these losses will exceed the pressure retention capability of the screen to produce ingestion of gas. Each trap was evaluated with respect to each of these pressure losses and their additive effect under 1 g to determine how much of the trap volume could be expelled as single-phase liquid.

1) Mission A_1 - A pleated-liner (150 pleats with a depth of about 0.3 in.) was selected since it will provide a minimum expulsion efficiency of 99.6%. The expulsion efficiency is the percent of the propellant loaded that can be expelled as gas-free liquid from the tank. (The residual propellant is that within the annulus.) The flow area between pleats is relatively large, so that pressure losses due to the reduction in flow area and friction will be small in comparison to the losses due to head and flow through the screen.

By using the 200 x 1400 Dutch twill screen, the maximum retention capability is provided. This fine screen, however, causes a considerable pressure loss as liquid flows through its complex weave (Ref IV-2). Figure IV-9 presents this pressure loss over the flow velocity range of interest for OF_2 and B_2H_6. Since the overall height of the trap (3.55 in.) is greater than the maximum height of OF_2 (3.37 in.) the screen can support, complete expulsion under 1 g using OF_2 is not possible. The critical pore will break down after 0.15 cu ft of propellant (or about 50% of the trap volume) has been expelled. This corresponds to 2.0 in. of the overall 3.55-in. height of the trap. While the trap for the B_2H_6 tank will not be as strongly affected by hydrostatic head because of its greater kinematic surface tension value, the loss due to flow through the screen is considerable. Only 3.3 in. of B_2H_6 can be expelled from the trap during the 1-g test.

From the above consideration of the pressure losses, it was established that there is a critical pore which will break down before any other pore on the annulus. Therefore, as far as the annulus is concerned, the 1-g test is a test of the size of the critical pore, or to be more general, the size of the pores near the tank outlet. When the 1-g test is considered in this sense, complete expulsion is not necessary. Prediction of the point at which breakdown will occur would show that the retention capability was as anticipated.

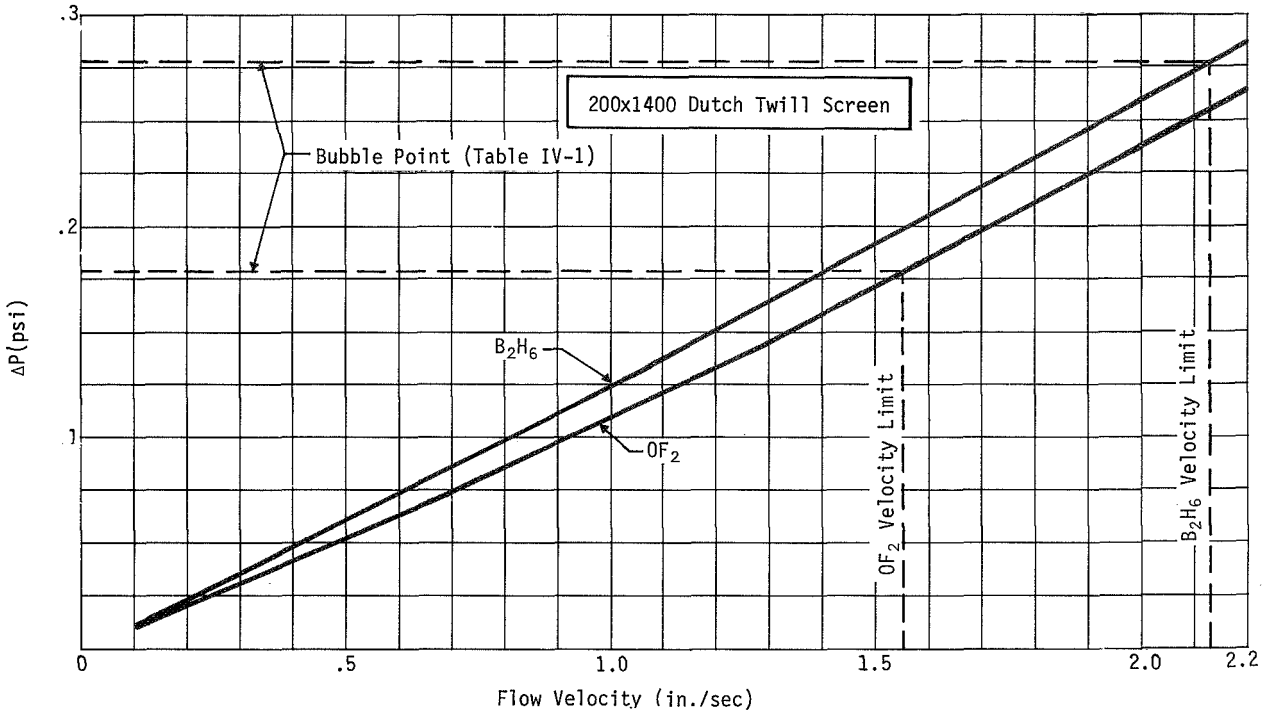

Figure IV-9 Pressure Drop Due to Flow through Screen, Mission A_1

2) Mission A_2 - For this mission, The pleated liner has 150 pleats with a depth of about 0.33 in. and a minimum expulsion efficiency of 99.6%. The flow area is such that the pressure losses due to friction and reduction in area are relatively small, since the 180 x 180 mesh twilled weave titanium screen is used for the annulus. Since the weave of this screen provides an open area to fluid flow (as mentioned, Dutch twill affords a tortuous flow path), the flow loss through the screen over the flow velocity range of interest (Fig. IV-10) is well below the bubble point (Table IV-1). This leaves the pressure difference due to the hydrostatic head as the major consideration in the analysis of annulus design.

Complete expulsion of the N_2O_4 tank trap during the 1-g test is not possible, however, because the height of the trap (3.7 in.) exceeds the maximum height of N_2O_4 (3.05 in.) that can be supported by the screen. Three inches of N_2O_4 only can be expelled from the trap. On the other hand, the trap in the fuel tank could be completely expelled using MMH during the 1-g test.

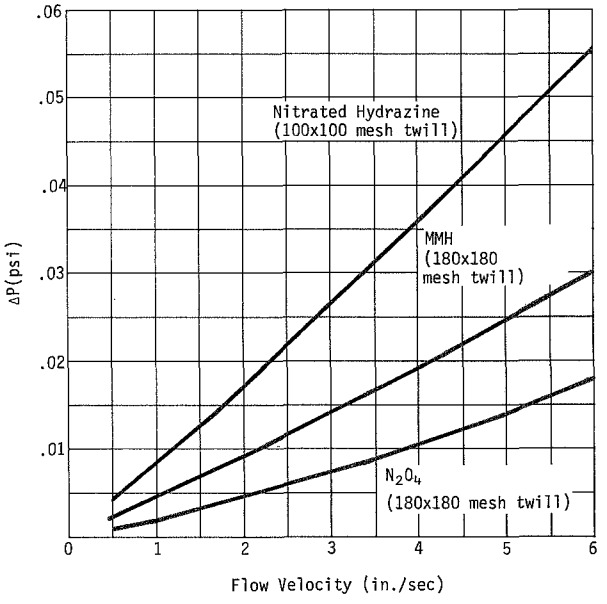

Figure IV-10 Pressure Drop Due to Flow through Screen, Missions A_2 and B

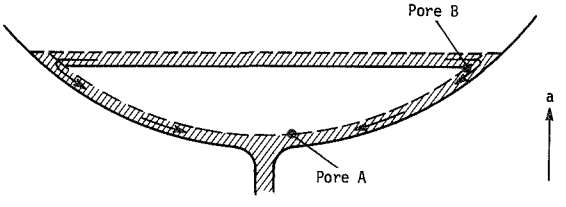

Figure IV-11 Worst-Case Configuration

3) Mission B - An Annulus with 120 pleats, approximately 0.27-in. deep, was selected. The minimum expulsion efficiency is 99.2%, which is lower in comparison to the other designs (99.6%) because it is based on the lower initial 50% propellant load. A 100 x 100 mesh, twilled titanium screen is adequate. The losses due to reduction of flow area, friction, and flow through the screen are all small, again leaving the hydrostatic head as the major consideration. Complete expulsion of the trap is possible under minus 1 g.

b. Low g - Each of the 1-g test designs must be analyzed for the mission accelerations to ensure that the device will function properly in flight. From the many possible configurations of the interface within the trap and the need for many engine starts, the configuration which produces the worst-case condition (Fig. IV-11) was selected for analysis. This worst-case condition is defined by the following conditions:

1) Immediately prior to the last engine burn;

2) Amount of propellant in the trap is just sufficient to start the engine and settle the propellant;

3) Propellant within the trap is initially oriented away from the outlet, due to the negative-axial acceleration acting on the spacecraft up to this point. A conservative assumption, to simplify the analysis, is that the interface is flat, though it will actually be curved and most likely the liquid will be in the sharp corner formed by the coverplate and annulus;

4) The engine starts and a positive, maximum axial acceleration (due to engine thrust) is imposed on the spacecraft. It was assumed that the thrust builds to its steady-state value instantaneously.

This worst-case condition occurs for only an instant. The pressure losses will be less at other times when there is more propellant in the trap, or when the propellant has settled over the outlet.

Rather than a single pore being the critical pore as it is under 1 g, there are two points on the annulus, either of which could be the critical pore. This is possible because the four annulus pressure losses are not maximum at the same point. This fact, by itself, will tend to make the 1-g test more stringent than the actual flight. The two possible critical pores are shown in Figure IV-11 as pore A and pore B.

Each of the annulus designs was analyzed based on these worst-case criteria. Even with these conservative conditions, the 1-g designs provided a greater pressure retention capability than required. Mission A_1 was the only mission in which the calculated pressure losses and the retention capability of the screen were on the same order of magnitude. A maximum pressure drop of 0.13 psi occurred at pore B; the retention capability is 0.18 psi. This resulted because the pressure loss due to flow through the screen, independent of acceleration, is large due to the Dutch twill screen. In Missions A_2 and B, the screen retention pressure and the maximum pressure loss in the annulus differed by at least two orders of magnitude (pressure drop of 0.007 psi at pore A compared to retention capability of 0.16 psi for Mission A_2 and pressure drop of 0.006 psi at pore A compared to retention capability of 0.2 psi for Mission B).

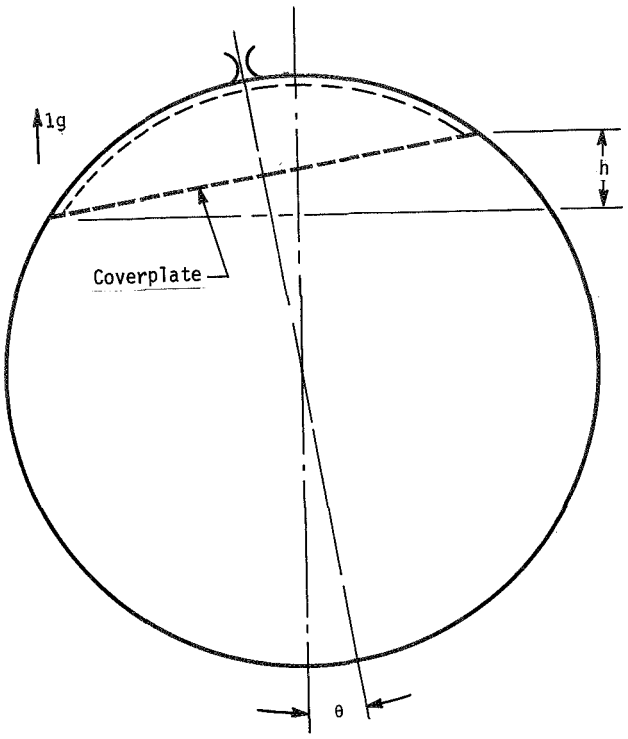

Figure IV-12 Tank Misalignment during 1-g Test

3. Coverplate

a. One g - The coverplate must support and contain the propellant in the trap under minus 1 g. The basic criteria which establishes the stability of the pores of the coverplate is the Bond number (Bo). For circular pores, the Bo must be less than 0.84 if the pores are to remain stable under an acceleration vector normal to foraminous materials (Ref IV-3). If the coverplate is completely horizontal (gravity perpendicular), this is the only design consideration. However, some misalignment will be present either from the installation of the trap or the test fixture, and the effect of the hydrostatic head (due to the lateral acceleration component) must be considered. This head is shown by the height (h), caused by the tilt angle (θ), as shown in Figure IV-12. When this angle of tilt is 2 or 3°, its resultant head becomes the controlling design criterion. A safety factor of 2 was used for the design of the coverplate for the 1-g operation.

During the mission, the coverplate must provide a wetted barrier so that the ullage pressure can support the liquid within the trap. If the coverplate has internal capillary passages, liquid will tend to be pumped into them to provide and maintain a wetted condition (Ref IV-3). There are at least two ways to provide these desired capillary passages. Dutch twill weave can be used or, during low-g conditions, two parallel, perforated plates may also be used. The void between the plates will tend to fill and remain full of liquid.

1) Mission A_1 - Adequate retention and structural strength were obtained by using the 200 x 1400 Dutch twill screen and supporting it with aluminum perforated plate. The Bo for this configuration is 6×10^{-4} during the 1-g test, and the pores will be stable. The retention provided by the screen is sufficient to allow for a total coverplate misalignment of five degrees during the 1-g test. Tolerances on the alignment of the coverplate within the tank can be closely controlled. By taking some care in the installation of the tank into the test fixture, a tolerance of

5° can be easily maintained. Since the screen material has very little rigidity, the primary purpose of the perforated plate is structural support. The plate has 0.5-in. diameter holes, spaced so that the openness (open-to-total area) ratio is less than 0.2.

2) Mission A_2 - The 180 x 180 mesh twilled weave screen provides an adequate pore size for the 1-g test but does not guarantee a wetted condition during the mission, since it does not have the capillary passageways (as does Dutch twill screen). If double perforated plates were considered instead of the screen, 0.005-in. diameter holes are required. Holes this size can be etched, but the plate must be no thicker than the hole diameter. Since these plates would need additional support and spacing between the plates would be difficult, this coverplate configuration was not considered attractive.

It is only during the mission that it is necessary to keep the coverplate wetted. For the 1-g test there will be liquid in contact with the coverplate. If the coverplate has the retention capability to hold the liquid, it will remain wetted; therefore, the coverplate was designed to ensure wetting during low g. Using this approach, a double-perforated plate configuration was selected. The size of the holes is practical (0.5-in. dia) and spacing between the plates of 1/8 in. is easily provided and maintained. A sheet of 180 x 180 mesh screen is added to the coverplate so that the 1-g test can be accomplished. This screen provides a Bo of 4×10^{-3} and will allow a maximum misalignment of 3° during the 1-g test. Alignment of the tank prior to the test is required to meet this requirement.

3) Mission B - The same configuration coverplate that was used for Mission A_2 was also used for Mission B. Perforated plate, 0.5-in. diameter holes and an 0.2 openness ratio, and 100 x 100 mesh screen were used for this case (Bo = 4×10^{-3}). The allowable misalignment of the coverplate for the 1-g test is 7°.

b. Low g - When flight accelerations are considered, some additional criteria must be applied to the coverplate design. Lateral accelerations and the damping capability of the coverplate must be considered in addition to the static containment criteria (discussed earlier).

The ϕ number can be used to determine the stability limits when the acceleration is parallel to the coverplate (Ref IV-3). The previously established maximum lateral accelerations were used to determine the required pore size using the ϕ number criteria.

At engine shutdown, the direction of the axial acceleration vector changes from positive to negative (drag). The motion of the liquid inside the trap, due to the shutdown maneuver and other accelerations, was considered in order to determine if the resultant dynamic motion will allow liquid to pass through the coverplate. The Weber number (We) can be used to establish the damping capability of the coverplate (Ref IV-3). Very good damping characteristics are provided by the coverplate configurations selected.

All of the coverplates are over-designed for the mission acceleration environment. For Mission A_1, 1.5-in. diameter holes in a single perforated plate would satisfy the ϕ and We criteria. The holes could be 3.3-in. diameter for Mission A_2 and 14.9-in. diameter for Mission B. The 0.5-in. diameter holes of the plate are more than adequate when each criterion is applied, providing a factor of safety on the order of 10. Considering only the actual mission, the screen on the coverplates for Mission A_2 and B is not required and, as mentioned, for Mission A_1 it is needed only to provide wetting of the barrier.

The coverplate design determines, to a great extent, if the trap can be refilled when the spacecraft engine is firing. If the pores are selected so that they would be unstable under the acceleration of the engine, gas may be purged from the trap permitting liquid to displace the gas. Since the engine accelerations during the mission are less than 1 g, the traps cannot be refilled. Use of the screen material on the coverplate makes them stable during boost when the acceleration can reach 3.8 g. Therefore, any gas which enters the trap, or is generated within the trap during the mission, will remain.

A summary of the propellant trap design for each mission is presented in Table IV-3.

Table IV-3 Propellant Trap Design Summary

	Mission A_1	Mission A_2	Mission B
Trap Volume (ft^3)	0.340	0.383	0.105
Trap Height (in.)	3.55	3.70	2.30
Material	Aluminum	Titanium	Titanium
Annulus			
Annulus Volume ($in.^3$)	61.3	69.7	26.1
Screen Material			
Mesh	200 x 1400	180 x 180	100 x 100
Weave	Dutch Twill	Twill	Twill
Number of Pleats	150	150	120
Pleat Depth			
At Coverplate (in.)	0.27	0.28	0.24
At Outlet Cup (in.)	0.32	0.33	0.28
Coverplate			
Diameter (in.)	20.1	20.9	13.9
Configuration	Screen on single plate	Screen on double plate	Screen on double plate
Screen Material			
Mesh	200 x 1400	180 x 180	100 x 100
Weave	Dutch Twill	Twill	Twill
Perforated Plate			
Thickness (in.)	0.10	0.06	0.06
Hole Diameter (in.)	0.50	0.50	0.50
Spacing between plates (in.)	---	0.125	0.125
Minimum Expulsion Efficiency (%)	99.6	99.6	99.2

C. FABRICATION AND ASSEMBLY

The propellant trap consists of a coverplate assembly, a pleated screen liner, and the outlet cup. Each part is fabricated and joined together before the entire trap is installed into the bottom of the tank. The outlet cup and the perforated plates of the coverplate assemblies are machined using conventional methods; therefore, their fabrication is not discussed.

1. Forming the Pleated Screen Liner

The pleated screen liner is formed with a die, from a single, flat sheet of screen material. To construct the die, the profile of the pleats must first be determined. By selecting the pleat depth at the point the liner meets the coverplate, the number of pleats, and the bend radius, the pleat profile can be determined.

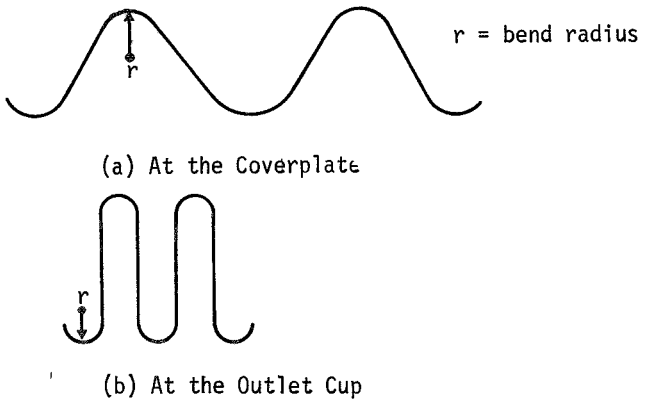

Figure IV-13 Pleat Configuration

A retangular sheet of screen may be used so the pleat depth increases as the outlet cup is approached, thus keeping the circumference constant. At the coverplate, the profile of the pleats looks like that presented in Figure IV-13a. The pleats cannot be any closer than shown in Figure IV-13b. Beyond this point, the pleats begin to fold back upon themselves and the flow passage is restricted. This limiting condition is usually reached at a point within 10° of the tank outlet, making the included angle of the outlet cup 20° (with respect to the center of the tank.

There is a tradeoff between the size of the outlet cup, the bend radius, and the number of pleats. The fineness of the teeth on the outlet cup is determined by the above factors. For these designs, the width (root) of a tooth on the outlet cup was limited to 0.05 in. and the included angle of the outlet cup is 20°. The best configuration was obtained with a bend radius of 0.025 in. and 150 pleats for the A Missions, and 120 pleats for Mission B. Another tradeoff consideration is that between expulsion efficiency and pressure losses (created by the flow of the propellant in the annulus). The expulsion efficiency and the pressure loss tradeoff is used to find the appropriate pleat depth.

From calculations of the shape of the pleat, a die with three (or four) consecutive pleats is manufactured. By advancing the screen material, one pleat at a time in the die, the pleated liner is formed. A press with such a die installed is shown in Figure IV-14. Before the screen material can be pleated, it must be conditioned* to improve formability of the screen. Any displacement of the wires relative to one another, tending to increase the pore size, is eliminated by this process.

In addition to the conditioning process of the screen material, the ultimate percent elongation of the metal must be considered. Pure aluminum has a 35% elongation and titanium has 20%, neither of which is very ductile in comparison to stainless steel, which has 55%. In the design of the pleated liner, the bend radius controls the amount of elongation. By comparing the bend radius to the thickness of the material, the relative elongation induced can be established. The aluminum screen is 0.006 in. thick and the titanium screen is 0.004 in. thick. A bend radius of 0.025 in. was used for all the designs, which is four times the aluminum thickness and about six times that of the titanium. This is not an overly-sharp bend and adequate elongation is available.

2. Joining Methods

Three different types of joints are required for the fabrication and are identified as follows:

1) Screen-to-screen - Joining of the ends of the screen section to form the liner;

2) Screen-to-plate - Joining of the screen to the outlet cup and the coverplate;

3) Plate-to-plate - Joining of the coverplate assembly to the tank wall.

The plate-to-plate joints are conventional, but joints involving screen material present certain considerations. Contaminant trap areas must be minimized and the screen's integrity should not be destroyed due to excessive heat (or force) during joining. Welding and brazing were considered for each joint. Mechanical attachment was not considered because of the inherent contaminant trap areas and the relatively poor rigidity of the

*The actual process is considered proprietary to Martin Marietta Corporation, Denver, Colorado.

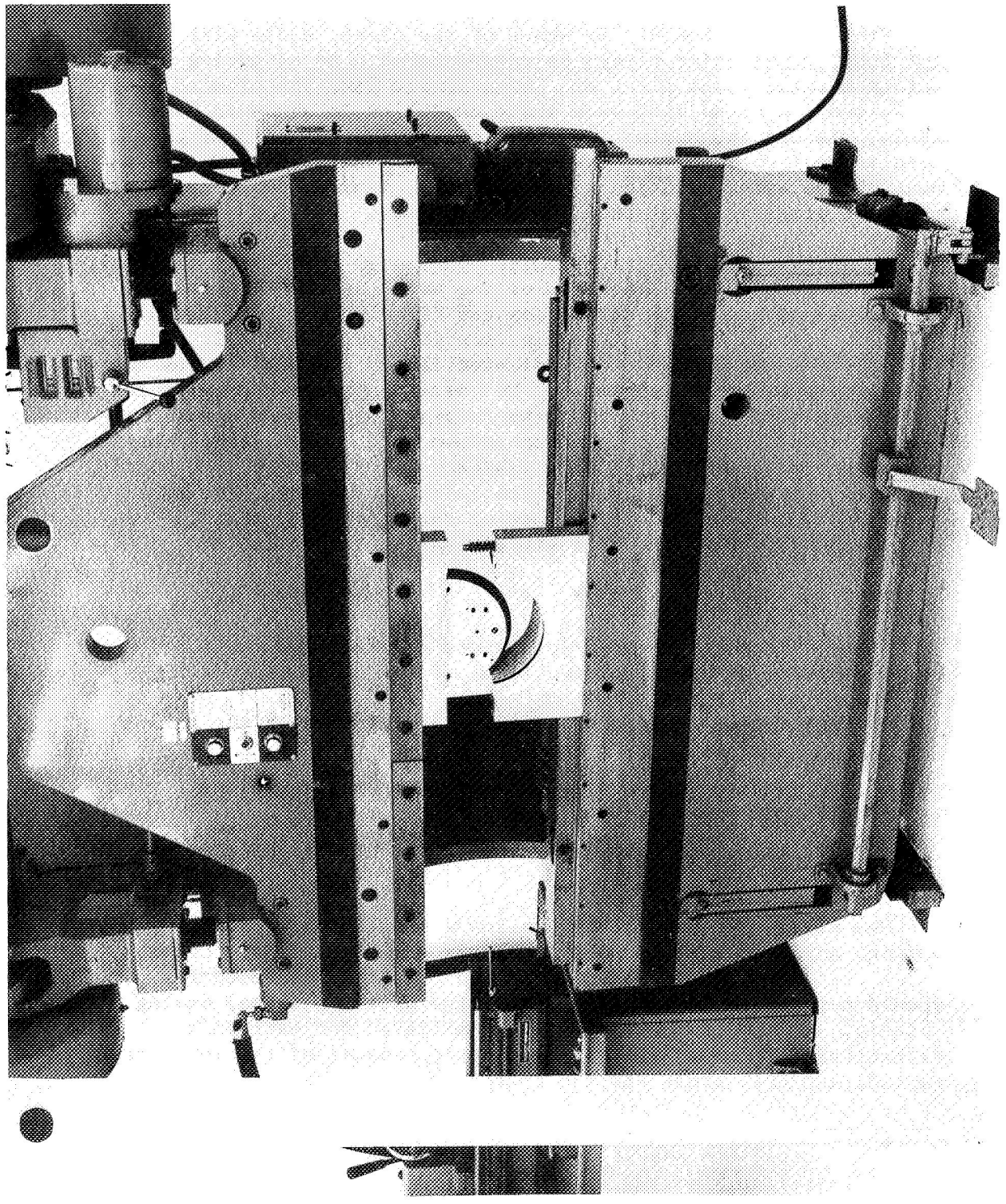

Figure IV-14 Pleating Press

joints. Explosive bonding was also not considered because of the delicate screen materials to be joined and the much simpler methods available (Ref IV-4).

a. Screen-to-Screen - Resistance welding is suitable for joining two sections of screen. The narrow weld joint produced is easily cleaned. Stainless steel screen has been resistance welded and cleaned and used with flourine (Ref IV-5).

Both the aluminum and titanium screen can be resistance welded. Figure IV-15 shows a fixture that has been successfully used to resistance weld pleated-screen liners.

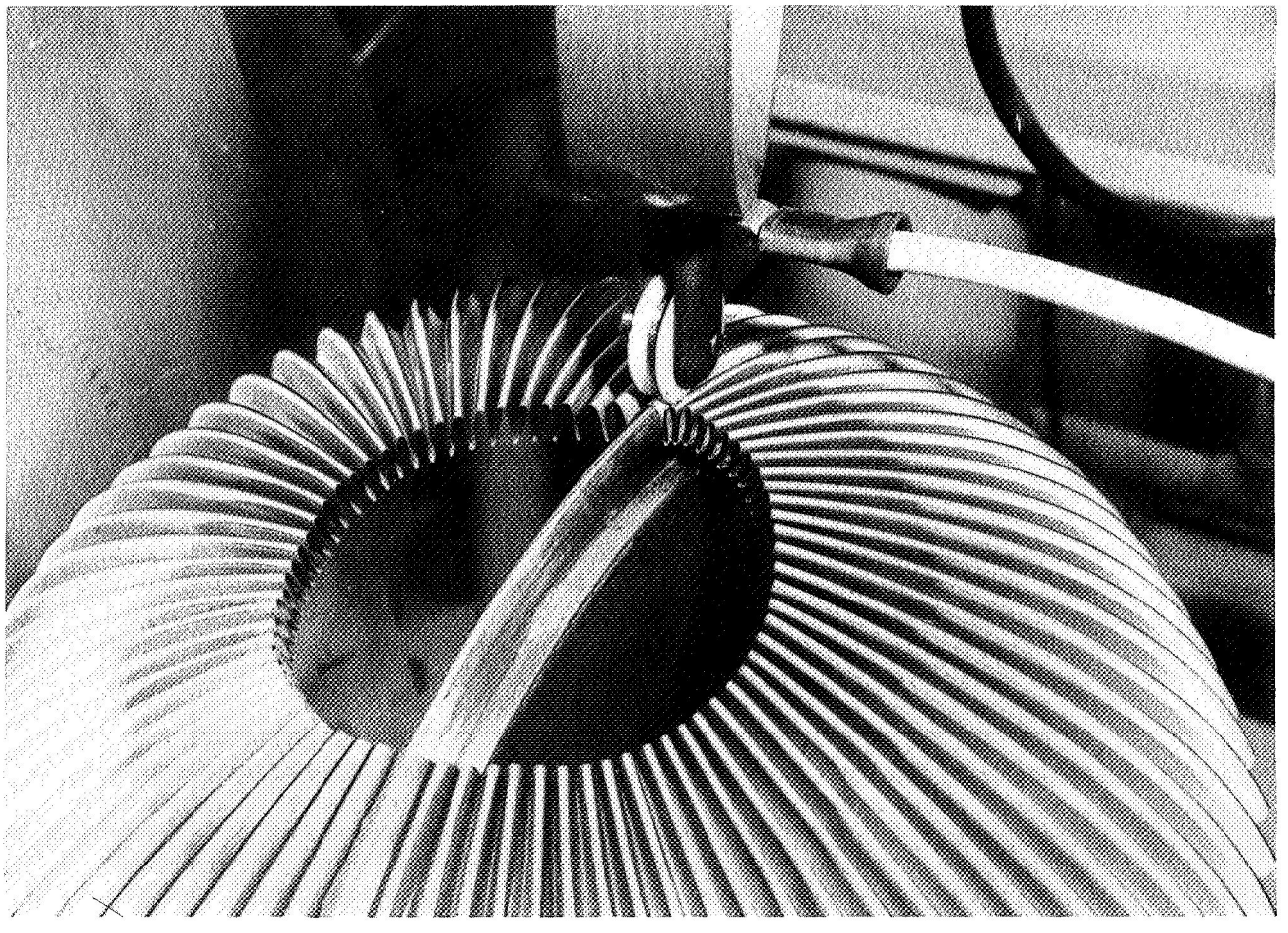

Figure IV-15 Resistance Welding Fixture

Electron beam welding (EBW) is also a candidate method for making screen-to-screen joints. However, additional experience in making and cleaning this type joint must be obtained before it can be recommended over resistance welding.

b. Screen-to-Plate

1) Brazing - The joints required between the screen and plate are complex, making brazing a simple method for accomplishing the joint. There are, however, considerations peculiar to aluminum and titanium. Because of an apparent lack of compatibility between the braze alloys and the fluorine-based propellants, brazing was not selected for aluminum. All braze alloys used for aluminum brazing have a high silicon content. Alloy 718, for example, contains 13% silicon. In addition, for most of these brazes a practically pure silicon flux is used (Ref IV-6). If silicon is present in a material in a quantity greater than 1%, fluorine or OF_2 will react with the silicon to form SiF_4 (Ref IV-7 and IV-8). Instead of adhering as a protective film, the SiF_4 will vaporize (SiF_4 melts at 321°R, and boils at 375°R - Ref IV-8). At the liquid OF_2 temperature of approximately 250°R, the SiF_4 will not liquify, but during gaseous fluorine passivation at ambient temperatures, any brazed aluminum joints will be attacked and weakened by the passivation. Also, even at 250°R, the integrity and protective nature of the solid SiF_4 film is questionable (Ref IV-8).

Only two techniques for brazing titanium are apparently available. One uses a 48Zr-4Be braze alloy; the other uses 3003 aluminum. The 48Zr-4Be, as far as braze integrity is concerned, appears excellent. Also, slight oxide coatings can be tolerated with this technique (Ref IV-9). However, upon examination of the available propellant compatibility information of braze alloys and zirconium alloys, there is some question as to whether this braze alloy is compatible with the propellants.

Zirconium has been rated as a Class 1 material for use with hydrazine (Ref IV-10), and due to its atomic structure it would theoretically not be a catalytic decomposer of hydrazine propellants (Ref IV-11). No compatibility data exist for zirconium with nitrated hydrazine, known to be corrosive with metals (Ref IV-12). Zirconium is rated incompatible with N_2O_4 (Ref IV-10), even though there is no apparent reason why zirconium should be subject to N_2O_4 corrosion (since it and titanium have similar properties). However, a zirconium alloy containing 5% titanium has been severely corroded in ordinary high temperature water (Ref IV-13). Another problem associated with the use of this braze alloy is beryllium poisoning. While the beryllium is very toxic, the hazard can be eliminated if used under the proper conditions.

The 3003 aluminum does not appear to present as many problems as the 48Zr-4Be braze. Aluminum, like titanium, is highly compatible with MMH, nitrated hydrazine, and N_2O_4; therefore, there should not be any compatibility problems with this braze alloy. Based upon preliminary data, the integrity of 3003 aluminum brazed titanium joints seems excellent. Also, any titanium alloy can be brazed to any other titanium alloy without lowering the quality of the braze joint. However, a completely clean surface is required for this procedure (Ref IV-14).

Wicking of the screen material may cause problems during brazing. Molten metal can be drawn into the screen sealing the openings. By applying a "stop-off" material (such as Cotronics Type A) to the screen before brazing, the wicking can be stopped. This type of stop-off is water soluble and can be removed with a water rinse.

2) Welding - Resistance welding can be used for joining screen-to-plate, but the joint is difficult to clean. Resistance welding of screen-to-screen is satisfactory because wire to wire joints are desired. When the screen is joined to plate, the joint should fill with molten metal.

Fusion welding is a means of providing sufficient molten metal to fill the area of the joint, but the application of heat must be carefully controlled. Considering the relative size of the wire compared to the plate thickness, the screen wire can be melted away before the plate weld areas are softened sufficiently to accomplish a complete weld. Also, because of the fine nature of the screen, relatively large areas of screen near the weld joint may be distorted due to heat during welding.

EBW is preferred compared to the resistance and fusion welding, since the amount of heat applied to the joint may be carefully controlled so that melting of the screen occurs only in the joint area. The welding machine is also capable of following the complex joint.

To summarize, the preferred way to accomplish the aluminum screen-to-plate joint is by EBW. Either brazing or EBW can be used for the titanium screen-to-plate joint, although brazing is preferred because of the joint complexity.

b. Plate-to-Plate - Adequate material is available at the joints so that they can be fusion-welded. The joint will be filled and no contaminant trap areas formed. Brazing of the titanium plate-to-plate joint is not desirable because the tensile strength of the tank will be reduced at the braze temperature of 1200°F.

Table IV-4 is a summary of the recommended joining methods for each of the different types of joints of the trap.

Table IV-4 Joining Methods for 1-g Testable Device

Type of Joint	Joining Method	
	Aluminum	Titanium
Screen-to-Screen	Resistance Weld	Resistance Weld
Screen-to-Plate	Electron Beam Weld	Braze (3003 Aluminum)
Plate-to-Plate	Fusion Weld	Fusion Weld

3. Assembly

a. Coverplate - Each of the coverplate assemblies for the traps uses a perforated plate as its base. This plate is a machined part and provides for the attachment of the liner to the coverplate and the attachment of the trap to the tank wall. The center portion of the plate has a pattern of 0.5-in. diameter holes, to provide an openness ratio of 0.2.

For Mission A_1, the coverplate assembly consists of the perforated plate and a disk of Dutch twill screen. EBW is used to attach the screen to the top of the perforated plate.

For Missions A_2 and B, two perforated plates and a disk of screen make up the coverplate assembly. The bottom perforated plate has attachment points and the upper has a 1/8-in. thick ridge to provide for the proper spacing between plates. The two plates, with the screen on top, are joined around the periphery by brazing. A bubble point test of the coverplate should be performed after assembly to ensure screen integrity.

b. Pleated-Screen-Liner - After the liner is formed, the ends are joined by resistance welding. The liner is machined to the proper size by an electrical discharge milling machine (Fig. IV-16). It is joined first to the outlet cup and then to the coverplate assembly.

The entire trap can be bubble checked. A fixture for the outlet cup is required so the inside of the trap can be pressurized. By submerging the entire trap in the test fluid, both the coverplate and the liner are checked. After the trap is installed in the tank, the tests will be similar to the 1-g tests, for which the trap was designed.

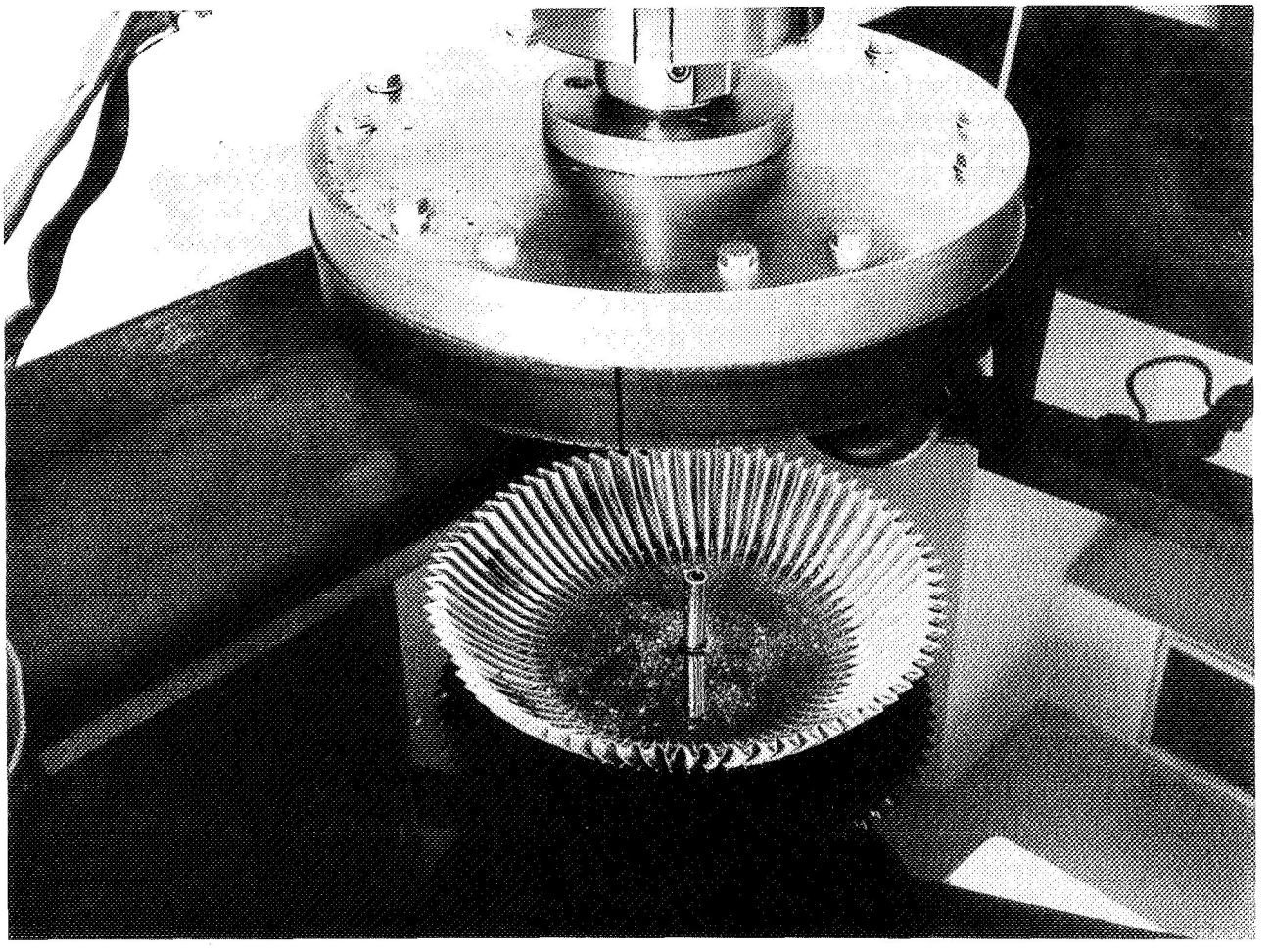

Figure IV-16 Electrical Discharge Milling Machine

4. Cleaning and Passivation

The following procedures, to guarantee that the trap and the tank are clean prior to propellant loading, should be followed for all three missions. Each trap component, except for the screen material, is degreased and then acid cleaned prior to assembly (Ref IV-12, IV-15, and IV-16). Degreasing consists of a vapor degrease or an acetone immersion, followed by air drying. The composition of the acid-cleaning solution and the specific procedure depends on the metal involved and the propellant to which it is to be exposed.

For titanium/hydrazine systems, the part should be immersed in a room temperature solution of HNO_3, HF, and water for approximately one minute. This is followed by a thorough, distilled water rinse and drying by either an oil-free, moisture-free nitrogen gas purge, or a vacuum oven bake at 120°F for a period of five minutes (Ref IV-12). The same cleaning procedure is recommended for cleaning titanium/N_2O_4 systems (Ref IV-15). Aluminum/B_2H_6 systems and aluminum/OF_2 systems can be cleaned by immersion in a room temperature HNO_3 + H_2O acid solution for a minimum of one hour (Ref IV-16). The rinse and dry are the same as recommended for titanium/hydrazine systems.

After cleaning, other treatment processes may be needed depending upon the specific joining operations to follow. When the process is complete, the cleaned parts must be stored under controlled conditions.

Screen material cannot be cleaned by the above processes because the amount of metal that would be removed by the acid solution would increase the size of the pores. Therefore, a vacuum annealing process is used to clean the screens. This is performed after assembly of the trap and completion of the bubble point tests. A vacuum annealing of the screens, subsequent to each previous bubble point test, is also suggested. All contaminants and residual alcohol would be removed. Stainless steel screens have been cleaned for fluorine service using this method (Ref IV-5).

Joining the trap to the lower-half of the tank, and joining the tank halves should be done under clean room conditions and in an inert atmosphere. A nonacid chemical cleaning procedure is then used to clean the assembled tank (Ref IV-8, IV-17, and IV-18). Vacuum annealing of the tank is not recommended because of the reduction in strength. When the nonacid chemical cleaning is complete, the tanks should be rinsed with distilled water and dried with a hot (150°F) helium gas purge. A chemical analysis of the rinse water is used to determine if all the cleaning solution has been removed. From this point on, the tanks should be maintained under a 3- to 5-psig blanket pressure with helium to prevent the entry of any contamination.

The OF_2 oxidizer tank, Mission A_1, must be passivated. Gaseous fluorine is used for the passivation, rather than gaseous OF_2, since fluorine is the most effective agent for passivation of metals (Ref IV-18). Passivation with fluorine gas appears to produce a more resistant and tenacious protective film. Procedures to be used for system passivation are presented in Ref IV-19. Passivation is accomplished immediately prior to loading the tank (Ref IV-20).

5. Fabrication Testing

To better evaluate forming and joining methods, as applied to screen materials, a test program was accomplished. The methods were evaluated by using small samples of either the actual or representative materials of the propellant trap.

a. Aluminum - The actual aluminum Dutch twill screen proposed for Mission A_1 was used in the test program (Ref IV-21). The first step was to determine the "as received" properties of the screen material. Bubble point tests were accomplished to determine the pore size. The measured pressure retention corresponded to an absolute rating of 16 microns (Kressilk Products quoted an absolute rating of 15 microns).

Some screen was cut into 1 in. by 4 in. strips for tensile tests. Three orientations were considered: warp wires in the longitudinal direction; shute wires in the longitudinal direction; and a diagonal orientation of the weave. When the load is applied to the larger number of shute wires, the screen has its greatest strength as shown in Table IV-5 and Figure IV-17. The values listed in the table are the amount of force required to break the 1-in. wide strips of screen material.

Table IV-5 Ultimate Strength of As Received Screen

Sample Number	Direction of Weave	Ultimate Strength (lb_f)
1	Longitudinal (warp)	17.6
2	Longitudinal (warp)	18.7
3	Longitudinal (warp)	17.2
4	Transverse (shute longitudinal)	52.9
5	Transverse (shute longitudinal)	57.0
6	Transverse (shute longitudinal)	58.2
7	Diagonal	16.7
8	Diagonal	16.4
9	Diagonal	17.5

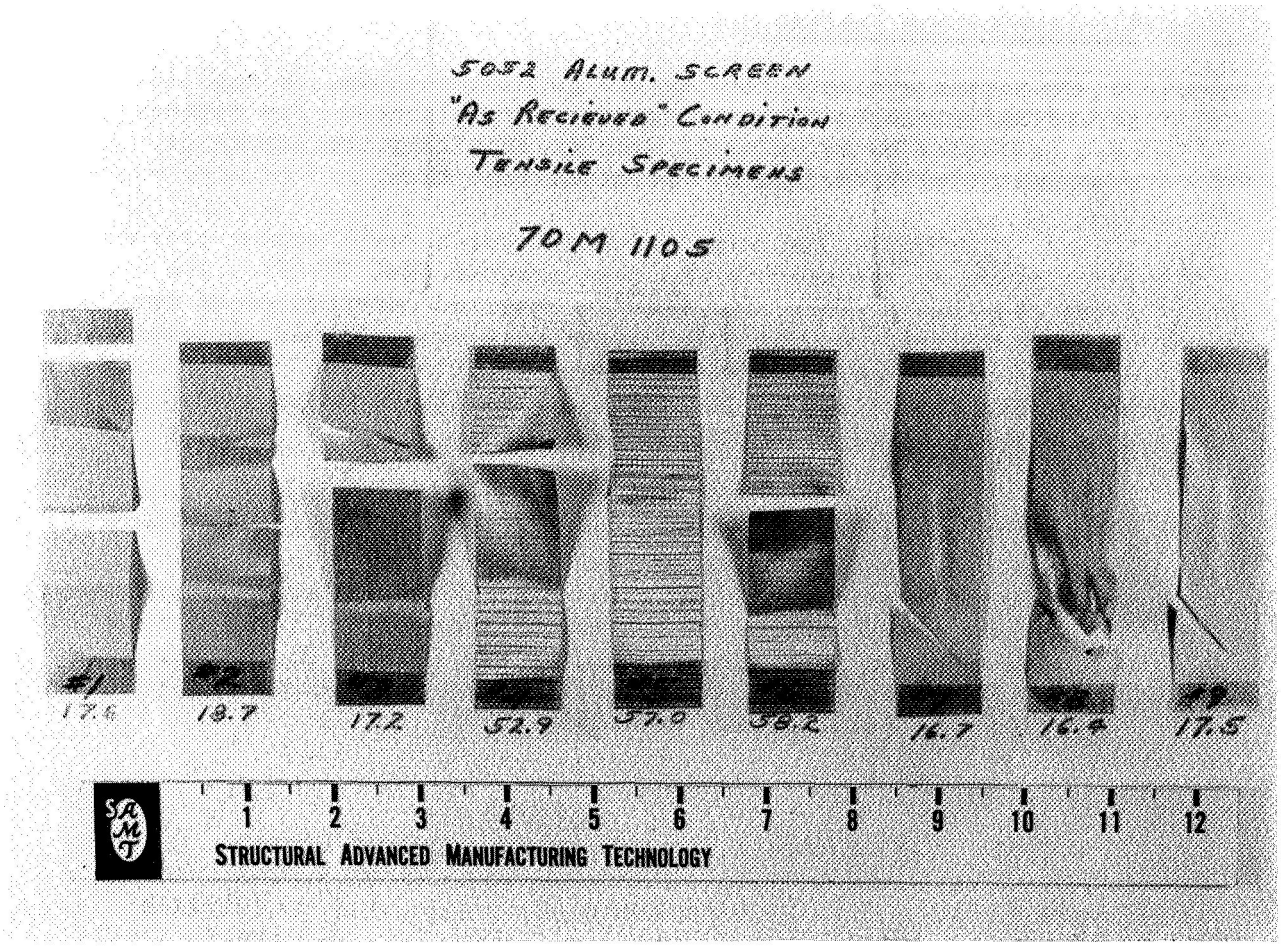

Figure IV-17 Tensile Test Specimens

Approximately 4-in. square sections of screen were pleated using a die. Seven pleats with a depth of 1/4 in., a pitch of 1/2 in., and a bend radius of 1/16 in. were formed. In the as received condition, the material does not retain the shape of the pleat. As can be seen from Figure IV-18, a wrinkled and rather flimsy liner section was formed.

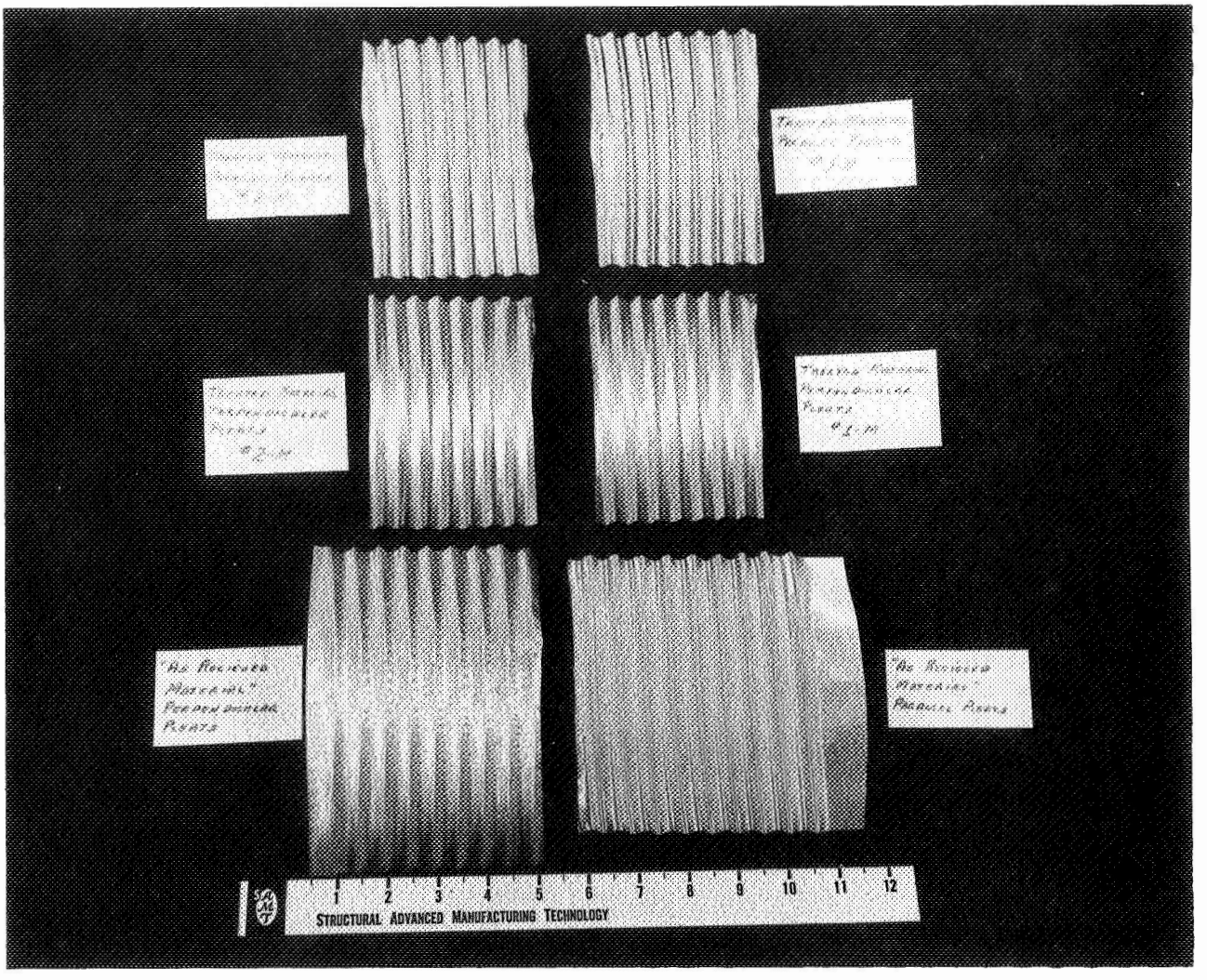

Figure IV-18 Pleated Aluminum Screen

After performing Martin Marietta's conditioning process, the properties of the screen were again measured. The absolute micron rating remained the same (16 microns). A 70% reduction in the ultimate strength occurred (Table IV-6), but the tensile strength of the screen is of secondary concern to the design. Since the liner contacts the tank wall and is rigidly attached at both ends, it does not experience any appreciable loads. A striking improvement in the formability of the screen is achieved by the conditioning process. The screen duplicates the shape and contour of the die exactly, as seen in Figure IV-18. The best rigidity is obtained with the pleats parallel to the warp wires.

Table IV-6 Ultimate Strength of Conditioned Screen

Sample Number	Direction of Weave	Ultimate Strength (lb_f)
1	Longitudinal	6.4
2	Longitudinal	6.1
3	Longitudinal	5.5
4	Transverse	17.4
5	Transverse	17.4
6	Transverse	17.9
7	Diagonal	9.6
8	Diagonal	7.8
9	Diagonal	8.2

Resistance welding of screen-to-screen was successful. A strong, narrow weld joint was produced, as seen in Figure IV-19. The strength of the weld joint was tested and found to be about 40% of the strength of the material (Table IV-7). Fracture of the joint occurred at the point the material met the weld area.

Table IV-7 Ultimate Strength of Resistance Welded Screen-to-Screen Joint

Sample Number	Direction of Weave	Ultimate Strength (lb_f)
1	Longitudinal	13.5
2	Longitudinal	14.6
3	Longitudinal	11.4
4	Transverse	33.7
5	Transverse	33.2
6	Transverse	32.0

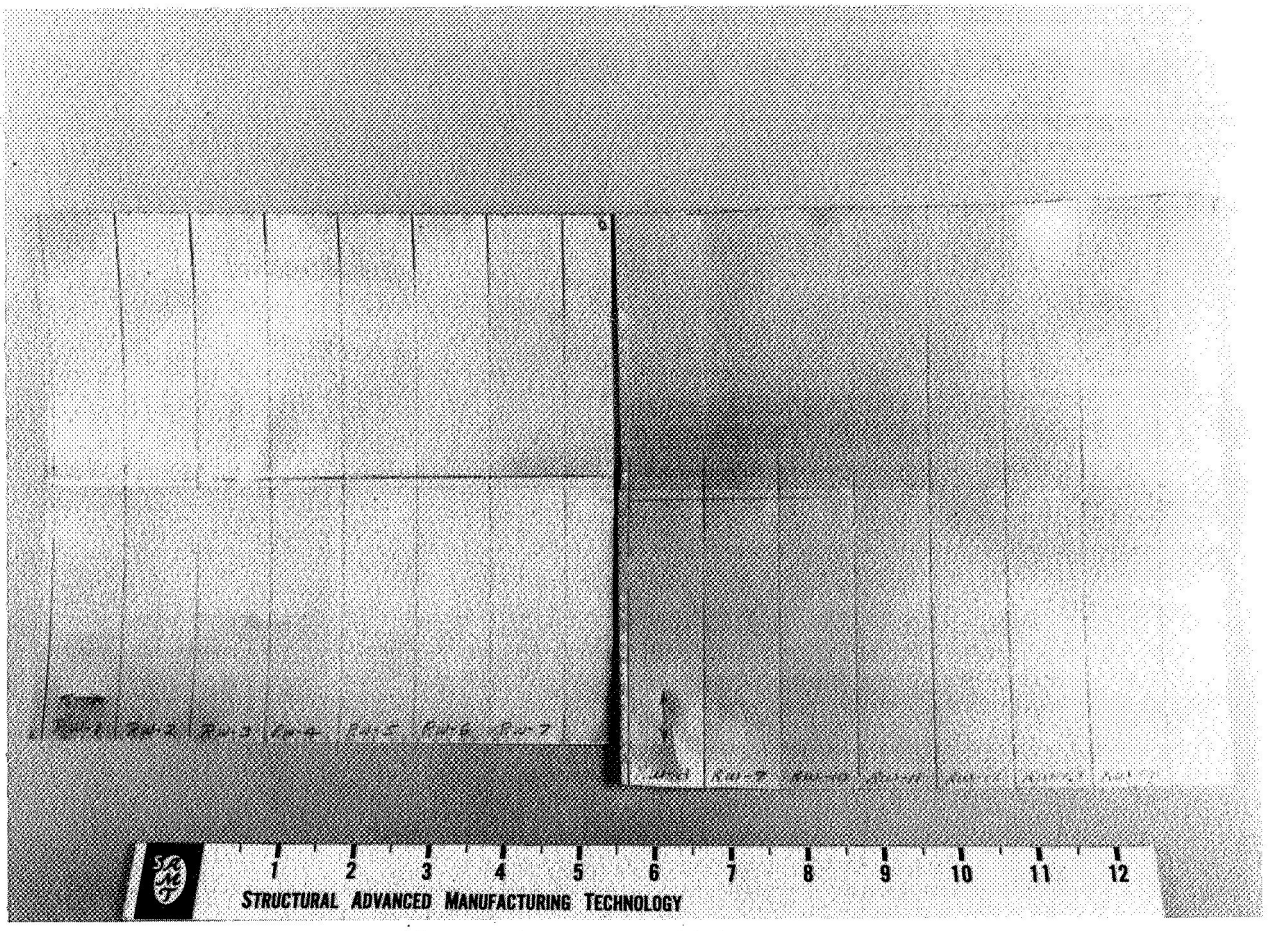

Figure IV-19 Resistance Welded Aluminum Screen

Screen-to-plate resistance welding was not successful. A high current is required when aluminum is welded because of its relatively low resistance. Problems arose because the conductivity of the plate was greater than the conductivity of the screen. With the high current, the pressure applied to the screen and the plate by the electrode must be carefully controlled or burning of the screen will occur. It was concluded that if higher pressures and current were used, the joint could be made; however, this does not appear to be a reliable means of joining screen-to-plate.

Fusion welding (tungsten-inert gas, TIG) of the screen-to-screen joint was found unacceptable, because the heat required to melt the metal cannot be applied to a small enough area. Heat is rapidly conducted by the fine wires, causing the screen to melt, and separate from the joint. A fusion welded screen-to-plate joint was made, but was of poor quality (Fig. IV-20). Again the screen was too easily melted and a continuous bead could not be maintained.

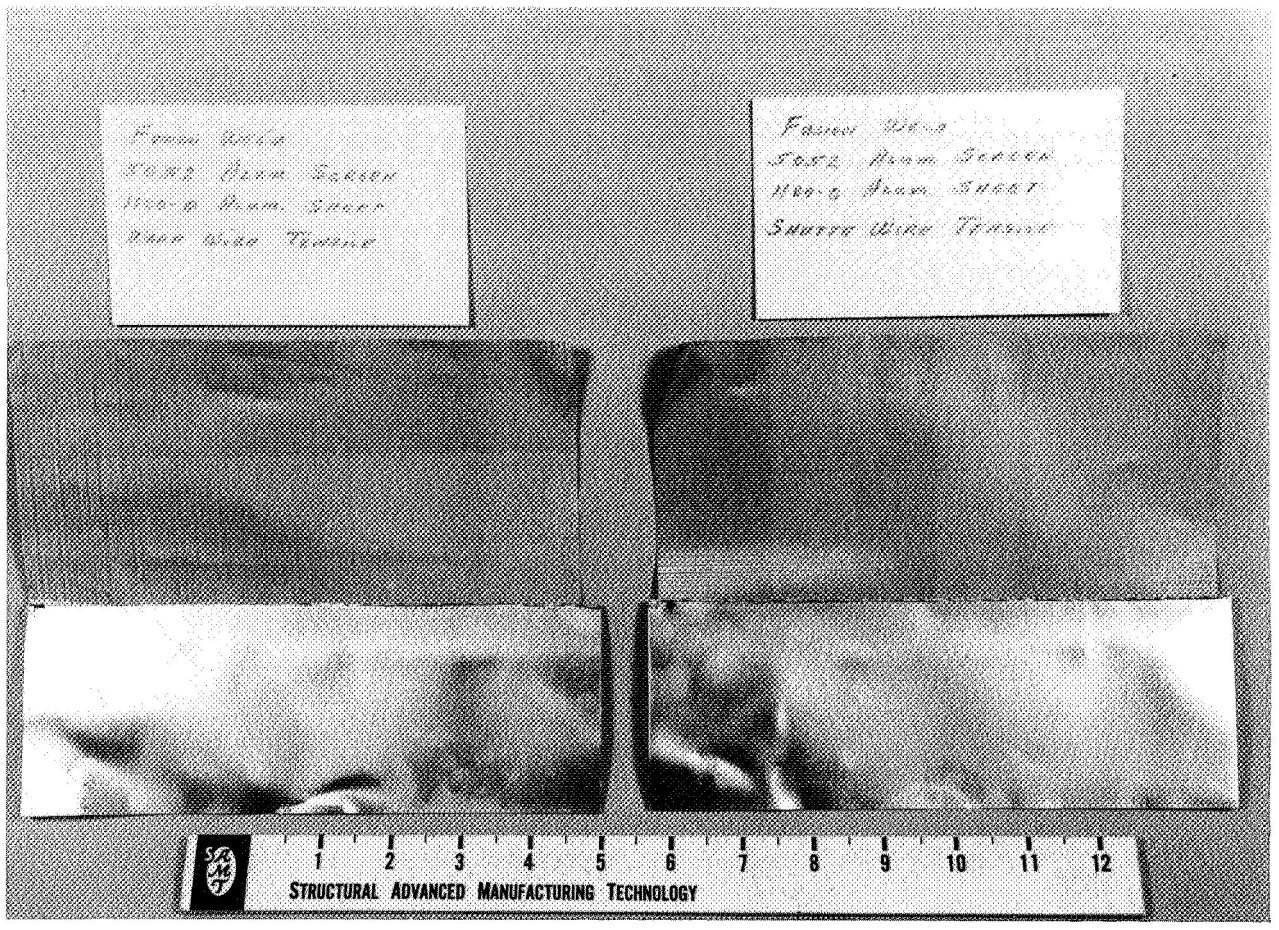

Figure IV-20 Fusion Welded Screen-to-Plate Joint

b. Titanium - Titanium screen is used to construct the traps for Missions A_2 and B. Only a small piece of the actual mesh size and material, which would be used in the Mission A_2 trap, could be obtained, because the vendors do not normally stock such screen. A coarser titanium screen is easily procured and was used to supplement testing. The actual screen is 180 x 180 mesh twilled weave with 0.0021-in. diameter wire. The coarser screen is 10 x 58 mesh with 0.019-in. diameter wire. Most of the fabrication and joining methods of interest were attempted. Bubble point tests and tensile tests were not considered, because of a lack of material (in one case) and too coarse a material (in the other). A qualitative evaluation of the techniques was possible.

Resistance welding of both screen-to-screen and screen-to-plate was successful using the coarse screen. To obtain a satisfactory joint, a high current and high electrode pressure were required. A 2 in. mandrel was used so that wires were not broken

by the pressure. As a result, a rather wide joint was produced. With the fine screen, pressure and current could be reduced to produce a narrow screen-to-screen joint.

Fusion welding (TIG) of screen-to-screen and screen-to-plate was accomplished using the coarse screen but a poor joint was produced. The openness of the mesh causes problems with the coarse titanium screen. As the weld progresses, variations result in the amount of material available to form the weld. It is expected that even the relatively fine 180 x 180 mesh screen will present this type of problem, though to a lesser (and possibly acceptable) degree.

While the coarse titanium screen could not be pleated, it was formed in order to determine the effect of the bend radius. A 130° bend with a radius 1.5 times the thickness (0.058 in.) was obtained without breaking wire. This is a much sharper bend than six times the thickness, as proposed in the designs.

D. OPERATIONAL DISCUSSION

1. Prelaunch

a. One-g Test - The 1-g test is accomplished by inverting the propellant tank and its surface tension device such that the tank outlet is oriented vertically upward. The tank is loaded so that the surface tension device is full of propellant prior to expulsion. The ullage is pressurized to flight pressure (or some lower level), the outlet is opened, and liquid is expelled from the tank until gas ingestion occurs. The liquid volume outflowed is measured to the gas ingestion point to check the predicted performance. Techniques for accomplishing the 1-g test and the results of some actual tests are documented in Ref IV-22.

A typical test apparatus for accomplishing the 1-g test is illustrated in Figure IV-21. The propellant trap is filled by pressurizing the receiver tank and flowing propellant through the pressurization line. The vent on the feed line is opened to allow complete filling of the test tank. Some gas might be trapped below the coverplate (with respect to the illustrated orientation) or within the reservoir but this will not affect the test. It merely changes the starting point of the expulsion. The tank is then pressurized and propellant is drained out of the bottom of the tank to expose the coverplate to the pressurant gas. The coverplate should be capable of retaining the propellant in this configuration.

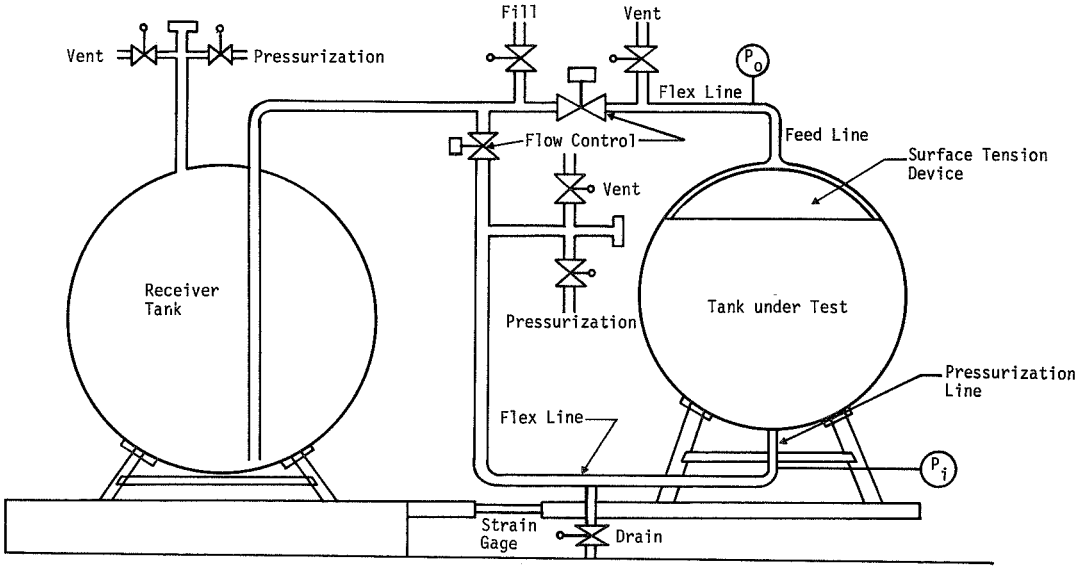

Figure IV-21 One-g Test Schematic

Outflow of the trap is accomplished by opening the flow control valve and allowing the propellant to flow from the trap to the receiver tank. One way of monitoring the liquid level is to measure the weight of the tank. A strain gage system on a cantilever beam has been used to measure the weight with good results (Ref IV-22). A recording of the tank weight by itself would provide sufficient information about the liquid level at gas ingestion. A flow meter and a sight glass on the feed line would better establish the flowrate and the presence of any gas bubbles. A differential pressure transducer, between the pressurant inlet and the feed line can also assist in determining the point of gas ingestion. Figure IV-22 represents the typical change in weight and pressure for a 1-g test (Ref IV-22).

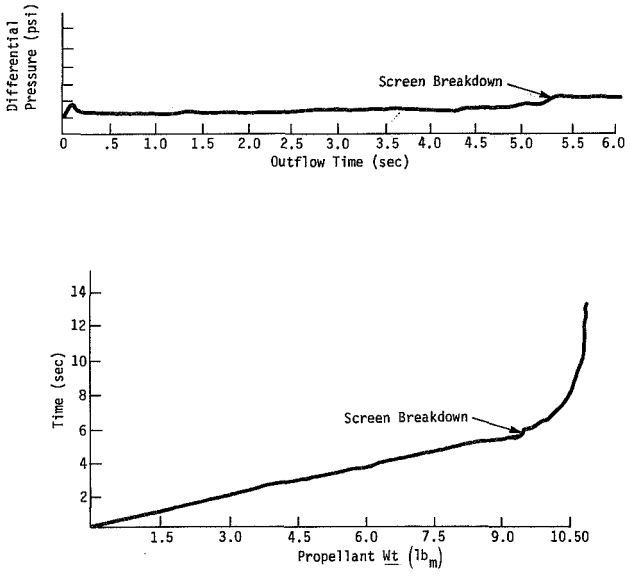

Figure IV-22 Pressure and Weight vs Time

The temperature of the propellant is controlled so that it will be within the range expected during flight. Tests with the propellant at the upper and lower temperature limits may be part of the qualification test. Since the MMH, N_2O_4, and nitrated hydrazine are used at temperatures near 500°R, thermal control presents no problem. The OF_2 and B_2H_6, on the other hand, stored at 250°R will require that some means of controlling the heat input into the test tank be used during test. A possible means for doing this would be to use the spacecraft's thermal control system and a vacuum chamber.

Using these techniques, the actual propellant could be expelled from the trap. By carefully controlling the pressurant supply and the flow control valve, the actual flow conditions that will occur in flight can be duplicated. Once the point at which gas ingestion occurs has been detected, the amount of propellant remaining in the trap could be determined from the instrumentation. The height of the liquid remaining should be equal to or less than the height determined by analytical methods.

b. Loading and Handling - The major impact that prelaunch procedures have on the 1-g test design concept is in the area of gas entrapment. If gas is trapped within either the reservoir or annulus during prelaunch operations, difficulties in completing the mission could arise. If gas is trapped within the annulus, gas will tend to be ingested during expulsion. This small volume of gas may cause some combustion instabilities but would probably not be catastrophic. If gas is trapped within the reservoir, there may not be enough propellant available to feed the annulus and satisfy all the engine burns. The degree of these difficulties depends upon the amount of gas trapped, the particular engine, particular burn, mission objective, etc. The following, therefore, is a discussion of the impact on the trap design of loading techniques and handling procedures with regard to gas entrapment.

1) Loading - Two possible loading techniques may be used; one is vented loading, the other, vacuum loading.

a) Vented Loading - A simple vented loading procedure is accomplished as follows. Consider the tank to be in the upright position and initially filled with an inert gas blanket. Liquid propellant is loaded into the tank through the feed line while the inert gas is vented through the pressurization port. Loading continues until the tank is filled to the proper level as determined either by tank weight or a gaging system (Ref IV-20).

Because of capillary pumping or wicking, screen material can fill with liquid. Consider the effect of wicking on the annulus of the trap during loading. Liquid will wick into the screen so that it will be wetted to a height above the rising liquid level. When the wicking reaches the coverplate, gas will be trapped within the annulus between the tank wall and the wetted concentric liner (Fig. IV-23a). The ability of screen material to wick depends upon the type of weave. Dutch twill screen is subject to wicking, while square weave and twill weave screen will not wick appreciably under 1 g (Ref IV-3). Therefore, the severity of gas entrapment within the annulus during vented loading is directly dependent upon the type of screen material employed for the annulus. For Mission A_1, the annulus screen material is Dutch twill so this trap will be subject to gas entrapment. The traps for Missions A_2 and B use a twill weave screen so the amount of gas entrapped, if any, will be small.

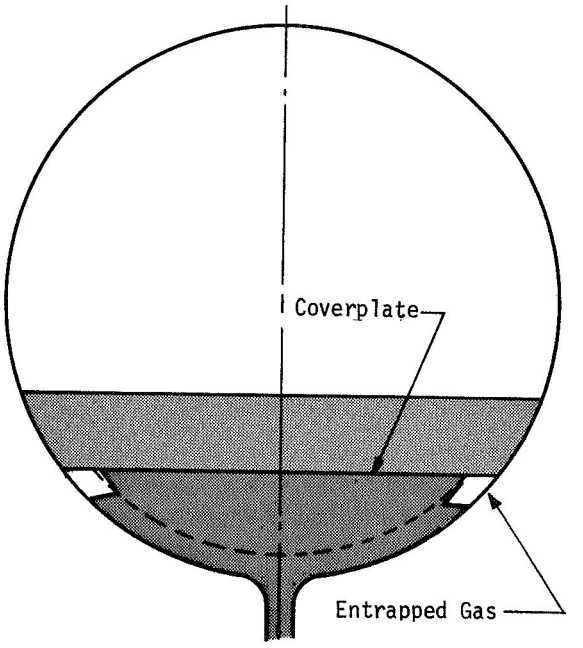

a) Entrapment within Annulus

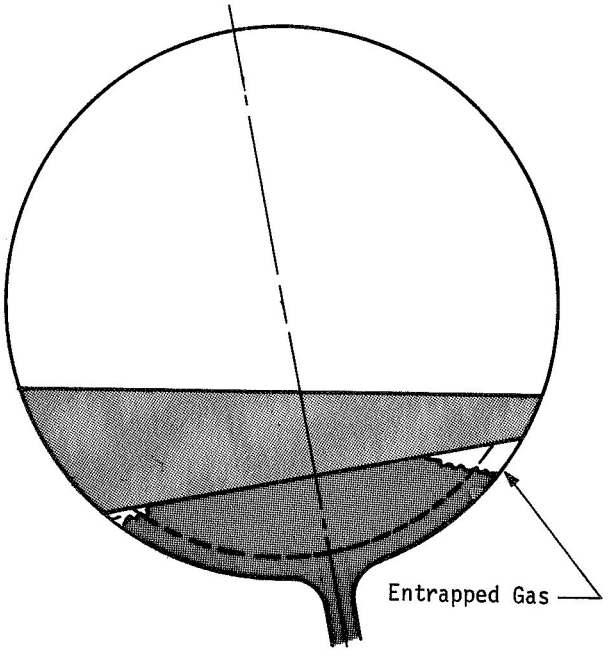

b) Entrapment within Reservoir

Figure IV-23 Gas Entrapment during Vented Loading

Inert gas may also be entrapped within the trap reservoir during the vented tank loading, because the coverplate is also subject to wicking (Ref IV-3). If propellant, during filling, contacts the coverplate unevenly, gas will be entrapped since a gas/liquid interface will form ahead of the ascending liquid level and block an escape route for the inert gas occupying the reservoir area. Uneven contacting of the coverplate by the propellant can occur if filling rates are such as to create sloshing or if the tank is at a slight tilt angle during loading as shown in Figure IV-23b. It should be noted, however, that severe gas entrapment problems within the reservoir seem fairly remote, because of the use of a flat coverplate (a conical coverplate would present definite gas entrapment problems). If the tank is filled at a rate faster than the wicking rate of the screen material, no gas will be entrapped. However, for practical filling rates which would not produce slosh, wicking of the screen will always precede the liquid level.

The size of the inert gas bubbles trapped within the annulus or reservoir will be greatly reduced upon tank pressurization. For all the missions, the tank is pressurized to 350 psia, which reduces the volume of the gas bubble by a factor of 0.05. The possibility exists,

therefore, that after pressurization, gas entrapment problems may be eliminated (size of gas bubbles in annulus reduced so as to not affect engine performance if ingested and amount of space occupied in reservoir by inert gas reduced to an insignificant amount). However, for Mission B, if the reduced inert gas bubbles are not dissolved by the propellant or expelled from the annulus or reservoir, they will increase in size throughout the mission since the tank pressure will decrease (blowdown pressurization system). This consideration does not exist for Missions A_1 and A_2 because a regulator maintains a relatively constant pressure within the tank.

To reduce the gas entrapment due to vented propellant loading, four possible solutions or combinations thereof could be incorporated. The coverplate could be designed so that it will be unstable due to the boost accelerations. By using this approach any entrapped gas would be purged from the trap; however, the 1-g test requirement prohibits this type of design. The coverplate pore sizes required for the 1-g test will be stable during boost and the gas could not be purged.

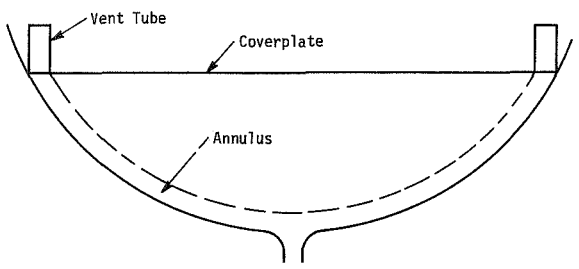

Figure IV-24 Propellant Trap with Vent Tubes

Another approach would be to add vent tubes to the annulus of the trap as shown in Figure IV-24 (Ref IV-23). The top of the tube would be covered with the same screen material used in the coverplate so the tubes would retain the propellant during the 1-g test. During loading, the tubes would provide a passage through which gas could be vented, eliminating the problem caused by the wicking screen. The major drawbacks of the design are that it further complicates the original design, adds some weight, and slightly decreases expulsion efficiency (propellant held in the vent tubes is wasted). Also, if the foraminous caps of the vent tubes become wetted prematurely because of sloshing during loading, gas may still be entrapped. During the mission, if the screen on the tubes should dry out, liquid would be lost from the trap.

A third way in which the annulus may be cleared of entrapped inert gas is to flush the annulus after loading, either before or after pressurization. A flushing procedure would consist of first rotating the tank 180°, so that the outflow port is vertically upward. Any gas bubbles in the annulus would then rise to the outflow port. Some propellant is then expelled from the tank, clearing the annulus of gas. Any gas within the reservoir, however, will not be cleared. The rotation of the tank, back to the upright position will also present gas entrapment problems (see Handling Impacts, below). Also, this technique could only be employed if the tanks are loaded before spacecraft assembly and encapsulation because of the difficulty of tank rotation during on-pad loading.

A possible way of avoiding gas entrapment within the annulus, is to load the tanks in the inverted position. This would eliminate gas from being trapped within the annulus but would now cause gas entrapment within the reservoir if the concentric liner screen material is subject to wicking as in Mission A_1. By inverted filling, the gas entrapment problem in the annulus is now shifted to one within the reservoir area.

b) Vacuum Loading - For this method, the tanks are evacuated before the liquid propellant is loaded. Any gas entrapped in the screen device would be propellant vapor. When the tank is pressurized the gas will completely condense, eliminating all entrapped gas. Compared to vented loading this is a much easier way of eliminating trapped gas. The propellant loading system would require a vacuum pump in order to accomplish this type of loading.

2) Handling Impacts - Two different approaches for loading and handling of the spacecraft (independent of the actual loading procedure) are possible for the three missions. These are on-pad loading of the tanks after assembly and encapsulation of the spacecraft, or loading prior to assembly and encapsulation followed by transport and mating of the spacecraft to the booster. Each has its advantages, but the latter would have the most impact on the trap because the tanks must be moved after loading. Based on the loading and handling procedures used for the Mariner and Surveyor spacecrafts and studies of prelaunch operations for this type of spacecraft (Ref IV-20), loading before encapsulation would be the preferred approach for these missions. Therefore, the following is a discussion of the impact of that mode upon the design of the propellant trap.

Entrapment of gas in the annulus or reservoir of the trap due to the rotation of the tanks is the major impact of loading prior to encapsulation. Rotation may be necessary during the assembly, system checkout, transportation to the launch pad, or mating of the spacecraft to the booster. If the Mission B propellant tank (loaded to 50% ullage) is rotated more than 53° from the vertical position, ullage gas will contact the coverplate. Only a small portion of the coverplate needs to be exposed to gas before it will break down due to the hydrostatic head. The 53° tilt is a practical limit beyond which the tank cannot be rotated. With the initial 10% ullage for Missions A_1 and A_2, these tanks could both be rotated 88° before gas would contact the coverplate. This angle would be used as the limit for the tank rotation.

Considering the loading procedures discussed earlier (in which the tank is inverted), rotating the tanks to their upright position would cause breakdown of the coverplate as discussed above, for all three missions; therefore, the flushing schemes are undesirable.

If a larger tilt angle is desired, the tanks could be completely filled for the period of time that tilting of the tank is required, and then the excess propellant could be unloaded. The thermal control system may be capable of maintaining a constant propellant temperature so that expansion of the propellant would not be a problem. If expansion is a problem, an accumulator to absorb the volume changes would be required. Unloading of the excess would probably have to take place after the spacecraft was mated with the booster. An accurate means of unloading the spacecraft in this configuration would be required. This approach would negate the primary advantage of loading before mating, i.e., obtaining a very precise propellant load (Ref IV-20).

A better solution, applicable only if the tanks are vacuum loaded, is to rely upon tank pressurization to condense all the vapor bubbles trapped in the reservoir and annulus. This would mean delaying pressurization, either partial or full, until all handling procedures have ceased.

Based on the considerations of both loading and handling, a vacuum loading procedure is recommended. This technique would eliminate all gas entrapment problems when pressurization is accomplished after handling is complete. Gas entrapment due to the Dutch twill screen used for Mission A_1 would not present any problems and a 180° rotation of the tank would be allowable. If the allowable tilt angles are not exceeded, vented loading could be used for Missions A_2 and B. The twill weave screen would not cause any problems if the propellant is loaded without producing any sloshing.

2. Boost Phase

During the boost phase of the mission, the propellant trap is completely full and covered with propellant. The device does not have any function to perform in this phase of the mission. One concern is propellant slosh induced by the acceleration and vibration of the booster. The question is whether the slosh could cause gas to be ingested into the trap. As part of this analysis, any slosh that could be induced by the wind (while the booster is on the launch pad) was also considered.

When a partially filled propellant tank is excited longitudinally (Ref IV-24), or laterally (Ref IV-25), either symmetrical or asymmetrical liquid surface displacement configurations can result (Fig. IV-25). Since asymmetric displacement can produce higher slosh amplitudes than symmetric surface displacement (Ref IV-26) it was given primary consideration. The asymmetric configuration can occur due to longitudinal tank excitation (Ref IV-24), but the possibility of this occurring during boost is remote. It would also be difficult to achieve on the pad, since wind loads are usually responsible only for lateral excitations. Therefore, only asymmetric sloshing due to lateral excitation is of concern. This type of slosh could reach high amplitudes if the excitation frequency is near the natural frequency of the propellant.

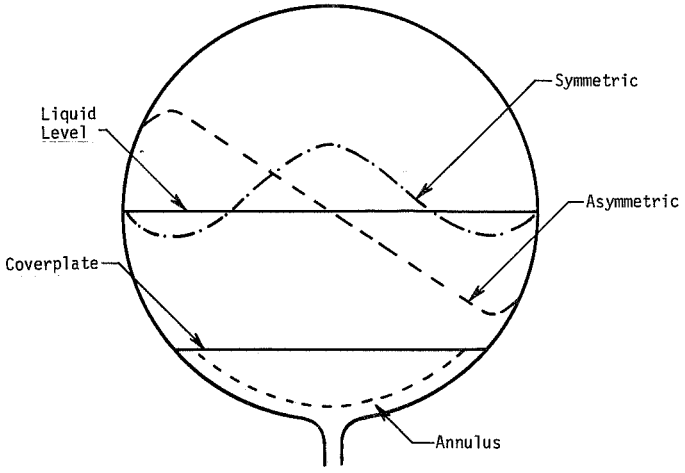

Figure IV-25 Liquid Surface Displacement in a Spherical Tank

The natural frequency parameter $\left(\omega_N^2 \frac{D}{a}\right)$ for different propellant levels in a spherical tank is shown in Figure IV-26 (Ref IV-27). From these curves, Figure IV-27 was generated. The first mode natural frequencies needed for the excitation of large amplitude asymmetric sloshing during ground hold for Missions A_1, A_2, and B and for the Mission A_1 boost phase are shown. The curves for the boost phase of Missions A_2 and B are parallel to the Mission A_1 curve with each starting at the ground hold value. Only the first mode frequencies were calculated since these give the largest

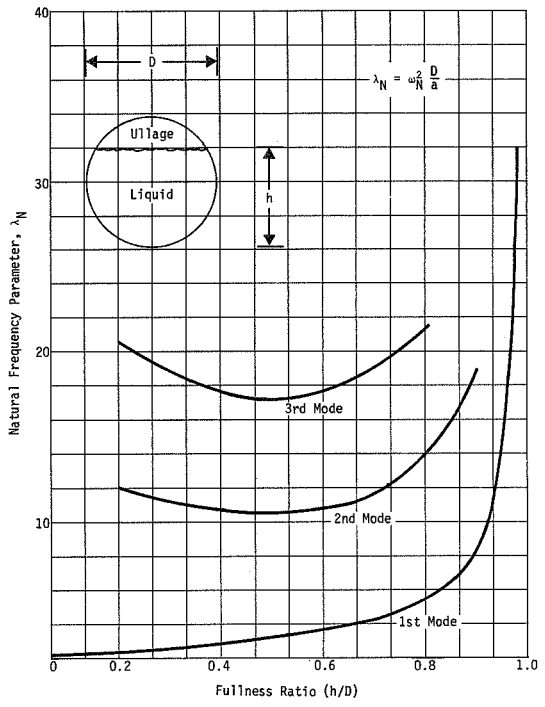

Figure IV-26 Natural Frequency Parameter Variation with Depth of Propellant in Spherical Tank

amplitudes (Ref IV-26). The range of natural frequencies is between 1 and 2.5 cycles per second. Based on Viking lander slosh testing, wind-induced excitation frequencies can be as high as 1.3 cycles per second (Ref IV-28). Also, during boost, low lateral excitation frequencies would probably exist within that range. Therefore, high amplitude sloshing may occur within the propellant tanks for all three missions both during ground hold and boost phase.

Even though high amplitude sloshing may be initiated, the size of the ullage must be considered. Since the ullage is 10% for Missions A_1 and A_2, the sloshing would be confined to the upper half of the tank and could not affect the trap. For Mission B, with a 50% ullage, the possibility of the slosh affecting the trap seems more likely, but there are two factors which reduce the possibility.

The first factor is that a spherical tank tends to dissipate high amplitude sloshing, because the waves break as they flow up the walls of the tank (Ref IV-26). The second factor is that the coverplate damps the effect of the slosh. Before gas ingestion can occur, the amplitude of the slosh must be large enough to have gas in contact with the coverplate. Then, the liquid inside the trap must have sufficient velocity so that it will flow through the coverplate and allow gas to be ingested. The coverplate of the Mission B trap (double perforated plate with twilled weave screen on the upper plate) has very good damping characteristics (Ref IV-3). It is unlikely that any gas would be ingested when the inherent damping of the tank and the coverplate is considered. Higher amplitude slosh than that generated by wind loads or boost vibration would be required to cause gas ingestion.

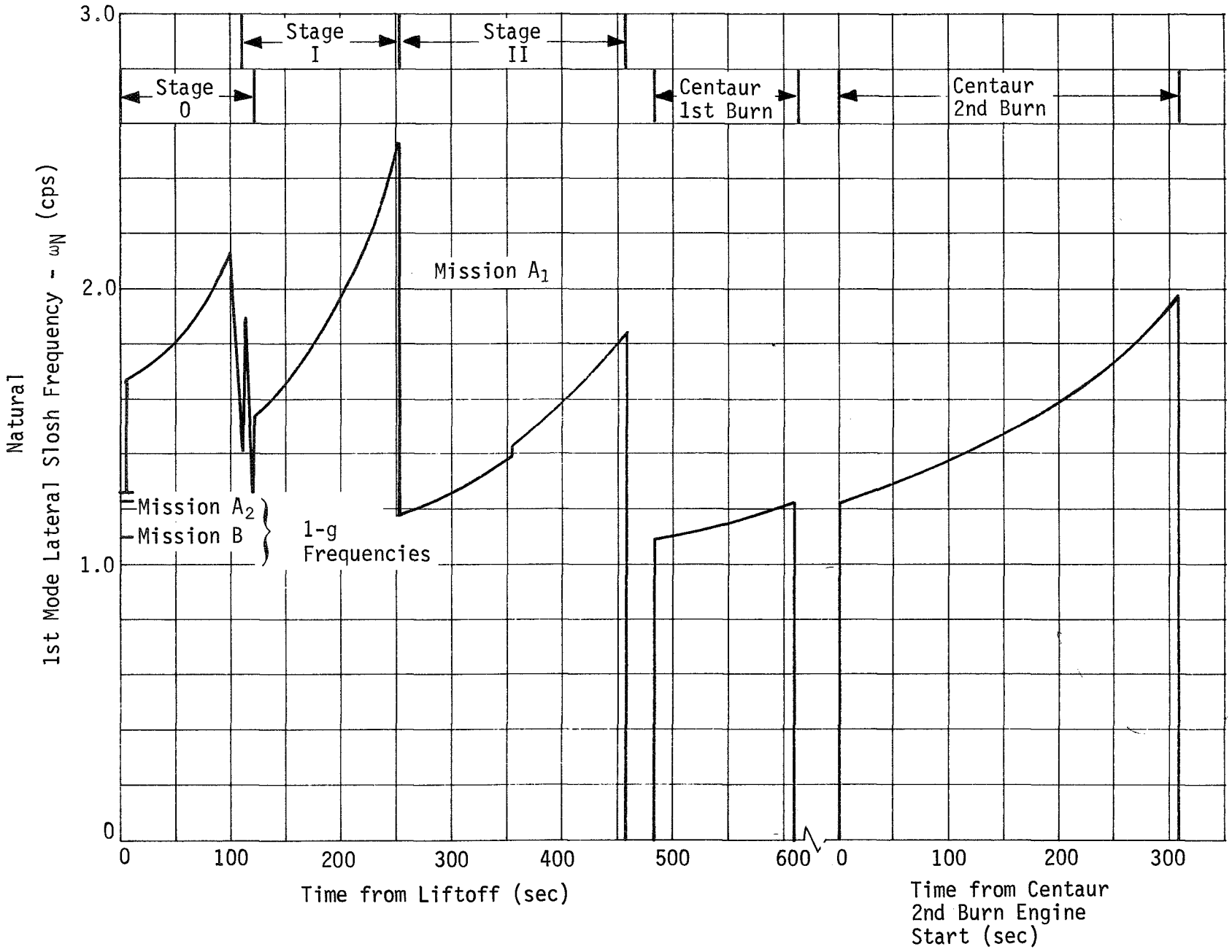

Figure IV-27 Lateral Slosh Frequency Variation with Acceleration

3. Low g

a. Thermal Analysis - Before finalizing the configuration of the 1-g test design, an analysis was conducted to determine what effect the thermal environments of the three missions have on the propellant trap. The ability of a propellant trap to retain liquid can be degraded by variations in the thermal environment. Propellant can be lost from the trap if vaporization, thermal expansion, or growth of a gas bubble occurs inside the trap. Therefore, each mission was considered in order to determine all the factors that could cause the thermal environment to vary. Since the thermal data for these missions are presently either preliminary or not available, the analysis identified the potential problem areas and yielded a tentative assessment of these problems.

Vaporization will occur whenever the partial pressure of the propellant vapor in the ullage is less than the saturation pressure of the liquid. Heat from the space environment will increase the temperature of the liquid, and vaporization will occur because of the increase in saturation pressure. Another source of heat is the engine of the spacecraft. During and subsequent to each operation of the engine, heat will be transferred from the engine to the propellant tanks. While the propellant is being heated by this source, vaporization will occur. The increase in the gas volume due to the consumption of propellant during a burn and the addition of helium pressurant during the outflow will also disturb the equilibrium.

Vaporization occurs at the gas/liquid interface. For a propellant trap, an interface will always exist at the coverplate because it must remain wet. Usually there will be a gas bubble inside the trap, which is another gas/liquid interface. When vaporization occurs at the coverplate, propellant vapor leaves the coverplate and enters the ullage. To keep pressure uniform throughout the tank, a volume of either gas or liquid, equal to the volume of liquid vaporized, must enter the trap. Unless liquid outside the trap is in contact with the coverplate, gas will enter the trap. On a much smaller scale, vaporization will occur at the interface of the trapped gas bubble to establish equilibrium. In this case, the size of the gas bubble will increase by the volume of liquid vaporized.

The liquid will be cooled by the vaporization, because the heat of vaporization must be supplied by the liquid. If the tank wall opposite the trap is cooler, some of the vaporized propellant will condense, heating up that wall. A complex process, which reestablishes the equilibrium between the liquid and the gas in the tanks, takes place whenever this equilibrium is disturbed.

Thermal expansion is a result of increasing the temperature of the liquid and thereby reducing its density. A wetted coverplate provides a barrier to gas, but it does not restrict the flow of liquid. As long as the liquid in the trap is in contact with the coverplate, which is usually the case under low g, it will be forced out of the trap in preference to any gas located in the trap. Therefore, the increase in liquid volume due to thermal expansion will be lost from the trap. If the liquid was then cooled, the contraction would draw liquid into the trap if it was in contact with the coverplate, otherwise gas would be ingested.

The growth of the gas bubble has already been a consideration in the above two effects; both resulted in an increase in the size of the bubble. Some additional factors that would cause an increase in the bubble volume must also be considered. If the liquid in the trap could boil, the resulting vapor would be added to the vapor bubble. The increase in temperature, required to boil these propellants at the tank pressure of 350 psia, would be impossible to attain. In order to boil, the vapor pressure must equal the tank pressure. Table IV-8 lists the saturation temperatures necessary to obtain a vapor pressure of 350 psia.

Table IV-8 Saturation Temperatures

Mission	Propellant	Nominal Temperature (°R)	Saturation Temperature at 350 psia (°R)
A_1	OF_2	250	340
	B_2H_6	250	480
A_2	N_2O_4	500	683
	MMH	500	900

A value for the saturation temperature of nitrated hydrazine at 350 psia was not available, but at 10 psia it is 690°R.

If the pressure inside the gas bubble in the trap could become greater than the ullage pressure, liquid would be forced out of the trap as the bubble expanded. A nonuniform addition of heat, at a high rate could produce this effect. Engine heat soakback is the only heat addition which is not relatively uniform; but, since it takes hours to reach equilibrium, its rate is low. Under these conditions the pressure in the tank would remain uniform and no pressure differentials would be created.

The volume of the gas bubble in the trap would be changed by the increase in the tank temperature and pressure. Increasing the temperature increases the volume and the increase in pressure would decrease the volume. The total effect would be negligible since both are of the same order of magnitude.

By considering each of the above effects, it has been established that liquid can be lost due to two effects, vaporization and thermal expansion. The volume of gas that could be ingested into the trap is equal to the volume of liquid that is lost due to these two effects. Since none of the propellant traps are refillable, due to the 1-g test requirement, the total loss of liquid from the trap during the entire mission must be evaluated. For Missions A_1 and A_2, the period prior to the insertion burn does not have to be considered because the interface will always be in contact with the coverplate. No liquid can be lost from the trap due to thermal effects during that period. The entire mission must be considered for Mission B.

The following paragraphs discuss the anticipated thermal environment for Missions A_1, A_2, and B. For each mission, the loss of propellant from the trap is assessed considering both the thermal environment and the tank thermal conditions. Vaporization and thermal expansion of each propellant was calculated based on the preliminary thermal data available.

1) Mission A_1 - This mission is characterized by propellants (B_2H_6 and OF_2) that are considered to be mild cryogens. Also, this mission is thermally affected by a long burn period (orbit insertion) during which 95% of the propellants are consumed. For these propellants and this mission, preliminary thermal control studies specify some form of insulation on both propellant tanks. Because of this insulation requirement, the environmental heating in space will be reduced.

An analysis of tank thermodynamics and heat transfer, for the purposes of the Task II Pressurization Studies, is presented in Volume I. Based on this analysis, it was found that 6.3 lb_m of OF_2 would be vaporized during the period from the end of the insertion burn to the end of the mission. This vaporization would result from environmental heating and reestablishment of equilibrium between the gas and liquid following an engine burn. Because of its low vapor pressure, the amount of B_2H_6 vaporized during the same period would be negligible. Any vaporization occurring prior to the insertion burn will not cause gas ingestion into the trap because the bulk liquid will be in contact with the coverplate.

A thermal analysis was conducted to assess the effects of engine heat soakback for Mission A_1. For this mission, engine heat soakback is significant only following the long-duration orbit insertion burn. The analysis calculated the temperature of the propellant as a function of time considering conduction through the feed line. This is the primary mode of heat transfer because the tank wall is insulated. A curve (supplied by JPL) of the engine head temperature as a function of time was used as the heat source (Fig. IV-28). The engine head included the bipropellant engine valves and the upper part of the thrust chamber. However, it should be noted that this data is preliminary and only an estimate for a similar type engine. Aluminum feed lines were considered because the tanks are constructed of aluminum; a feed line length of five feet was assumed. The propellant node included the heat capacities of the propellant, screen trap, and adjacent tank wall. Only 3.8% of the propellant loaded remained in the tank at this time. Results of the analysis showed that a 5° temperature rise in the propellant occurred over a 30 minute period following engine shutdown. This analysis is conservative in that the heat capacity of the propellant in the feed line and the heat of vaporization which would be absorbed by the vaporizing propellant were neglected. For the OF_2, a 5° temperature rise in propellant temperature vaporizes approximately 0.6 lb_m.

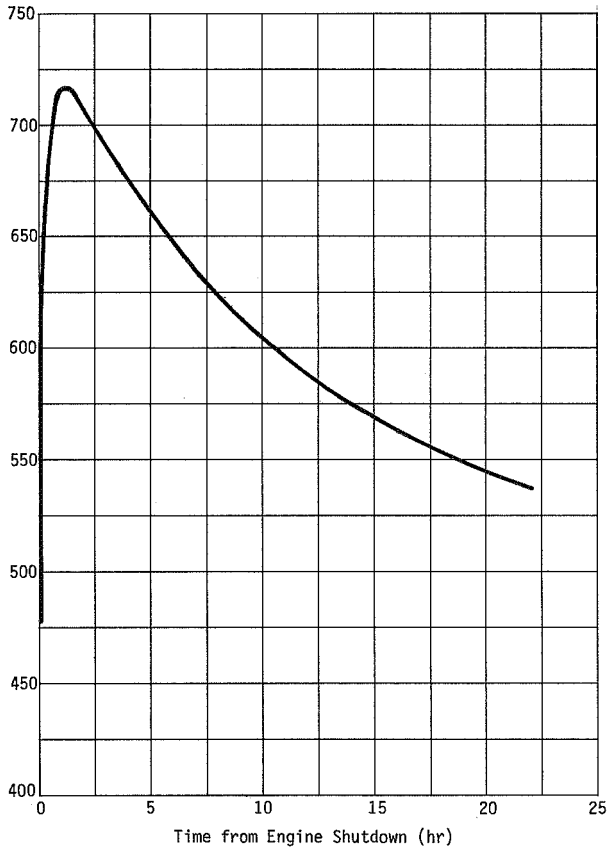

Figure IV-28 Temperature History of Engine Head-End after Engine Operation

According to the pressurization study, the OF_2 temperature would increase 5° and the B_2H_6 temperature would increase 2° due to environmental heating during the period between the end of the insertion burn and the end of the mission. Thermal expansion, due to environmental heating and engine heat soakback, would force 0.8 lb_m of liquid OF_2 out of its trap. For the B_2H_6 propellant, vaporization and thermal expansion are negligible, because of its low vapor pressure and small change in density with temperature.

2) Mission A_2 - This mission is characterized by propellants (N_2O_4 and MMH) that have operating temperatures at approximately 500°R. The thermal control system must provide heat to prevent the oxidizer from freezing. For the purposes of the pressurization analysis it was assumed that the thermal control system maintains the propellant at a relatively constant temperature and there would be no environmental heating.

The reestablishment of equilibrium between the gas and liquid following the engine burns would cause the vaporization of 0.9 lb_m of N_2O_4 during the period of time between the end of insertion burn and the end of the mission. Due to the low vapor pressure of MMH at temperatures near 500°R, vaporization in the fuel tank during this same period would be negligible.

The results of an engine heat soakback analysis conducted by JPL for the Viking Orbiter were assumed to be a good estimate of the heat soakback for Mission A_2 because of the similarities in propellants, engine size, and burn profiles. The data supplied by JPL were in the form of temperature histories at the outlet flange and bottom dome of the propellant tanks. The analysis showed that the only burn that resulted in a significant temperature rise was the orbit insertion burn. This burn period produced a 60° temperature rise at the outlet flange and bottom tank dome within 100 minutes of the completion of the insertion burn. This analysis is considered to be "worst-case" since it did not consider the heat capacity of the propellants nor the heat of vaporization absorbed by the vaporizing liquid. The heat transfer considered was primarily radiation between engine and tanks. Since these data are very conservative, the analysis was extended to approximate the temperature rise by including the heat capacity of the propellants. The temperature rise was obtained by the following:

$$\left[\left(mc_p\right)_{wall} + \left(mc_p\right)_{liquid}\right] \Delta T = \left(mc_p\right)_{wall} \times 60°$$

where m_{liquid} is the mass of liquid in the trap, and m_{wall} is one half of the total tank mass. For this assumed heat balance, the temperature rise was calculated to be 6.8°. This temperature rise, in turn, produced 0.6 lb_m of N_2O_4 vaporization.

A 6.8° temperature rise will not produce any measurable thermal expansion of the N_2O_4 or the MMH. The vapor pressure of MMH at these temperatures is less than 1 psia so that the vaporization is negligible.

3) Mission B - This mission is characterized by a monopropellant (nitrated hydrazine) system operating at approximately 500°R. Unlike Missions A_1 and A_2, this mission does not have one long burn where engine heat soakback effects are significant. Thermal data in any form for this mission are not available. An environmental control system must supply heat to the tank to prevent the propellant from freezing; therefore, environmental heating is not a consideration for this mission.

The assessment of engine heat soakback effects is difficult since data does not exist. However, since nitrated hydrazine has a very low vapor pressure at the operating temperature ranges and will behave in a manner similar to MMH, the results for MMH from Mission A_2 can be extrapolated. The qualitative assessment would indicate negligible effects of engine heat soakback on the acquisition device.

4) Summary - The size of the propellant trap was selected to compensate for the thermal effects. By keeping as much propellant as possible in the vicinity of the outlet, a heat sink that reduces the effect of engine heat soakback is provided. At the same time, a surplus of propellant is provided so that the loss of some of the liquid from the trap is permissible.

Table IV-9 is a summary of the results of the thermal analysis. In the right column, the amount of surplus liquid that will be in the trap is listed. The performance of the trap is evaluated on the basis of how much of the surplus is lost due to the thermal effects. If the amount of liquid lost exceeds the surplus, there will not be enough propellant to start the engine and settle the propellants for all of the burns.

Table IV-9 Results of Thermal Analysis

Mission	Pounds of Propellants Lost from Trap (lb_m)			Surplus Propellant in Trap (lb_m)
	Environmental Heating and/or Return to Equilibrium	Engine Heat Soakback	Thermal Expansion	
A_1				
OF_2	6.3	0.6	0.8	13.45
B_2H_6	N*	N	N	4.48
A_2				
N_2O_4	0.9	0.6	N	21.83
MMH	N	N	N	14.07
B				
Nitrated Hydrazine	N	N	N	2.40

*None or Negligible

Only the two oxidizer tanks are affected to any extent by the thermal environment. According to this analysis, 7.7 lb_m of OF_2 and 1.5 lb_m of N_2O_4 would be lost from their traps. Both of these losses are much less than the surplus available in the trap, which creates an adequate margin of safety for every tank.

Based on this analysis, it appears that the thermal environment would never be a problem to the propellant trap for this type of mission and these propellants. Nevertheless, a propellant trap is sensitive to the thermal environment. As more detail becomes available concerning the anticipated thermal environment, the evaluation of its effect on the trap can be refined.

One effect, which could have a significant impact, is thermal cycling. If cyclic variations of the liquid temperature on the order of a few degrees could occur, the liquid would expand and contract in phase with these cycles. As the liquid expands, liquid would be forced out of the trap. If liquid were in contact with the coverplate, liquid would be returned to the trap during the contraction; if liquid were not in contact, gas would be ingested. Even if the volume change that occurred each cycle was small, the effect could be cumulative. For a large number of cycles, liquid would be pumped out of the trap due to this phenomena. If some liquid were kept in contact with the coverplate, this effect would be reduced to just a flow of liquid in and out of the trap. Techniques used in the following section for the low-g device could be used with the trap to provide a volume of liquid at the coverplate. Figure IV-29 shows one way this could be done. The fins are added on top of the existing coverplate. Under low g, liquid will collect in the sharp corners formed by the fin and the tank wall.

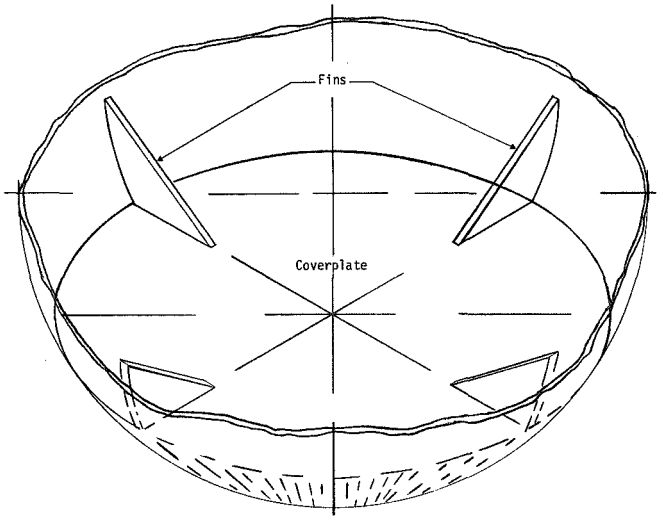

Figure IV-29 Fins Added to Coverplate

If the trap could be refilled during the engine burns, some of the effect of the thermal environment could be overcome. All the liquid would be returned to the trap during the burns. Then the concern would be the amount of liquid that could be lost in the period of time between any two burns, rather than how much is lost during the entire mission.

b. Mission Profile

1) Missions A_1 and A_2 - In the baseline missions, the duration of the midcourse correction and orbital trim burns is the maximum anticipated duration. An actual correction burn could range anywhere between the minimum impulse bit, to the impulse specified for that burn in the baseline mission. The minimum impulse bit is the shortest duration burn that can be accomplished by the engine in conjunction with the guidance and control system. The minimum impulse bit of 400 lb_f-sec for these missions results in a 0.4-second duration burn for Mission A_1 and a 1.33-second burn for Mission A_2.

With respect to the trap, that portion of the mission which is of the most concern is the period between the end of the insertion burn and the end of the mission. The design approach was to retain all the propellant remaining after the insertion burn in the trap. Of the total amount of propellant in the trap, a portion was considered as surplus (could be lost from the trap without degrading the capability of the system to accomplish the burns). The time required to start the engine and settle the propellant determines the size of the surplus. For the amounts of propellant remaining after the orbit insertion burn, the settling time was conservatively calculated as three seconds for Mission A_1 and six seconds for Mission A_2.

The duration of a minimum impulse bit burn is less than the settling time. If a minimum impulse bit burn is accomplished, the amount of surplus propellant in the trap will be increased. Whenever a burn is of shorter duration than that specified in the baseline mission, the total propellant load would not be consumed and the unused propellant would remain in the trap. Both of these factors improve the worst-case operating conditions. More propellant will be available in the trap so the pressure losses in the annulus would be reduced. Loss of liquid from the trap is less of a problem since the surplus was increased. Therefore, any reduction in the burn duration without changing the number of burns will not cause problems.

To determine the flexibility of the propellant trap designed for the basic mission, variations in the number and duration of the orbital trim burns were considered. The total amount of propellant available to accomplish the orbital trim burns is assumed to remain the same (changes in total propellant load are not being considered).

Two factors limit the number of burns the trap is capable of providing. The first is the effect of the thermal environment. There must be some way of providing for the loss of liquid from the trap due to thermal effects. As discussed in the previous section, the loss can be provided for by having more liquid in the trap than is required to start and settle for each burn. This applies only if the burn duration is greater than the settle time.

For example, consider the Mission A_1 oxidizer tank where the amount of propellant available for orbital trim burns is 30.78 lb_m. Since it requires three seconds to settle propellant located outside the trap, 5.77 lb_m of propellant would be consumed during settling. With the three burns of the baseline mission, each of approximately five seconds duration, there would be a surplus of 13.45 lb_m of propellant that could be lost from the trap. If five burns of three seconds duration, and consuming the same amount of propellant were desired, the surplus would only be about 2 lb_m of propellant; however, this is not enough to provide for the loss of liquid from the trap due to thermal effects. The trap is limited as far as how many equal duration burns can be provided if all the propellant must be consumed. The limits are four burns of approximately three seconds duration for Mission A_1 and eight burns of approximately six seconds duration for Mission A_2.

Another approach, which would provide a larger number of burns, could be taken. Consider the OF_2 tank again. According to the thermal analysis, 7.7 lb_m of OF_2 would be lost from the trap, leaving 23 lb_m in the trap. Any duration and number of burns that will consume 23 lb_m of propellant could be accomplished. For example, 20 burns of 0.6 second duration could be accomplished. But now the expulsion efficiency would be reduced to 98.6% because the 7.7 lb_m lost from the trap could not be burned. Since only 1.5 lb_m of N_2O_4 would be lost from the trap, the effect on the expulsion efficiency is less; it would become 99.4%.

The second factor that limits the flexibility of the trap is the duration of the last burn. As explained in the analysis of the annulus under low g, the last burn establishes the worst-case condition for the pressure losses in the annulus. As the amount of propellant remaining for the last burn is decreased, the pressure losses under the worst-case condition are increased.

Using the criteria for the worst-case condition, the last burn for Mission A_1 must be at least 1.8 seconds in duration. If the duration was shorter, the amount of propellant in the trap would be less and the magnitude of the pressure losses would cause breakdown of the annulus. The pressure loss due to the flow through the Dutch twill screen causes the pressure losses to be large. If a shorter last burn was required, the amount of propellant needed for a 1.8-second burn would still have to be provided. Only part of the remaining propellant would be consumed, so the expulsion efficiency would be decreased.

For Mission A_2 the last burn could be as small as the minimum impulse bit. In this case none of the pressure losses are excessive under low g. With this small a burn, the expulsion efficiency must enter the consideration of whether the last burn could be accomplished. About 3.7 lb_m of N_2O_4 and 2.2 lb_m of MMH are required to fill the annulus and it is expected that this remainder cannot be expelled from the trap. A minimum impulse bit burn consumes 0.54 lb_m of MMH and 0.78 lb_m of N_2O_4. It seems that the 4% margin added to the propellant load (22.5 lb_m MMH and 34.8 lb_m N_2O_4) should provide enough propellant to allow for the expulsion efficiency, especially if it can be shown that the typical variation in propellant consumption is less than 4%.

2) Mission B - The characteristics of this mission are much different than those of Missions A_1 and A_2. Nine burns are accomplished in the basic mission. The velocity increment required for each of these burns will fall somewhere between an anticipated minimum and maximum. It was assumed that the maximum velocity increment would be required for all of the burns when the size of the propellant load was determined.

A minimum impulse bit of 1.0 lb_f-sec is specified for this mission. This would require a 0.04-second burn and 0.004 lb_m of propellant would be consumed. It requires between five and six seconds to settle the propellant for this mission, depending upon how much propellant is remaining in the tanks.

If additional burns were to be added, the size of the trap would have to be changed. For this mission, the effect of the thermal environment on the trap was concluded to be negligible. Therefore, the size of the trap is determined only by the amount of propellant required to start the engine and settle the propellant for each burn. If the duration of the additional burn was less than six seconds, the total amount of propellant must be added to the trap. If the duration is greater than six seconds, the increase would be the amount of propellant required to start and settle.

The worst-case condition at the start of the last burn is also a consideration when variations to Mission B are considered. All of the pressure losses are very small under low-g conditions, so theoretically a minimum impulse burn could be the last burn. The amount of propellant required for this burn $(0.004\ lb_m)$ is very small compared to the 1.05 lb_m propellant that would remain in the tank due to the expulsion efficiency. All of the burns will not actually be the maximum velocity increment, so there should be a sizable amount of propellant (in comparison to that required for a minimum impulse bit) remaining in the tank.

c. Variations in Propellant Properties - Another factor that remains to be considered is the effect of the variation in the properties of the propellants. Surface tension and density are the properties which most affect the design of a surface tension device. The effect of these properties can best be evaluated in terms of kinematic surface tension, which is the ratio of surface tension to density. Since the retention capability of the screen is directly proportional to the surface tension and, the pressure losses in the annulus are directly proportional to the density, it is the smallest kinematic surface tension that is of concern.

The effect of the variation in the properties could be evaluated as part of the 1-g test, but those effects will not be considered here. The criteria established were for a test accomplished at the nominal temperature. During the mission, the temperature can vary above and below the nominal value, causing a variation in propellant properties. The values of the surface tension and density are listed for upper and lower temperature limits in Table II-6. The minimum kinematic surface tension occurs at the maximum propellant temperature. When the designs were analyzed for the low-g condition, it was usually found that the trap was extremely over-designed because of the 1-g test requirement. The annulus of the Mission A_1 oxidizer tank was the only exception, so it was reevaluated for the worst-case liquid property values.

Based on the criteria for Mission A_1, the minimum kinematic surface tension of OF_2 occurs at 280°R. The pressure losses in the annulus and the retention capability of the screen were reevaluated at that temperature. It was found that the screen still would provide adequate retention under the worst-case flow condition. Therefore, the variation in properties will not adversely affect any of the designs.

V. PROPELLANT ACQUISITION SYSTEM - LOW-G DESIGN

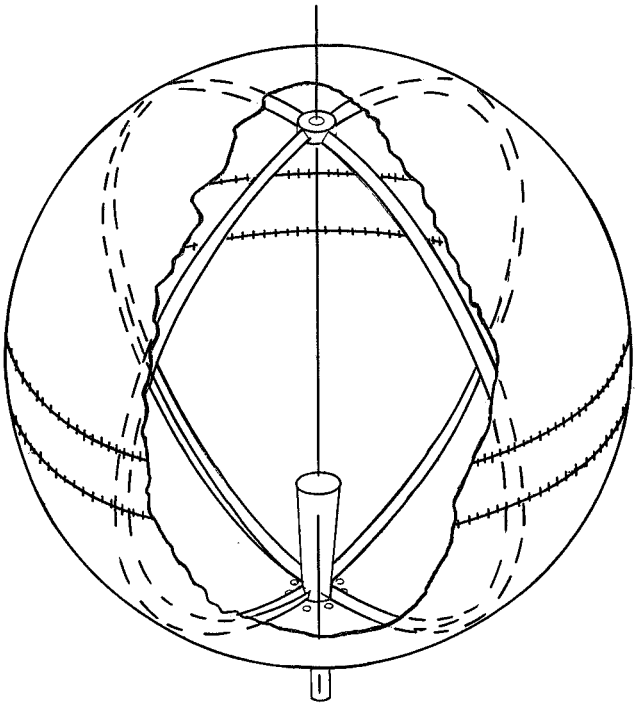

Figure V-1 The Fruhof, a Low-g Propellant Acquisition Concept

The Martin Marietta surface tension concept (the Fruhof) consists simply of an ullage stand-off post located over the tank outlet, and connected to communication channels circling the tank wall (Fig. V-1). This chapter describes the concept, fabrication and assembly considerations, and its operational performance for Missions A_1, A_2, and B.

A. CONCEPT

A rather stringent design requirement, imposed on the capillary devices presented in the previous chapter, was that liquid expulsion be demonstrated on Earth with the tank held upside down. This requirement is considered stringent since the primary objective of the propellant acquisition system for Missions A_1, A_2, and B is to acquire and hold sufficient liquid propellant over the tank outlet prior to main engine burns in the low-g environment. The acceptable design provides gas-free propellant to the engine by preventing gas ingestion into the feed line until the propellant tank is nearly depleted.

Removal of the 1-g test requirement eliminates the need for fine-mesh capillary devices. The use of surface tension to stabilize a liquid/vapor interface in Earth g requires that the radius of curvature of that interface be exceedingly small (micronic). Fine mesh screen serves this function well, as proven by screen trap and liner tests (Ref V-1). The use of surface tension to stabilize a liquid/vapor interface in low g, requires that the radius of curvature of the interface be smaller at the desired place than at any other location inside the tank. This is discussed further in this section.

One physical description of the effect of surface tension is based on pressure. The liquid pressure at a curved, free surface, is less than the ullage (gas) pressure by the amount of the free-surface membrane stress,

$$P_{\ell} = P_g - \sigma\ (1/R_1 + 1/R_2), \qquad [V\text{-}1]$$

where

R_1 and R_2 = principal radii of curvature of the surface;

σ = liquid/gas surface tension (Ref V-2).

The static equilibrium condition in zero g requires that pressure be uniform throughout connected liquid regions. At equilibrium, the two principal radii of curvature are such that $1/R_1$ and $1/R_2$ add to the same value everywhere on the free surface. In a nonequilibrium state, any pressure gradient will cause liquid flow to the low pressure region. Therefore, liquid will tend to flow and orient itself inside a tank where the radius of curvature is minimum.

The liquid/solid contact angle is another physical constraint in the design of surface tension systems. It determines the effects of tank and internal hardware configurations on the static interface shapes. The contact line is formed by the locus of the intersection between the free and rigid boundaries of the confined liquid. For example, the contact line for a liquid with an axisymmetric free surface inside an axisymmetric container is a circle. The contact angle is the angle between two straight lines drawn normal to the contact line, one tangent to the free surface and the other tangent to the rigid surface at a point on the contact line (Fig. V-2).

The equilibrium contact angle is a physical property of the particular liquid, vapor, and solid substances (Ref V-3). If the substances are uniform throughout the inside of the tank, then the contact angle must be uniform wherever the liquid is positioned. (In contrast, contaminants can introduce local variations in the equilibrium contact angle.) If a contact line is located on an irregularly-shaped solid surface, then there generally must be considerable distortion of the free surface shape to satisfy the contact angle condition. The low pressure regions in the liquid created by the surface distortions cause flow that must move the contact line until both uniform contact angle and surface curvature are achieved. This can be somewhat complicated by the

effects of the nonequilibrium contact angle. Liquids with non-zero equilibrium contact angles tend to exhibit a larger angle when advancing on a dry surface, and a smaller angle when receding. This range of possible angles may persist for days, since the nonequilibrium effects may dissipate very slowly, particularly for angles greater than 20° (Ref V-4). If possible, large contact angle conditions are to be avoided because of the inherently long times required for equilibrium orientation, particularly in the vicinity of irregularly-shaped solid surfaces.

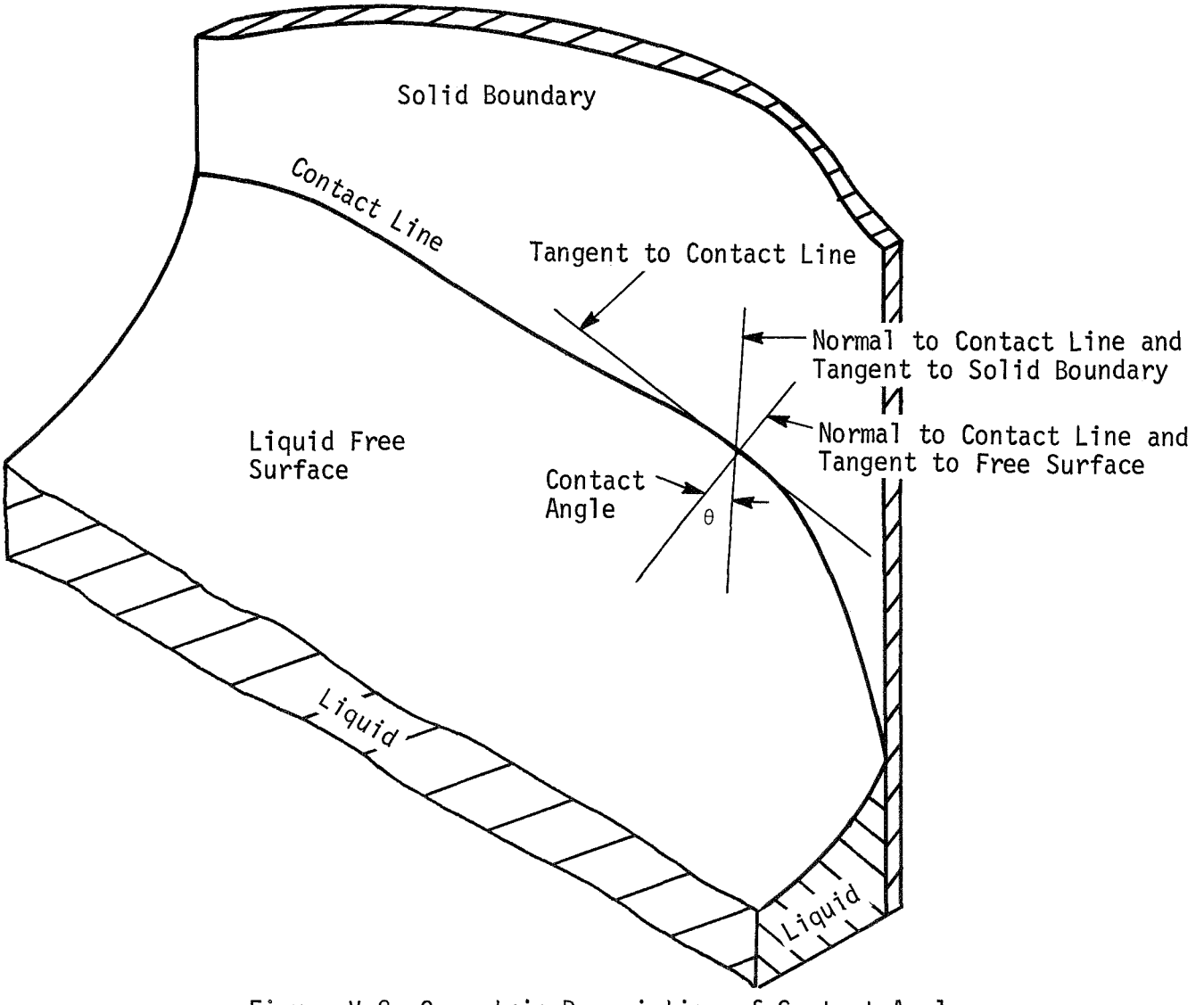

Figure V-2 Geometric Description of Contact Angle

The strength of the surface tension positioning forces is proportional to the cosine of the contact angle (Ref V-5). Therefore, fluid with a contact angle of 20° has only about 6% less orientation capability than a fluid with a contact angle of zero. The value of the contact angle for the propellants considered for Missions A_1, A_2, and B depends primarily on the liquid surface tension and the solid boundary surface energy. Solid surface energy can be expressed as a "critical surface tension" (Ref V-6). If the liquid surface tension is less than the critical value, the contact angle is zero. If the surface tension is greater than the critical value, the cosine of the contact angle is approximately linearly proportioned to the difference between the liquid and the critical surface tensions. Clean metal surfaces have very high critical surface tensions and nonmetallic liquids completely wet them. However, maintaining a thoroughly clean metal surface requires care. Most monolayer contaminant films (except fluorocarbons) have critical surface tensions between 20 and 45 dynes/cm (Ref V-7). It is important, therefore, to guarantee careful cleaning procedures in order to keep contact angle to a minimum. A study has shown that with standard spacecraft tankage cleaning procedures, expected contaminants such as stearic and oleic acids do not significantly raise the contact angle of liquid propellants (Ref V-8).

Using surface tension phenomena and the constraint of considering only spherical tankage, the design approach was to add a minimum of internal hardware such that its shape and location would position the liquid/vapor interface (or free surface) away from the tank outlet with liquid at the outlet. Since the surface tension effect is essentially that of a membrane stress, and since the liquid propellants in this study are wetting or nearly wetting (contact angle zero to 2°), we may consider that the liquid/vapor interface acts somewhat like a balloon with gas on the inside and liquid on the outside. Using this analogy, one can visualize that a single, straight rod located at the tank outlet will tend to hold the ullage bubble (except for small ullage volumes) away from the outlet in zero g.

The ullage standoff post (or pillar) creates a region where the liquid free surface at equilibrium must be curved more sharply than for regions away from the post. As mentioned earlier, the greater the curvature the lower the liquid pressure. Therefore, if, under dynamic conditions, the free surface moves down along the pillar and positions itself over the outlet, liquid will flow into this lower pressure region (created near the outlet) pushing the surface away from the outlet. In this manner, the simple post guarantees liquid at the outlet in zero g.

The post geometry factors (height, diameter, and taper) are design choices. The primary consideration is the amount of liquid that must be held over the outlet for restart. A 50% liquid load can be held with a post height equal to 0.21 times the sphere diameter.

A second consideration is the control of the liquid center-of-mass for guidance and control. The post establishes a preferred location for the propellant if there is sufficient ullage volume. A post height equal to 0.5 times the sphere diameter controls the liquid location up to an 87.5% load. Smaller ullage bubbles may drift about within a limited region inside the tank; the smaller the bubble, the larger the region for movement. However, the small amount of mass movement with these small ullages is probably negligible.

For Missions A_1 and A_2, the ullage volume at the orbit insertion burn will be about 10% of the tank volume. It was assumed that movement of this volume has a small effect on the vehicle control system (Ref V-18). Thus, no attempt was made to control the location of a 10%, or less, ullage bubble, except to keep it from sitting directly over the tank outlet. After the orbit insertion burn, the remaining liquid propellant is about 5% of the tank volume and will be located over the outlet.

Mission B with a blowdown pressurization system has an initial liquid load of about 50%. In the near zero-g environment of interplanetary space, the spherical ullage bubble is held away from the outlet in a fixed axisymmetric position by a post height 0.21 times the sphere diameter. The post height required to hold a spherical bubble in place in a spherical tank is governed by the simple geometric relation:

$$H/D = 1 - \left(V_{ullage} / V_{tank}\right)^{1/3}, \qquad [V\text{-}2]$$

where H = post height, D = tank diameter, V = volume.

The diameter of the post directly affects the surface tension holding power of the post. Liquid pressure at the post is less than the ullage pressure by an amount equal to the product of surface tension and the sum of the two principal radii of curvature for the free surface (Eq [V-1]). At the post, the second principal radius of curvature (i.e., the inverse of curvature) is negative and is directly proportional to the post diameter; thus,

the larger the post diameter, the greater is the surface tension effect. Tapering the post achieves this larger diameter for larger amounts of liquid while holding small residual propellant quantities more closely over the outlet.

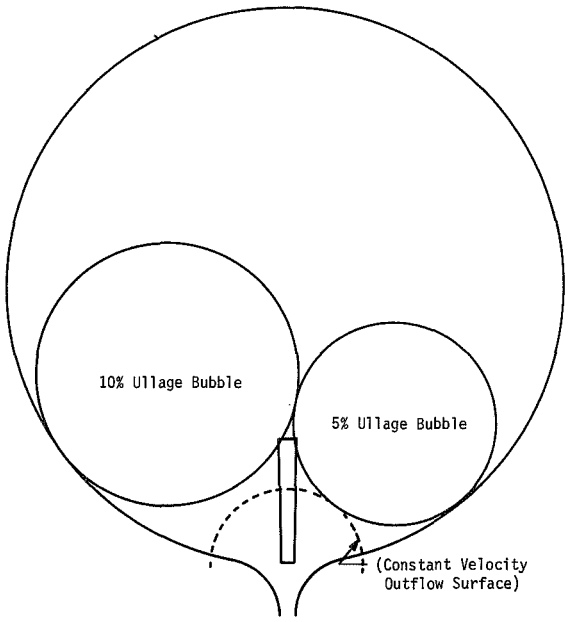

Figure V-3 Spherical Tank with Ullage Standoff Post, Showing Closest Approach of an Ullage Bubble to the Tank Outlet

The presence of the post device also prevents small ullage bubbles from sitting directly over the outlet (Fig. V-3). The probable static positions that various-sized bubbles (5 and 10% ullage volumes) can attain near the outlet are pictured. The proximity of a given-sized ullage bubble to the outlet at which ingestion may occur at engine start can be estimated as follows. Assume that the bubble velocity toward the outlet at startup is the volume flowrate divided by the surface area of the spherical-shell shown by a broken line in Figure V-3. Further assume that engine startup time is 200 milliseconds. A simple calculation will then show that a 5% ullage bubble tends to move less than 5% of its distance to the outlet before the buoyant force resulting from the engine thrust starts to move the bubble toward the top of the tank (away from the outlet). This is the case for either Mission A_1 or A_2.* This estimate indicates that the standoff post will prevent any relatively small ullage volumes from being ingested during engine startup.

As the ullage volume grows with liquid outflow, the bubble surface will eventually contact the post. If the post height equals the tank radius, this will occur at ullage volumes greater than about 12.5% of the tank volume for the A Missions (for shorter posts, this contact will occur at larger ullage volumes). When the free surface contacts the post and grows down along the post it distorts to satisfy contact angle. A balance between the two principal radii of curvature (to create a uniform pressure throughout the liquid) is possible only if the free surface is axisymmetric

*Mission B has an initial ullage volume of 50%.

about the axisymmetric post. Any asymmetry in the surface shape will tend to be eliminated by liquid flow to the liquid regions of lower pressure. Thus, an added feature of the Fruhof design is that liquid can be held axisymmetric in zero g with a predictable center-of-mass for ullage volumes in excess of 12.5%. This is also true for very low liquid volumes (which tends to ensure the desired expulsion efficiency of 99.5%, or more).

Two approaches were taken to verify the Fruhof concept: a numerical calculation of the static-equilibrium interface shape, as influenced by the presence of the post; and an experimental demonstration of the zero-g interface shape using the Martin Marietta drop tower facility.

The analysis is a solution of the surface tension equation (Eq [V-1]). In cylindrical coordinates, the axisymmetric free surface may be described by the surface height as a function of radius, $Z = \eta(r)$. The surface curvature is then (Ref V-9):

$$\frac{1}{R_1} + \frac{1}{R_2} = \frac{1}{r}\frac{d}{dr}\left[r\left(\frac{d\eta}{dr}\right)\Big/\sqrt{1 + \left(\frac{d\eta}{dr}\right)^2}\right] \qquad [V-3]$$

The curvature may be expressed in a general coordinate system through the use of surface tensors (Ref V-10) or vectors (Ref V-11). The liquid pressure in an axial gravity field is expressed as:

$$P_L = P_O - \rho a \eta \qquad [V-4]$$

Thus, the surface tension equation can be written as a second order, nonlinear, ordinary differential equation for the free surface height as a function of radius:

$$\frac{\sigma}{r}\frac{d}{dr}\left[r\left(\frac{d\eta}{dr}\right)\Big/\sqrt{1 + \left(\frac{d\eta}{dr}\right)^2}\right] = \rho a \eta + p_G - p_O. \qquad [V-5]$$

Nondimensionalizing r and η by division by the tank radius R allows Equation [V-5] to be expressed as

$$\frac{1}{r}\frac{d}{dr}\left[r\left(\frac{d\eta}{dr}\right)\Big/\sqrt{1 + \left(\frac{d\eta}{dr}\right)^2}\right] - Bo\eta = b \qquad [V-6]$$

where

$Bo = \rho a R^2/\sigma$, the Bond number (Ref V-12);

$b = \left(P_G - p_O\right) \cdot R/\sigma$, an unknown constant.

Equation [V-6] is the Young-Laplace equation (Ref V-9 and V-13).

The contact angle at the post and tank wall and the liquid volume are the three boundary conditions needed to uniquely define the free surface position and shape. The second order differential equation (Eq [V-6]) requires two conditions and the unknown b requires a third. The importance of contact angle in the positioning surface is indicated by this mathematical requirement. A numerical solution is readily found using the Bashforth-Adams integration technique (Ref V-14). Equation [V-5] cannot be integrated directly since $d\eta/dr$ passes through infinity as the slope passes through 90°. Adapting the angle of the slope of the free surface as the independent variable allows construction of parametric relations. Let

$$\tan \theta = d\eta/dr. \qquad [V-7]$$

Then Equation [V-6] becomes

$$\frac{1}{r}\frac{d}{dr}(r \sin \theta) - Bo\eta = b,$$

which can be manipulated to

$$dr = \cos \theta \, d\theta/(b + Bo\eta - \sin \theta/r). \qquad [V-8]$$

Equation [V-7] thus becomes

$$d\eta = \sin \theta \, d\theta/(b + Bo\eta - \sin \theta/r). \qquad [V-9]$$

Equations [V-8] and [V-9] are two simultaneous equations for the free surface radius and height, which may be solved to yield the parametric representation $r = \dot{r}(\theta)$ and $\eta = \eta(\theta)$. The method of solution is a numerical integration starting at one boundary and progressively incrementing θ to the other boundary, e.g., starting at some contact point on the Fruhof pillar and integrating until the free surface contacts the sphere wall. Two boundary conditions specify the height and slope of the free surface contact on the pillar at some specified radius. The angle of slope is the contact angle plus the angle of slope of the pillar.

The initial guess of the unknown b in Equations [V-8] and [V-9] is best based on the experience gained in calculating interface shapes. Generally, a value of 0.5 for b is a reasonable starting point $\left(p_0 \approx p_G - 2\sigma/r \text{ in Equation [V-6]}\right)$. The choice of a reasonable θ increment depends on the method of integration. The minimum truncation error, fourth order Runge-Kotta method (Ref V-15) with $\Delta\theta = 0.5°$ has proven quite accurate and provides efficient use of computer time.

The nondimensional position of the spherical tank wall may be represented in parametric form in terms of the slope of the wall:

$$\eta_\omega = \eta_\omega \left(\theta_\omega\right) \text{ and } r_\omega = r_\omega \left(\theta_\omega\right).$$

If we place a coordinate system at the center of the sphere, the wall height and radius are given in terms of the slope of the wall as:

$$\eta_\omega = -\cos \theta_\omega \qquad [V\text{-}10]$$

$$r_\omega = \sin \theta_\omega \qquad [V\text{-}11]$$

Note that

$$d\eta_\omega \Big/ dr_\omega = \tan \theta_\omega. \qquad [V\text{-}12]$$

If, in the process of integration, a point is reached where $\theta = \theta_\omega$ - contact angle, we have $r = r_\omega$ and $\eta = \eta_\omega$. Then, the spherical surface contact has been found and the interface shape, $\eta = \eta(\theta)$ and $r = r(\theta)$, has been determined. However, this can only occur if the correct value of b has been used in Equations [V-8] and [V-9]. If the incorrect value of b is used, then when $\theta = \theta_\omega$ - contact angle and $r = r_\omega$ simultaneously, the difference between η and η_ω measures the error in b, $\varepsilon_o = \left(\eta - \eta\omega\right)\Big|_{b=b_o}$. Incrementing the estimate of b and reintegrating establishes a second error, $\varepsilon_1 = \left(\eta - \eta_\omega\right)\Big|_{b=b_1}$. Extrapolation to zero gives an improved estimate of b,

$$b_{i+1} = \left(b_i\, \varepsilon_{i-1} - b_{i-1}\, \varepsilon_i\right) \Big/ \left(\varepsilon_{i-1} - \varepsilon_i\right). \qquad [V\text{-}13]$$

This procedure can be continued until the error is within some small bound, typically $\varepsilon_i < 10^{-6}$. At this point, an accurate approximation of the free surface shape, $r = r(\theta)$, $\eta = \eta(\theta)$, is obtained that satisfies a specified position and contact angle on the pillar and contact angle on the sphere wall. A typical computer plotted picture of such a solution is shown in Figure V-4. The volume of liquid may be computed by integration, assuming a sphere whose radius is one:

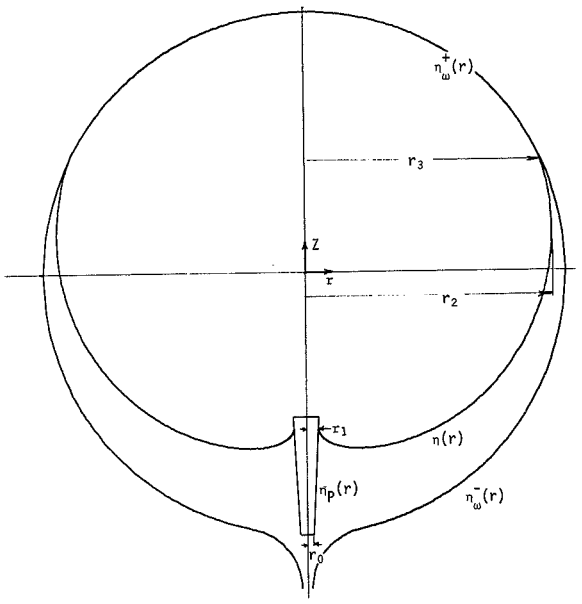

Figure V-4 Free Surface Shape Distortion by Standoff Post (Percent Liquid = 22.49, Bond No. = 0)

$$\text{Volume} = 2\pi \int_{r_0}^{r_1} \left(\eta_P - \eta_\omega^-\right) r\,dr + 2\pi \int_{r_1}^{r_2} \left(\eta - \eta_\omega^-\right) r\,dr + 2\pi \int_{r_3}^{r_2} \left(\eta_\omega^+ - \eta\right) r\,dr + 2\pi \int_{r_2}^{1} \left(\eta_\omega^+ - \eta_\omega^-\right) r\,dr, \quad \text{[V-14]}$$

or

$$\text{Volume} = 2\pi \int_{r_0}^{r_1} \left(\eta_P - \eta_\omega^-\right) r\,dr + 2\pi \int_{r_1}^{r_3} \left(\eta - \eta_\omega^-\right) r\,dr + 2\pi \int_{r_3}^{1} \left(\eta_\omega^+ - \eta_\omega^-\right) r\,dr.$$

When the liquid contact point is not above the sphere equator, the last integral is set to zero. Equation [V-14] is valid for either $r_0 < r_1$ or $r_0 > r_1$.

To determine the interface position for a specified amount of liquid, the liquid contact height on the Fruhof pillar is estimated to be equal to the height of the pillar and the contact angle is estimated as the physical contact angle. The interface shape and the resulting liquid volume are then calculated. If the calculated liquid volume is greater than the desired volume, the estimated contact height on the pillar is decreased and the calculation of interface shape and liquid volume is repeated until the desired liquid volume is obtained. If the initial calculated volume is less than the desired amount, the estimate of contact angle is increased (since the physical contact angle at a corner is not defined) until convergence on the correct interface shape to match the specified liquid volume is obtained.

Computer pictures showing the static-free surface location of the propellants before each burn during Mission A_1 are presented in Figure V-5. The first picture (a) is representative of possible location of the ullage bubble ($\sim$10% volume) before the midcourse corrections and the orbit insertion burn. The bubble is free to move anywhere inside the tank except over the tank outlet. The change in ullage size following the midcourse burns is not significant. Since no data are available on contact angle exhibited by either diborane or oxygen difluoride, a contact angle of 0° was assumed for the two propellants. A similar series of pictures, showing the static-free surface position before each of the engine burns during Mission B, is presented in Figure V-6. The propellant margin required by mission criteria was conservatively assumed to be used during the last burns.

Tests were performed in the Martin Marietta drop tower (Ref V-16) to verify (at least qualitatively) certain key operational features of the Fruhof. The test objectives were to:

- Provide zero-g equilibrium interface configurations for different liquid volumes and pillar orientations;
- Show ability of pillar to position ullage away from the tank outlet under zero and low-level, constant accelerations;*
- Demonstrate the ability of the pillar and communication channels to refill with liquid.

*These axial accelerations tend to move liquid away from the tank outlet.

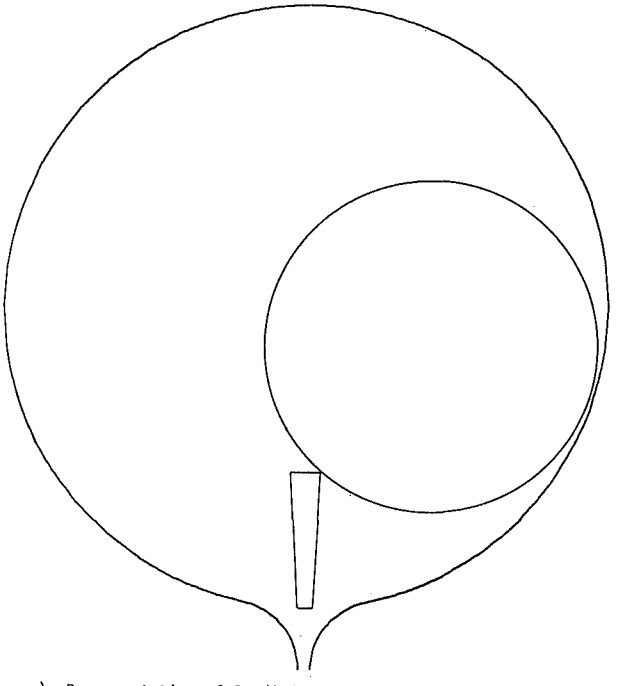

a) Representative of Conditions Prior to First and Second Midcourse Burns and Orbit Insertion Burn (Percent Liquid = 90 to 88.9, Bond No. = 0)

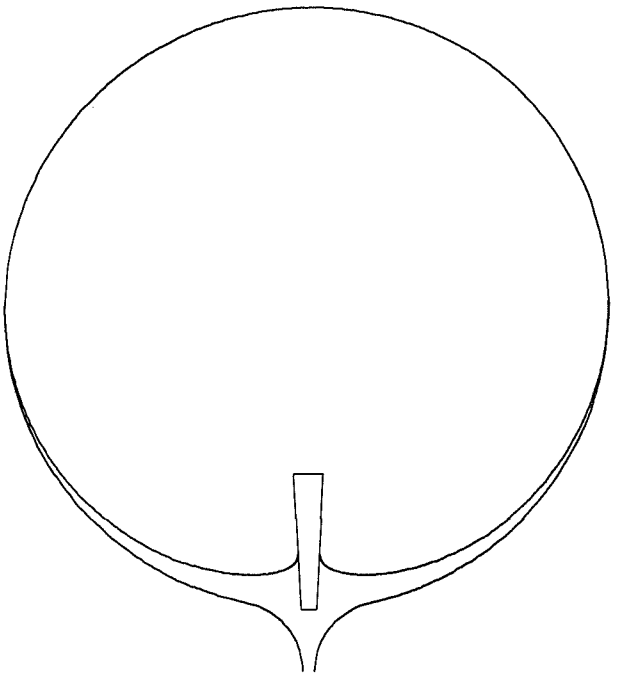

b) Prior to First Orbit Trim Burn (Percent Liquid = 3.42, Bond No. = 0)

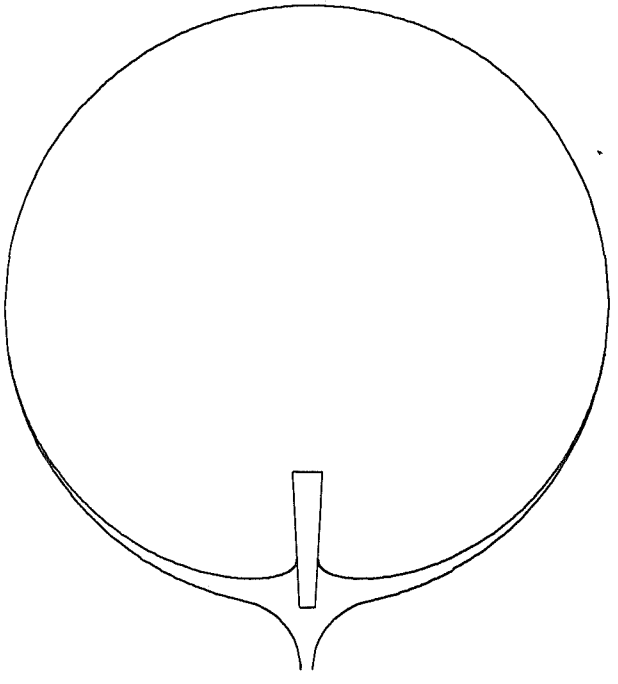

c) Prior to Second Orbit Trim Burn (Percent Liquid = 2.25, Bond No. = 0)

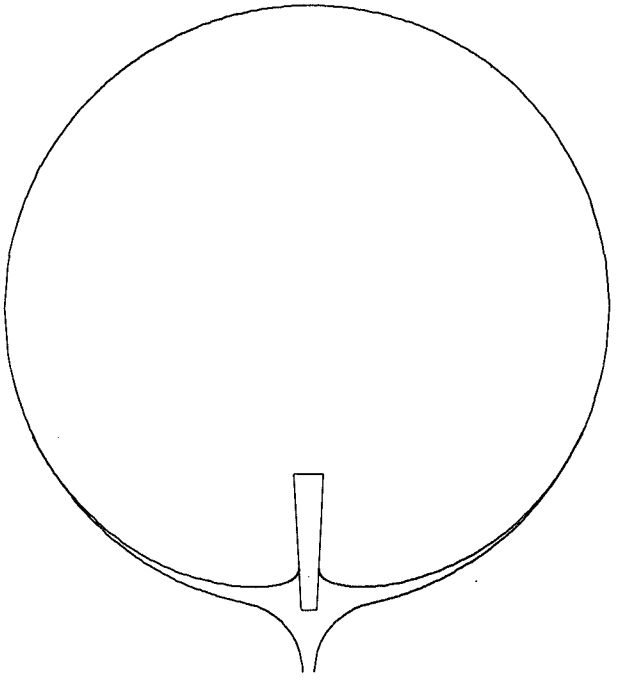

d) Prior to Third (Final) Orbit Trim Burn (Percent Liquid = 1.17, Bond No. = 0)

Fig. V-5 Liquid Orientation by the Fruhof Device before Each Burn on Mission A_1

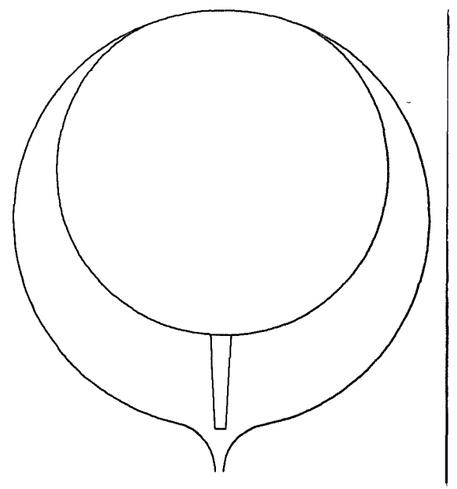

Percent Liquid = 50.00, Bond No. = 0

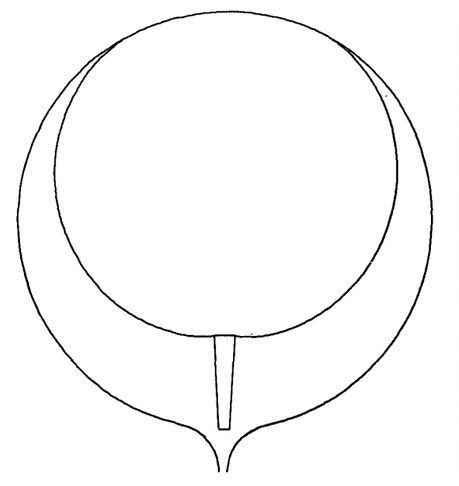

Percent Liquid = 45.10, Bond No. = 0

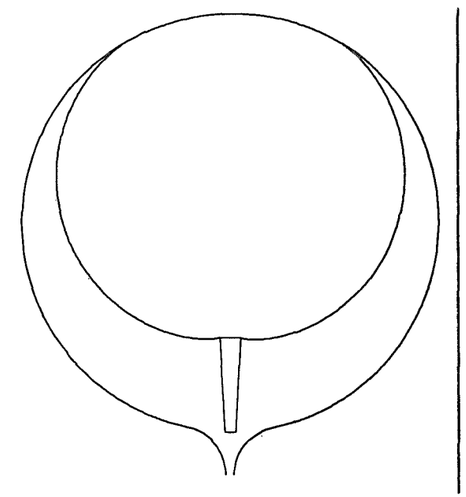

Percent Liquid = 44.00, Bond No. = 0

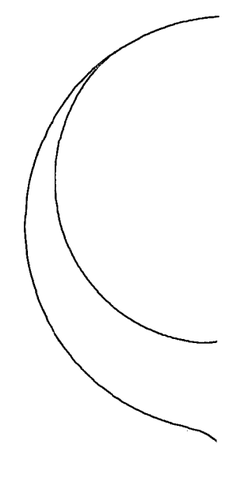

Percent Liquid =

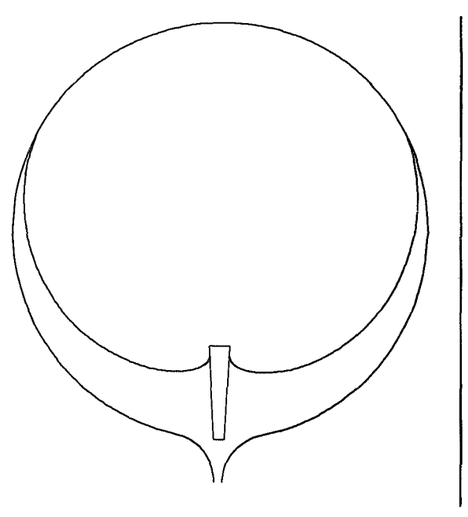

Percent Liquid = 22.10, Bond No. = 0

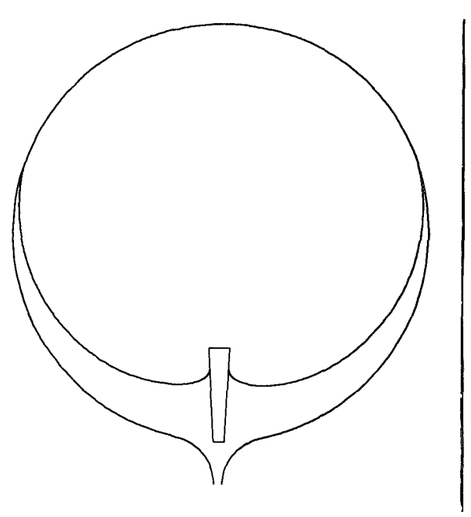

Percent Liquid = 16.70, Bond No. = 0

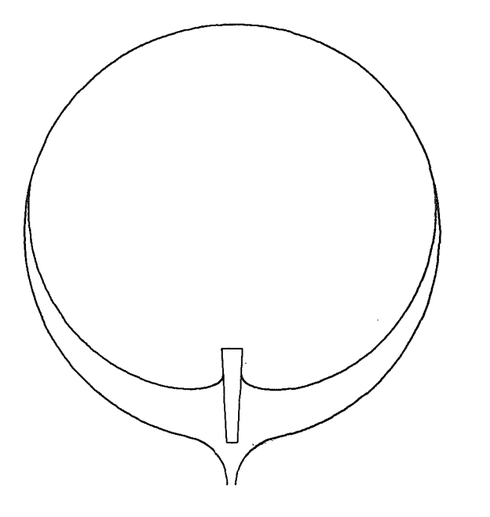

Percent Liquid = 14.60, Bond No. = 0

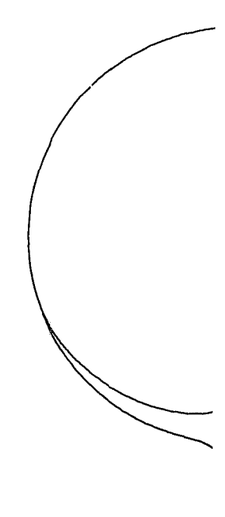

Percent Liquid =

Fig

Percent Liquid = 45.10, Bond No. = 0

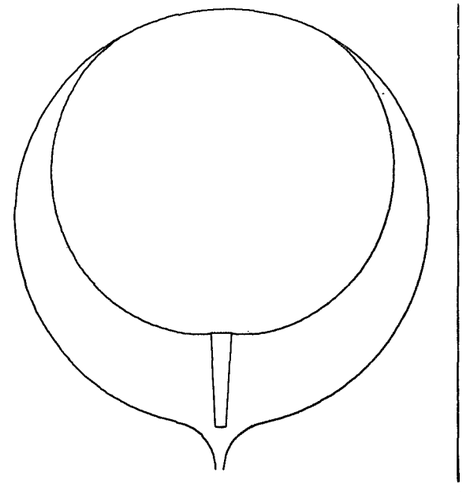

Percent Liquid = 44.00, Bond No. = 0

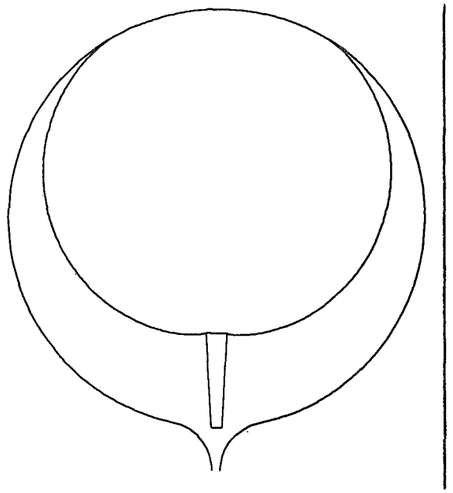

Percent Liquid = 41.20, Bond No. = 0

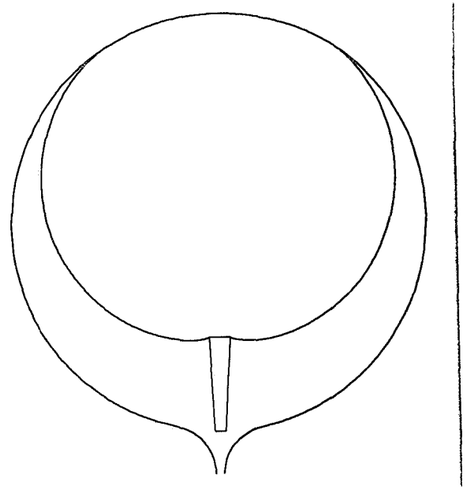

Percent Liquid = 39.30, Bond No. = 0

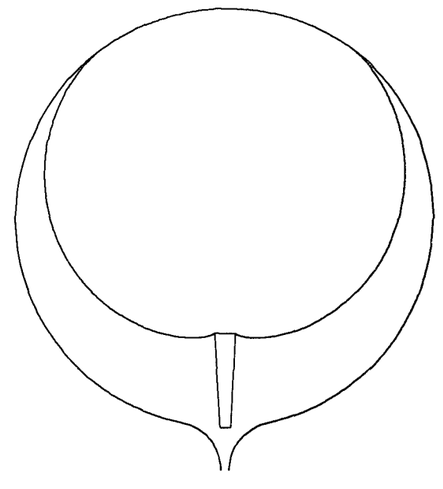

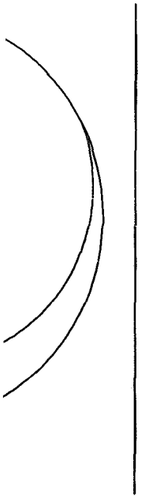

Percent Liquid = 16.70, Bond No. = 0

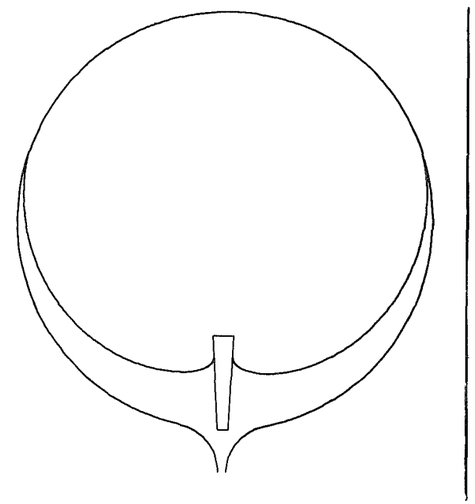

Percent Liquid = 14.60, Bond No. = 0

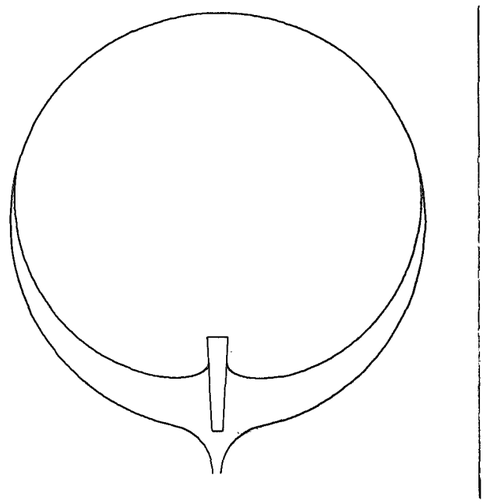

Percent Liquid = 4.20, Bond No. = 0

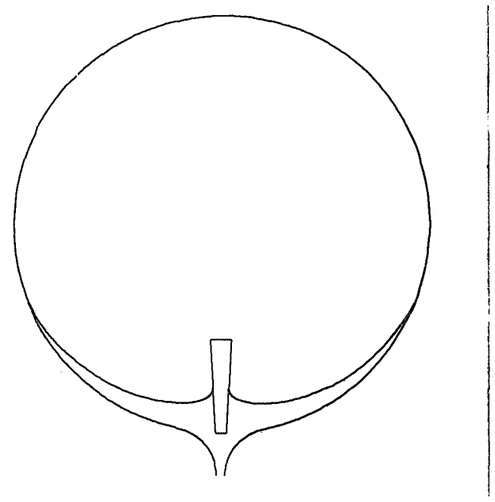

Figure V-6 Liquid Orientation by the Fruhof Device, before Each Burn on Mission B, Showing Free Surface Shape Distortion by the Standoff Post

The qualitative results were determined from 16mm color film records. Film speed was 200 frames per second to provide at least 400 frames for each 2.1-sec drop. The test specimens were glass and spherical to satisfy the visual and similitude requirements. The baseline tank geometry for the three planetary missions is spherical. The pillars were untapered, metal rods.

Benzene was chosen as the test liquid because of its high kinematic surface tension ($\beta = 11.6 \times 10^{-4}$ ft^3/sec^2) and low surface tension $\left(\sigma = 1.98 \times 10^{-3} \text{ lb}_f/\text{ft}\right)$. Attainment of the liquid/gas equilibrium configuration during the limited test duration was desired for most tests. The time to establish the zero-g curved interface from the 1-g flat shape (prior to the drop) is proportional to the parameter, $\sqrt{r^3/\beta}$ (Ref V-17). The high β value for benzene reduced the reorientation time, since its low surface tension value ensured that it would wet the glass specimens (assuming proper cleaning).*

Complete descriptions of the free-fall facility and testing procedures are presented in Ref V-16. The tests, summarized in Table V-1, are discussed in the following paragraphs.

In the first series of tests, three different sized spheres (1.9, 2.8, and 3.8-in. dia) were tested simultaneously with the same percentage of liquid. Different liquid levels were used. One purpose of the initial tests was to select the sphere size that allowed orientation of the free surface from the 1-g flat position to the zero-g shape in a reasonable fraction of the 2.1-sec free-fall time available.

Enlarged frames selected from the films of the first tests are presented in Figure V-7. The zero-g interface positions verify that liquid is held over the outlet. The 2.8-in. diameter sphere was chosen as the test item for the remaining test series since it represents the best compromise between clarity (of the filmed results) and reorientation time demands.

---

*The critical surface tension value to wet glass is 3.42×10^{-3} lb_f/ft, i.e., liquids possessing surface tensions of greater value will not wet glass. The detergent wash, water rinse, and air dry cleaning technique used in the drop tests did, however, yield contact angles with the benzene to 20° (as observed from the filmed results). Even with this relatively large contact angle, the Fruhof appeared to function adequately and as predicted.

Table V-1 Summary of Drop Tower Tests on Fruhof Design Concept

Run*	Test Specimen†	Acceleration (a/g)	Liquid Load (% of sphere volume)	Post Diameter/ Sphere Diameter	Test Purpose	Test Results
1	1	0	2	0.05	Demonstrate zero-g interface shape on post	Stable equilibrium interfaces formed in three spheres with qualitative agreement with analysis
2	1	0	10	0.05		Stable equilibrium interfaces formed in three spheres
3	1	0	25	0.05		Liquid in smallest sphere stabilized to zero-g interface shape; the others still had residual sloshing at end of test
4	1	0	50	0.05		Equilibrium interface shapes formed in three spheres in agreement with analysis
5A	1	0	2	0.025		No effect of smaller post diameter was seen (Run 5 was defective)
6	1	0	10	0.025		Sloshing persisted in largest sphere to end of test; other two reached equilibrium interface shapes
7	1	0	25	0.025		Sloshing persisted in all spheres to end of test
8	1	0	50	0.025		All spheres achieved equilibrium zero-g conditions; however, smaller post diameter slowed slosh damping
9	2	0	80	0.05	Demonstrate surface tension force of post in pushing ullage bubble away	Surface tension force was too small to see any difference between hydrodynamics in sphere with post and sphere without post
10	2	0	85			Surface tension force on ullage bubble was too small to be seen
11	2	0	90			Ullage bubble formed more slowly in sphere with post; but bubble velocity away from top was higher in sphere with post
12	2	0	95			Ullage bubble acceleration by surface tension force at post was easily seen
13	3	0	10		Demonstrate lateral post orienting ullage bubble to side of sphere	No liquid came in contact with post during test because of low liquid level
14	3	0	25			The post surface force began pumping liquid to side of sphere with post by end of test
15	3	0	50			An ullage bubble was formed and pushed away from post
16	3	0	70			An ullage bubble was formed and pushed away from post
17	3	0	90			The ullage bubble was too small to come in contact with post
18	4	-0.0015	10		Demonstrate liquid retention capability under negative accelerations	Liquid interaction with flange dominated the flow, obstructing the effect of the post
19	4	-0.0015	25			Liquid interaction with flange dominated flow
20	4	-0.0015	50			Post retained most of liquid, while liquid in sphere without post settled away from outlet
21	4	-0.0079	10			Post retained most of liquid
22	4	-0.0079	25			Slosh dynamics persisted through test, obscuring results
23	4	-0.0079	50			Post appeared to retain some liquid
24	4	-0.039	10			Acceleration settled liquid away from outlet in both spheres
25	4	-0.039	25			Acceleration settled liquid away from outlet in both spheres
26	2	0	10		Demonstrate post and channel refill	No liquid came in contact with post during test because of low liquid level
27	2	0	25			No liquid came in contact with post during test because the flange interrupted the flow
28	2	0	50			The post was filling with liquid at end of test, whereas liquid in sphere without post did not reach outlet region

*Test liquid was benzene; test duration was approximately 2.1 seconds.

†Test specimen designation:
1 = Three spheres, 1.9, 2.8, and 3.8 in. dia (sphere consisted of two flanged hemispheres joined at equator; post was a drill bit imbedded in outlet stopper). Each sphere had a post at the bottom (length = 0.4 x sphere diameter).
2 = Two spheres, 2.8 in. dia. One sphere without post (control) and one sphere with post at top (length = 0.2 x sphere diameter). 3-mil wire loops used as communication channels.
3 = Two spheres, 2.8 in. dia. One sphere without post (control) and one sphere with post at side (length = 0.2 x sphere diameter). 3-mil wire loops used as communication channels.
4 = Two spheres, 2.8 in. dia. One sphere without post (control) and one sphere with post at bottom (length = 0.2 × sphere diameter). 3-mil wire loops used as communication channels.

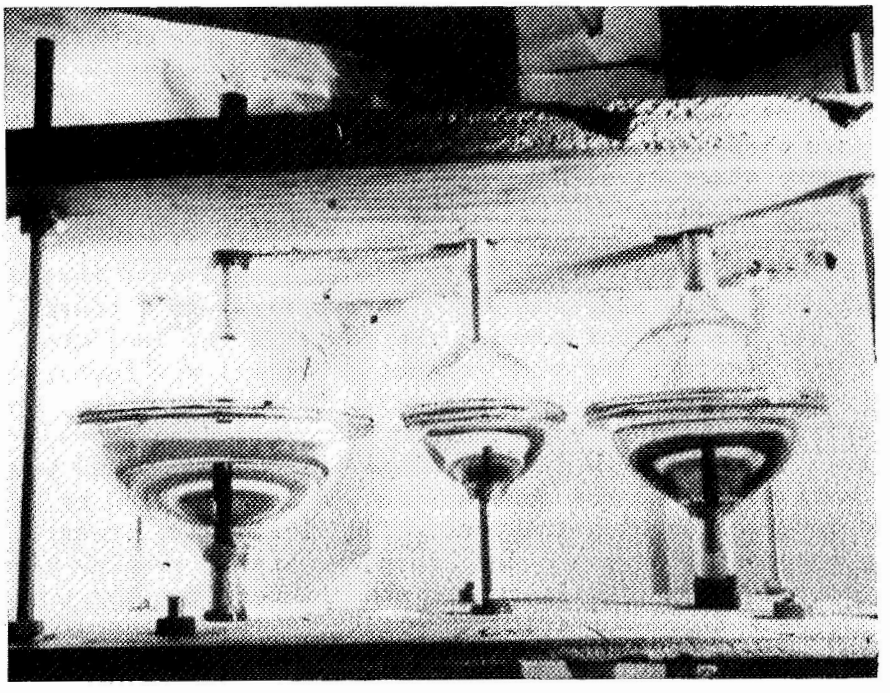

a) Initial 1-g Configuration (50% liquid load)

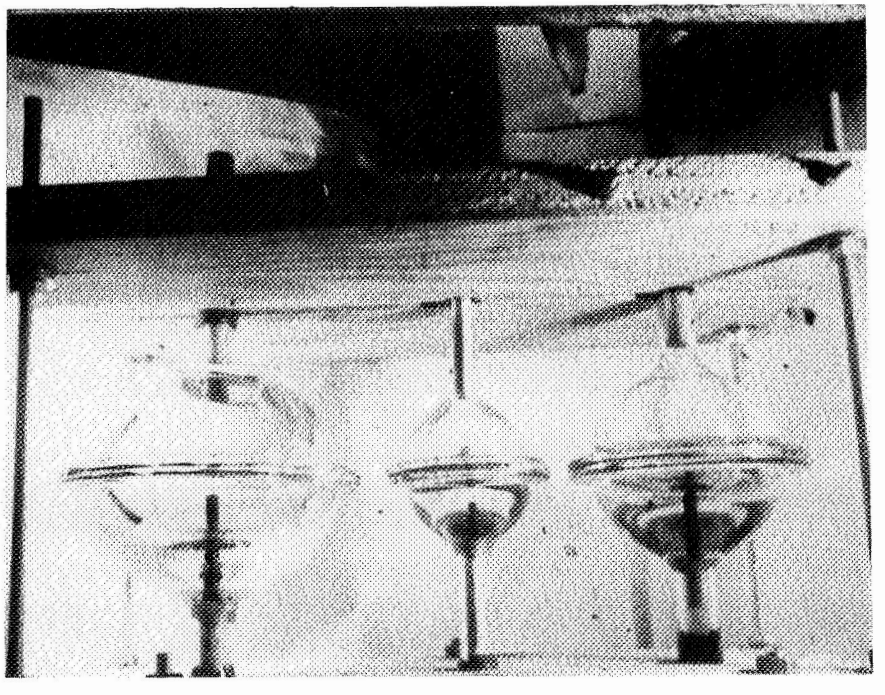

b) Zero-g Configuration (seen best in left sphere)

Figure V-7 Frames from Motion Picture Film of Fruhof Test Run No. 4

The second series of tests was designed to see how the pillar functioned with a relatively small ullage bubble. Two identical spheres were observed side-by-side, one with a standoff pillar at the top of the container, the other with no pillar. Comparison of the free surface motions in the two spheres allowed isolation of the effects of the pillar. Six liquid levels were tested: 25%, 50%, 80%, 85%, 90%, and 95%. In the first four tests, the flat 1-g surface did not contact the post; in the last two, the initial flat surface did make contact. For all six tests, the base of the post was dry (not wetted). During the tests, the free surface in both spheres changed from near-flat to near-spherical. For the high liquid volume tests, the ullage bubble formed more slowly in the sphere with the post, caused by liquid surface interaction with the post. The liquid flow created in forming these bubbles continued after formation, causing them to move from the top of the sphere toward the bottom. For the 95%-full case, the force the standoff pillar exerts on the ullage bubble to push it away from the outlet was clearly evident. The bubble in the clean tank, once formed, moved about 80% of the diameter of the sphere. The bubble in the sphere with the post left the post at a higher velocity and collided with the bottom of the container. Figure V-8 shows a sequence of frames selected from the film coverage of the 95%-full test.

The third series of tests was designed to demonstrate that the holding power of the ullage standoff pillar, as seen in the earlier tests, was not due to the test sphere orientation. Again, two spheres were used (one with a post, the other without), but they were positioned on their sides. The results showed that the zero-g ullage bubble formed in the sphere with the post achieved an offset position (away from the post). The ullage bubble in the clean tank remained axisymmetrically positioned (Fig. V-9).

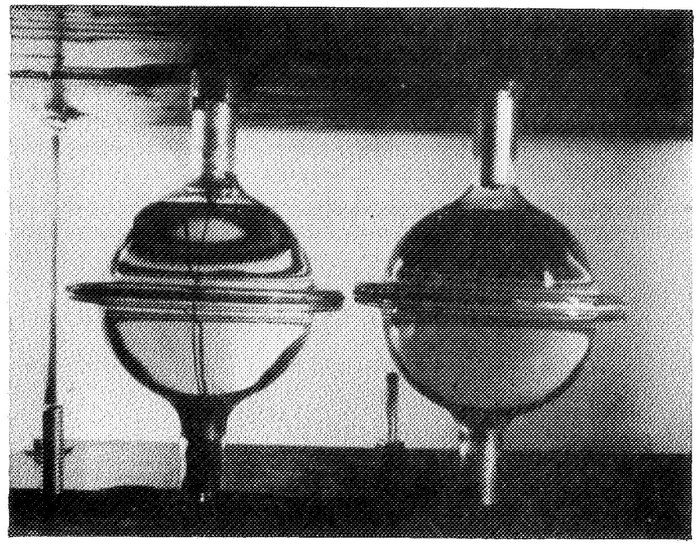

1) Initial 1-g Configuration (95% liquid load)

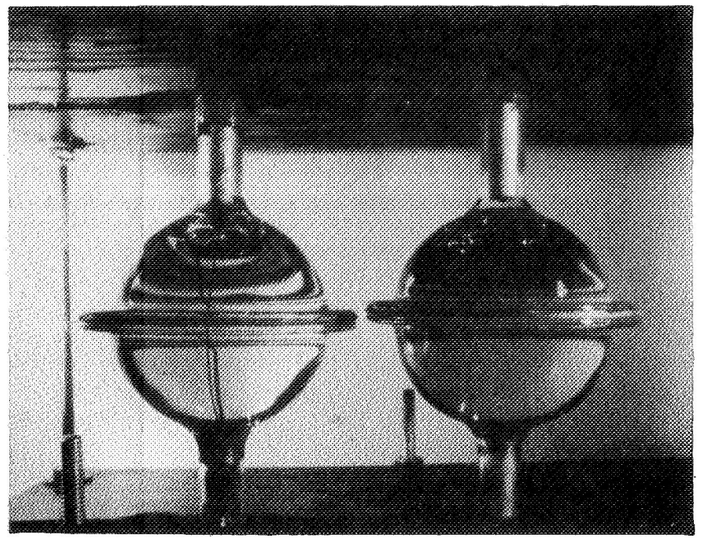

2) Initially Identical Bubble Formation

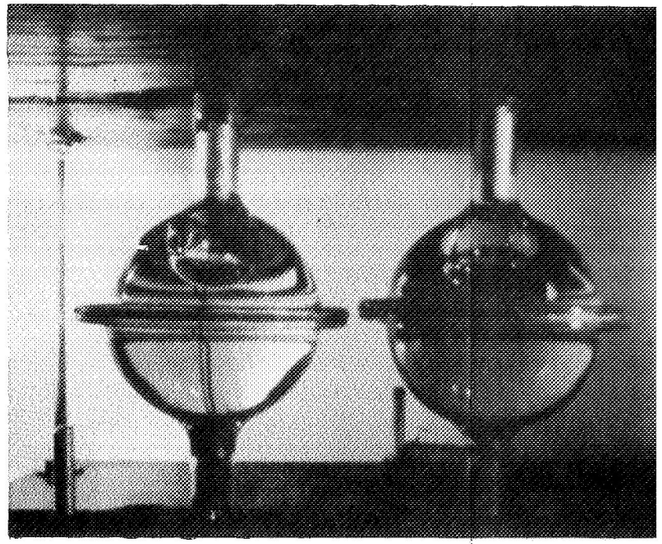

3) Post Begins to Interfere, Slowing Bubble Format

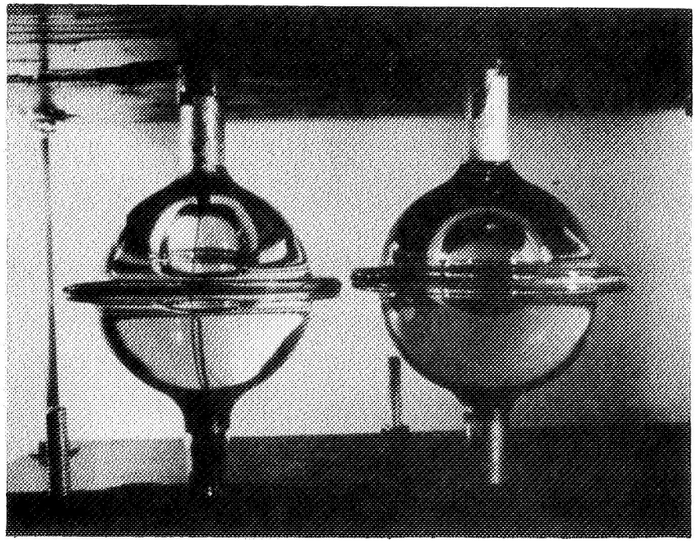

5) Post Accelerates Bubble toward Bottom

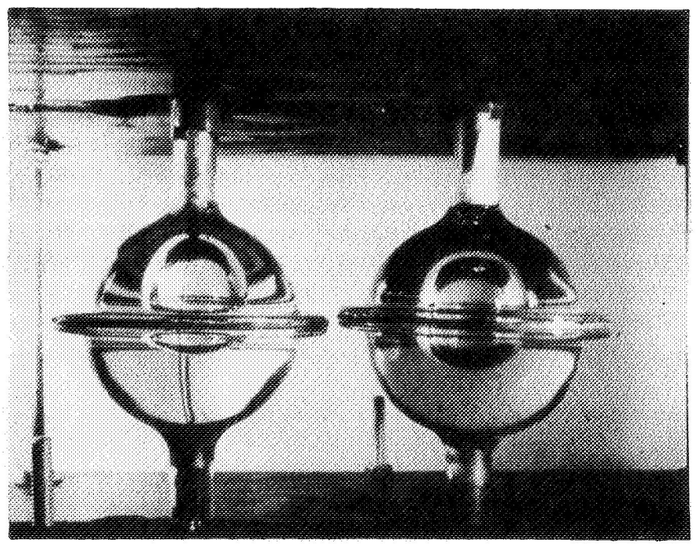

6) Bubble on Left Still Behind Bubble on Right

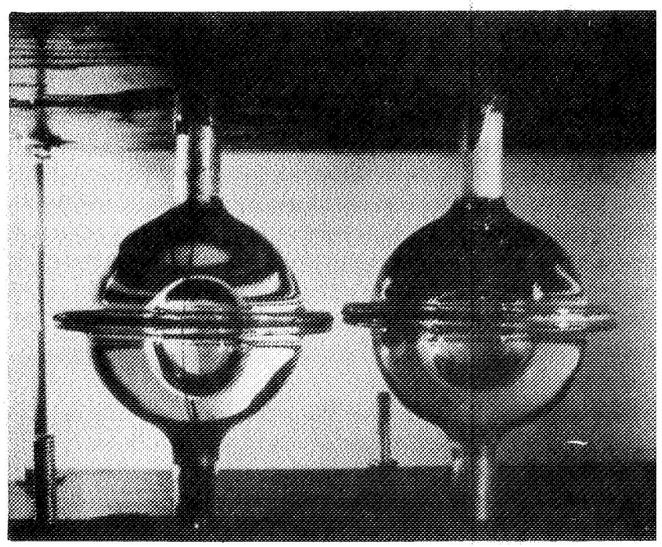

7) Bubble on Left Passes Bubble on Right

Figure

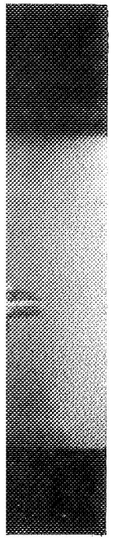

oad)

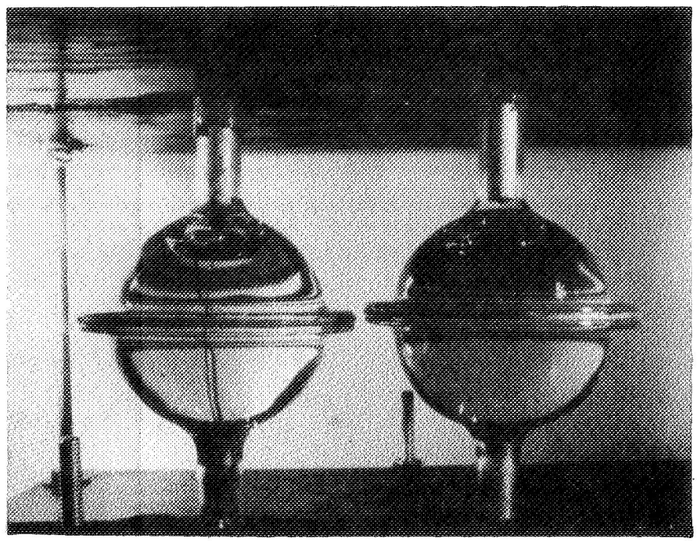

2) Initially Identical Bubble Formation

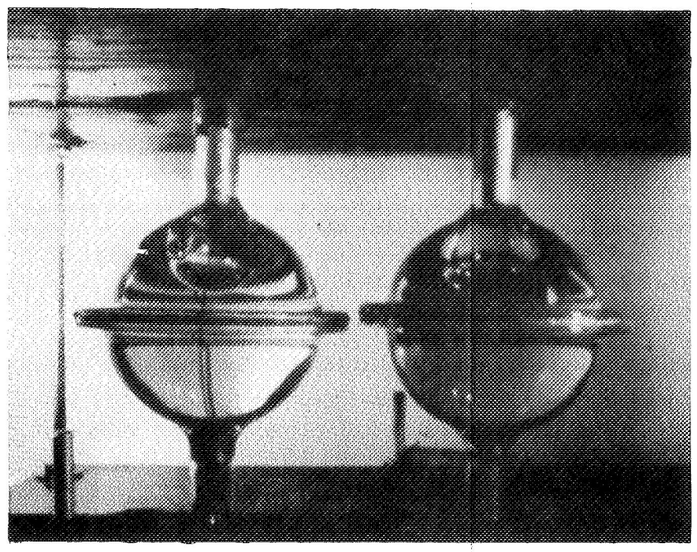

3) Post Begins to Interfere, Slowing Bubble Formation

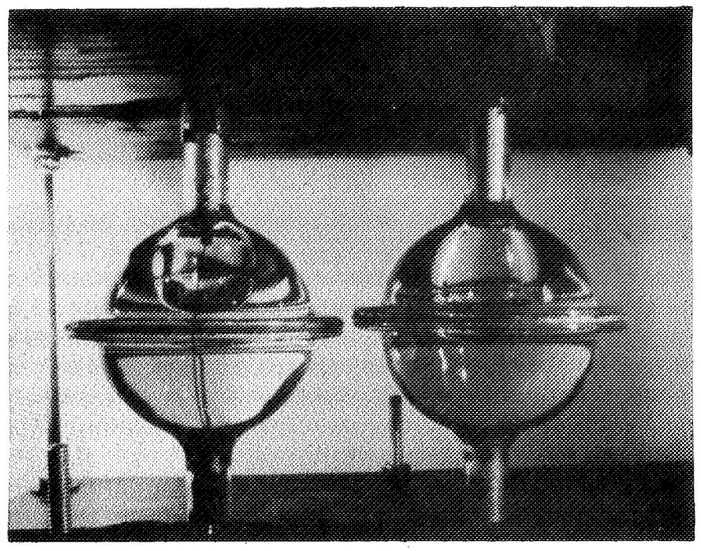

4) Meniscus Forms at Post

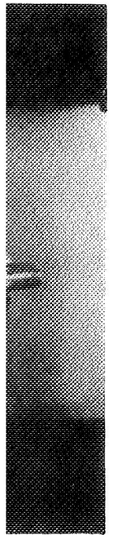

ɔm

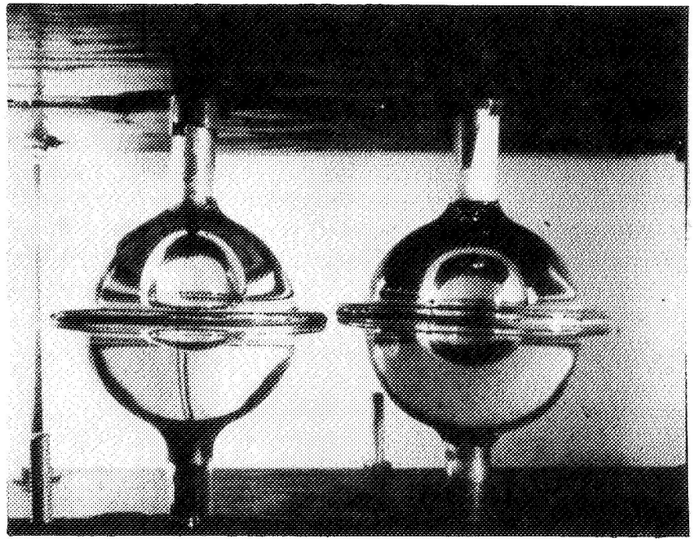

6) Bubble on Left Still Behind Bubble on Right

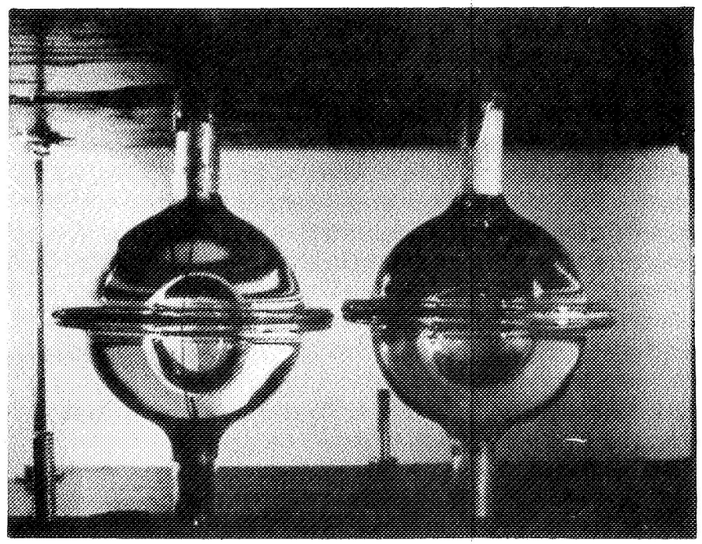

7) Bubble on Left Passes Bubble on Right

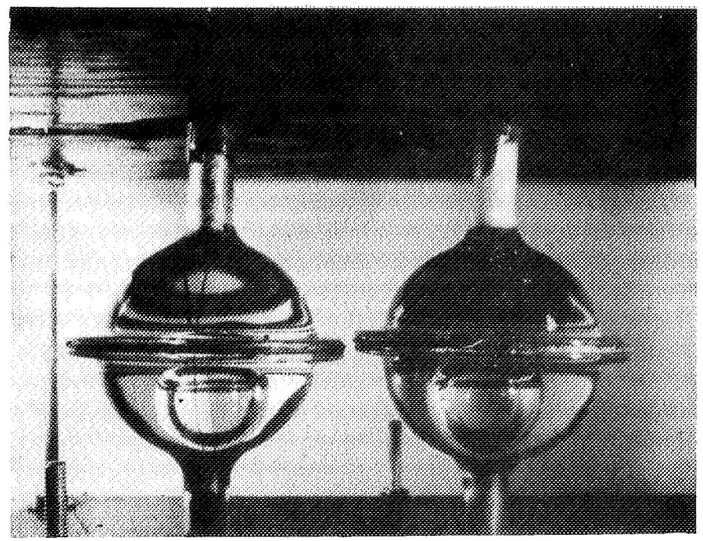

8) Bubble on Left Strikes Bottom First

Figure V-8 Frames from Motion Picture Film of Fruhof Test Run No. 12, Showing Progressive Fluid Motion through Test

2 3

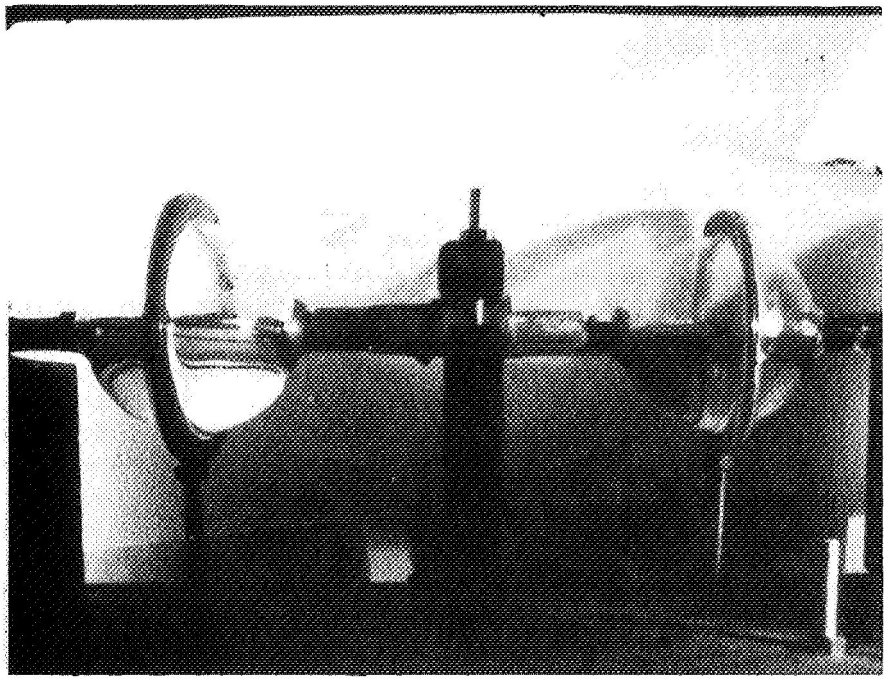

a) Initial 1-g Configuration (50% liquid load)

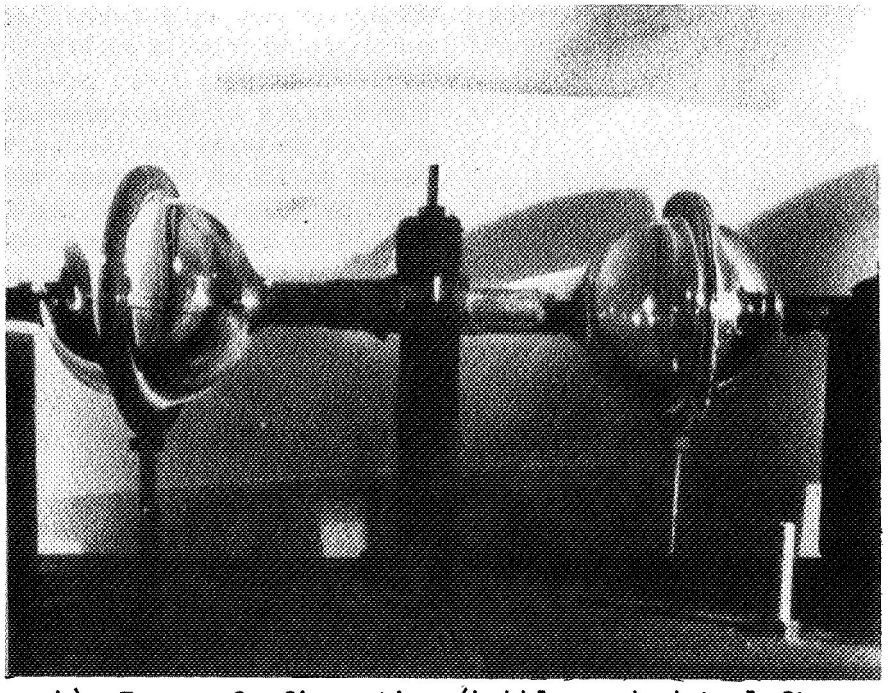

b) Zero-g Configuration (bubble pushed to left side in left sphere; bubble symmetric in right sphere)

Figure V-9 Frames from Motion Picture Film of Fruhof Test Run No. 15

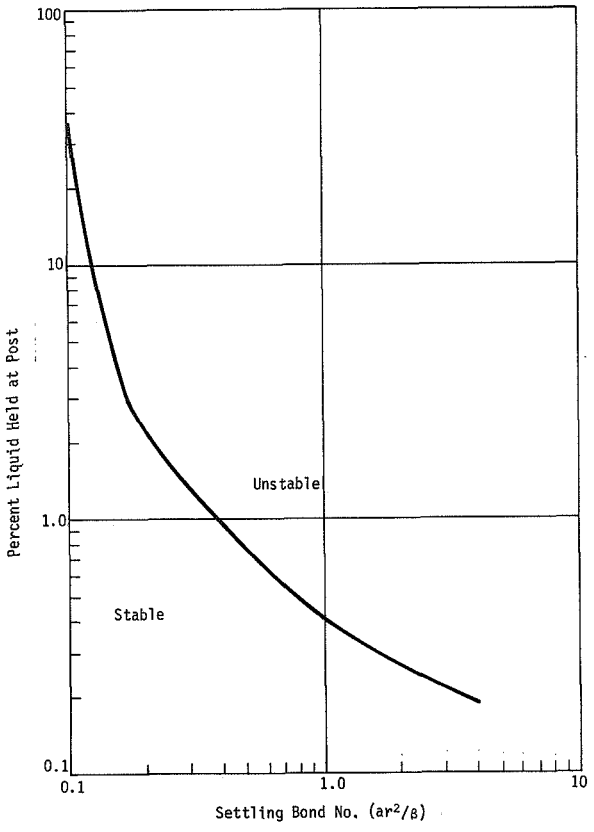

Figure V-10 Effect of Negative Acceleration on the Holding Power of the Ullage Standoff Post

The results of the test program show that the ullage standoff pillar performs well in zero g. A critical question is the ability of the device to hold liquid over the outlet under an axial acceleration tending to position ullage at the outlet.* Computer calculations of interface shapes for negative, nonzero Bond numbers were made. For a given liquid level, a sequence of increasing negative Bond numbers were input to the computer until the numerical technique could no longer find a static equilibrium interface condition. The failure to find a solution was due to rapidly increasing program convergence difficulties. The last solution found serves as a conservative estimate of the stability criterion. Figure V-10 presents the results of the calculations. If, for example, a liquid volume equal to 1% of the tank volume must be positioned at the tank outlet to guarantee successful engine start, then the magnitude of the Bond number acting to move liquid away from the outlet due to drag must be less than 0.4. This requirement is equivalent to holding the gravity level below 2.2×10^{-6} g before engine start on Mission A, and below 2.3×10^{-5} g before engine start on Mission B. The mission acceleration environments (Tables II-2 and II-4) show that this is satisfied by more than one order of magnitude on Mission A_1 and by more than two orders of magnitude on Mission B.

*This type of acceleration is termed a negative acceleration since it tends to move liquid away from the tank outlet; a positive acceleration tends to position liquid at the outlet.

The 10^{-7} g environment acting prior to an engine burn for Missions A_1, A_2, and B, has no perceptible effect on the holding power of the standoff pillar. However, for other missions such as Earth orbit and lower altitude Mars orbit missions, the drag force on the spacecraft could be large enough to overcome the required liquid holding capability of the standoff device. There are a number of design steps that may be used in the spectrum between the simple pillar and the fine mesh screen trap (Chapter IV) to hold liquid under gravity, or acceleration, forces between 10^{-7} and 1 g. Some modifications are presented in the following paragraphs.

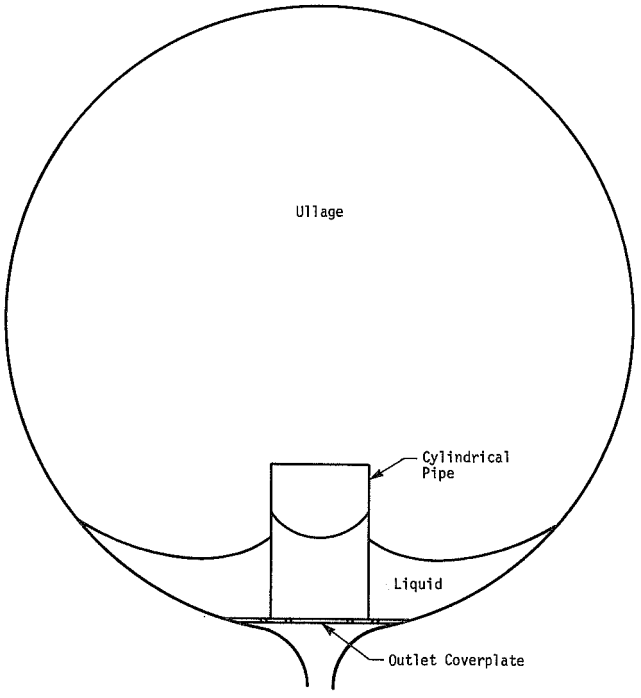

Figure V-11 Hollow Ullage Standoff Pillar or Standpipe Concept

A hollow ullage standoff post (or standpipe) will hold more liquid at the outlet (Fig. V-11). The pipe diameter can be optimized to provide the maximum surface tension stabilization. A perforated coverplate may be required over the outlet, however, to avoid free-surface pull-through during the transient settling at engine startup. Multiple, concentric standpipes can be used to further increase the surface tension holding capability by decreasing the free-surface radius of curvature inside the annuli. This type of configuration is shown in Figure V-12.

Another approach to improving the surface tension holding power of the ullage standoff device is to add vanes at its base, as first proposed by Martin Marietta in 1968 (Ref V-18). The vanes (Fig. V-13) divide the liquid into separate compartments that afford smaller radii of curvature to the free-surface of the liquid. The smaller radii increase the surface tension force acting on the liquid. Some possible advantages of vanes over the standpipe configurations include a lessening of the surface dropout problem and antivortexing. The addition of vanes is equivalent to adding

concentric standpipes. As the negative gravity holding requirement increases, a point is reached where a closed trap device is simpler and more attractive.

A simple trap design consists of a plate with large openings positioned above the outlet. The holes are sized small enough to hold (stabilize the interface) against the design g-level, but large enough to permit any trapped ullage gas bubbles to escape during thrusting. It is designed to be full of liquid prior to engine firings. The trap volume is large enough to supply gas-free liquid to the engine until the bulk propellant is settled. Once settling is accomplished, buoyancy forces will tend to purge ullage from the trap.

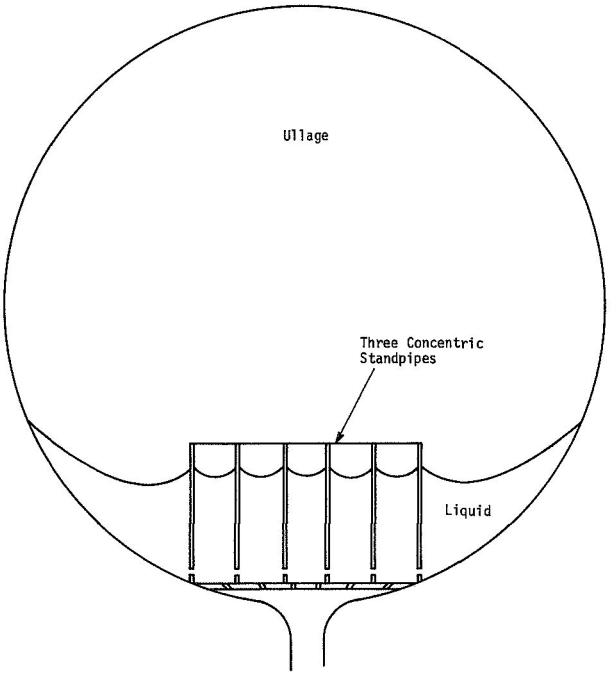

Figure V-12 Multiple Concentric Standpipe Concept

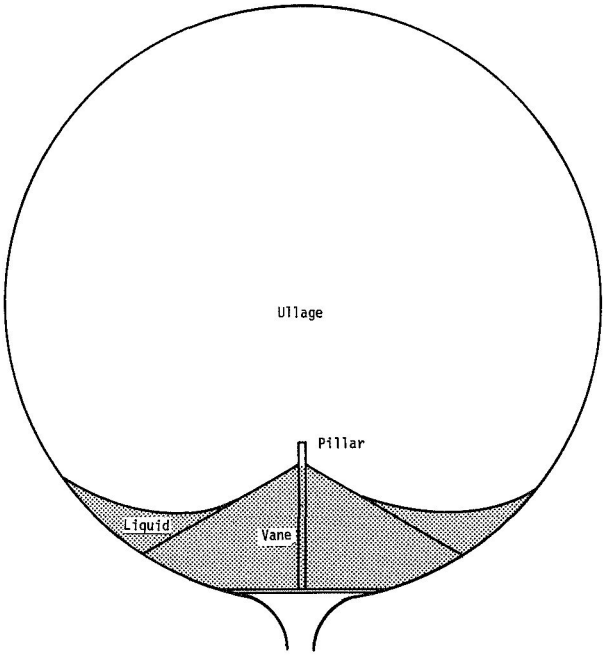

Figure V-13 Ullage Standoff Pillar with Vanes Concept

Successful trap operation in a high negative-g field precludes the use of a plate with holes large enough for trapped ullage gas purging. Descriptions of these systems are presented in detail in Chapter IV.

The Fruhof concept is an acquisition device that depends on liquid being located in its most stable configuration, i.e., over the outlet and in contact with the single post. A second, less stable liquid configuration exists where the liquid is not in contact with the outlet under certain conditions, namely: the tank is not perfectly spherical; the liquid contact angle is not zero; or the gravity level is not zero. Two stable configurations in zero g for a sphere 20% full of liquid having a nonzero contact angle are shown in Figure V-14. In the right-hand figure, the small amount of liquid over the outlet is at a lower pressure than the bulk liquid at the opposite end of the tank. Since there is no liquid communication between the two regions, the condition shown is stable. The bulk liquid free surface is spherical with its radius of curvature defined by the amount of liquid and its contact angle with the spherical wall.

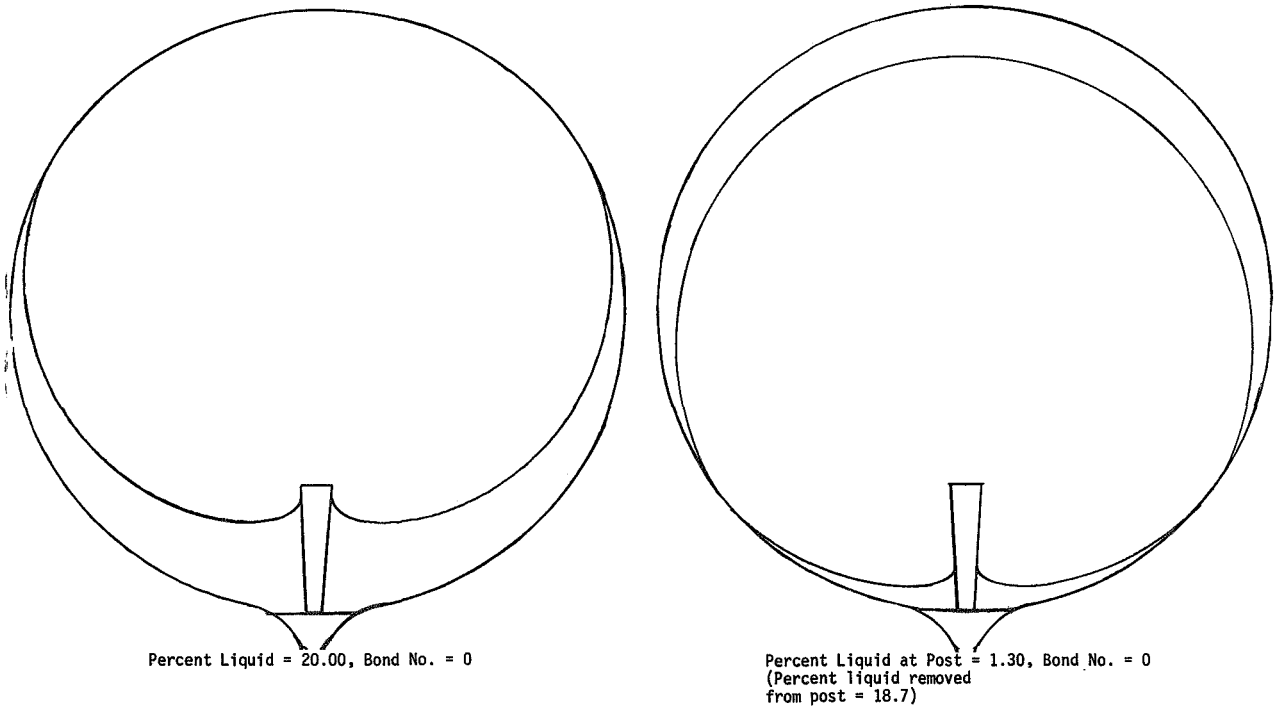

Figure V-14 Comparison of Two Stable Liquid Configurations, Showing Free Surface Shape Distortion by Standoff Post

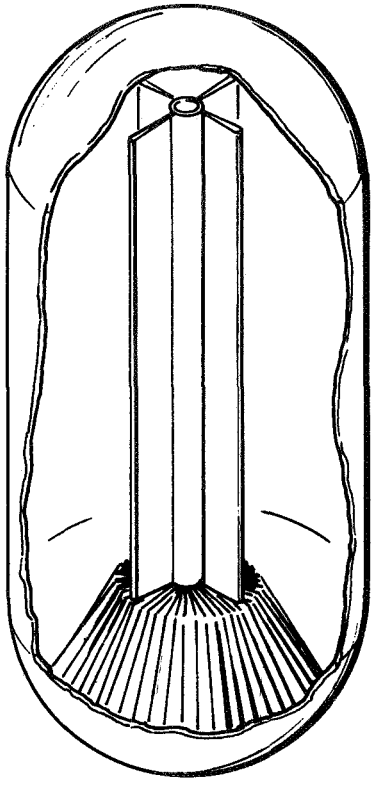

Figure V-15 Capillary Duct and Sump Concept

The Martin Marietta capillary sump and duct concept (Ref V-18) shown in Figure V-15, is one way to provide communication between the two stable regions. Such a device is similar to the current design for the Viking Orbiter (Ref V-19). The cruciform between the top of the tank and the vanes at the outlet fills with liquid to satisfy contact angle and free-surface curvature requirements. Once the liquid in the cruciform connects the bulk liquid at the top of the tank to the liquid over the outlet, the pressure difference will cause nearly all of the propellant to flow to the outlet region, which is its most stable position.

A major disadvantage of having the communication channel on the axis of the tank is that a considerable amount of liquid may possibly orient itself on the tank in contact with neither the tank top nor the tank bottom. Simple algebraic calculations on the intersection of two spheres representing a liquid with a 2° contact angle show that such an isolated liquid pocket could be over 2% of the tank volume. Another consideration is that the channel on the axis acts to orient liquid at both ends of the tank. At low liquid load levels, the half of the liquid oriented at the top of the tank will undergo large amplitude settling motion at engine start. This motion may cause vapor ingestion. Placing the communication channel on the tank axis also creates the possibility of large scale propellant asymmetry at engine startup. Liquid asymmetric settling can cause vehicle control stability difficulties (Ref V-19).

The direct method to minimize liquid pockets removed from the outlet is to place communication channels along the tank wall instead of on the tank axis. Any fluid pocket away from the post will be on the wall and will have a higher pressure than the liquid at the post. Providing a continuous liquid path along the wall between the two liquid regions causes the liquid to flow to the low pressure region at the post.

The number of channels placed on the wall from the post to the top of the tank determines the size of liquid pockets that are not in communication with the pillar. Four channels, 90° apart, connected to the pillar and to each other at the tank top reduce the maximum liquid pocket to less than 1% of the tank volume. Eight channels, 45° apart, further reduce the maximum liquid pocket size to less than 0.4% of the liquid volume.

Vehicle accelerations can move liquid away from the outlet and drain most of the liquid from the exposed portions of the communication channels. After an acceleration is terminated, the channels first refill with liquid by capillary pumping, and then carry the propellant back to the pillar. The channel cross-section shape and size determines the refill capability and the time required to reorient the liquid over the outlet.

The liquid pumping capability of the communication channels was tested as part of the drop test program to verify the ullage standoff post concept. Loops fashioned from three-mil diameter wire were positioned adjacent to the interior sphere wall and attached to the post (Fig. V-8 and V-9). Two loops, 90° apart, were used. The wires, as seen in drop tower motion picture results, pumped so slowly that they did not fill in the test time available. However, the V-groove at the junction of the two sphere halves filled very rapidly. The radius of curvature required in the V-groove was much smaller than that at the wire loops, increasing its pumping power considerably. These tests confirmed that sharp corners on the channels aid in guaranteeing a continuous liquid path between the standoff post and any isolated liquid. Filling the channel by surface tension pumping requires that a stable interface not form in the channel. A stable interface requires uniform curvature, which cannot occur in a sharp-cornered channel with the propellants considered in this study, because of their near-zero contact angle.* For this reason, V-shaped channels, as shown in Fig. V-16, are proposed.

*As the liquid moves up the sharp corner to satisfy contact angle, the second principal radius of curvature of the liquid/gas interface becomes smaller, resulting in a lower liquid pressure in this region (Eq [V-1]). This pressure gradient causes liquid to flow along the channel.

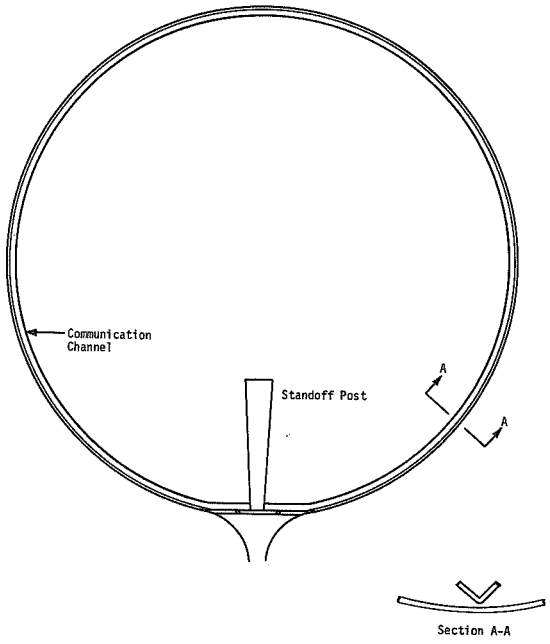

Figure V-16 Ullage Standoff Post with Communication Channel Concept

Communication channels are not required with liquids having a zero contact angle. However, to provide a more universal design, it is felt that the system should be capable of accommodating nonzero contact angle situations and communication channels should be incorporated in the low-g design.

A gap between the channel and the tank wall must be maintained to prevent contact and rubbing against the wall. The smaller the gap, the faster the channel refills; however, a large gap yields a larger liquid cross-section, which increases the volumetric flow rate.

Modeling of the hydrodynamics of the reorientation process was not possible during this study. However, reorientation time can be estimated from the characteristic capillary response time, $\sqrt{\rho r^3/\sigma}$ (Ref V-17). For the missions and propellants considered in this study, the estimate ranges from 100 to 500 seconds.

The liquid retention capability of instrumentation probes, cooling coils, and other protuberances is similar to the retention at the standoff pillar. Each probe will retain liquid in zero g as confirmed by drop tower tests of liquid/vapor sensors (Ref V-20). Therefore, the location and configuration of any instrumentation probes or other protuberances in the propellant tank must be considered in the detailed analysis and design of the propellant acquisition system flight hardware. If cooling coils, for example, are required within the tank for the space storable propellants they may be incorporated as part of the communication channels.

In summary, the search for a propellant acquisition device using surface tension that satisfied the requirements of Missions A_1, A_2, and B, but did not have to satisfy minus 1-g testability, has yielded a very simple design that consists of an ullage standoff post with communication channels near the tank wall.

B. FABRICATION AND ASSEMBLY

Aluminum is required for propellant compatibility on Mission A_1, and the alloy chosen for the tankage was 2219, as discussed in Volume I. It is recommended that the post and communication channels be made of 6061 Aℓ since it is easily welded, readily available, and the strength of 2219 Aℓ is not required. Figure V-17 shows an assembled propellant tank with the low-g acquisition device installed for Mission A_1. The tank, itself, consists of two hemispherical shells joined at a support ring with a pressurant inlet fitting at the top and an outlet fitting at the bottom. The ullage standoff post is a solid, machined metal piece formed so that its bottom serves as an outlet coverplate, as shown. Its height, equal to 42% of the tank radius, was chosen to provide precise axisymmetric ullage control for volumes greater than 50% of the tank volume. The post is joined to the outlet fitting at the rim of the coverplate section.

Propellant compatibility requires that the tankage for Missions A_2 and B be titanium, and the alloy 6Aℓ-4V Ti was chosen. The material selected for post and communication channels assembly is Ti-40, since the pure metal is more ductile and is easily welded.

Figure V-18 is a detail design drawing and shows fabrication and assembly details of the Mission B low-g acquisition device. The Mission A_2 design is identical (scalable to the tank dimensions), and for this reason a separate drawing is not presented. Figure V-19 shows the detail design of an alternate Mission B device (discussed in Section A); the ullage standoff pillar with vanes. The vanes provide greater liquid holding ability at the outlet. The design presented in Figure V-19 permits engine restart at three orders of magnitude greater vehicle drag than required for Missions A_2 and B. This performance increase, as seen, increases system complexity.

An alternate assembly with pressurant supplied through the outlet, requiring only one tank penetration, is included in Figure V-18. The concept is valid for all three missions. Two alternate hole patterns on the coverplate over the outlet are also shown. Both patterns are adequate to prevent gas ingestion if the post area should for any reason become dry. The Bond number stability criterion is

$$\left|a\rho r^2/\sigma\right| < \text{Bo critical} = 0.84, \qquad \text{[V-15]}$$

for no bubble breakthrough under a negative gravity or acceleration.

Considering all the propellants for Missions A_1, A_2, and B, it would require a negative acceleration greater than 0.07 g for ullage to be ingested into the feed line through the 0.25-in. diameter holes. The critical acceleration level (negative) is more than three orders of magnitude greater than anticipated on any of the missions. The second criterion is the interface stability provided by the holes against hydrostatic heads created by a lateral acceleration (parallel to the surface of the coverplate);

$$|\rho a h| < 4\sigma/r, \qquad [V\text{-}16]$$

for zero ullage breakthrough (where h is the maximum distance between holes). From Equation [V-16], the lateral acceleration for breakdown is greater than 0.02 g for Missions A_1, A_2, and B, which is again at least three orders of magnitude greater than that anticipated. The coverplate provides structural support for the post, as shown. If vanes are used (Fig. V-19), the coverplate is not needed.

Flat areas are machined at the base of the post to facilitate joining the communication channels to the post. The channels are also joined to the tank wall near the equator and to a free-standing junction hub at the top of the tank. A constant gap size is maintained between the tank wall and the channels. The gap chosen is large enough for ease of installation without severely penalizing its surface tension pumping capability. The V-shape purges ullage from the channels and was also chosen because of the ease of manufacture and assembly of the sharp-cornered sections.

The attachment and joining procedures are of particular concern. As with the 1-g testable design, at least four joining procedures are possible. Because both resistance welding and mechanical fastening tend to create contaminant trap areas, these procedures were eliminated from consideration.

For Missions A_2 and B titanium tankage, the 3003 Aℓ brazing process could be used for the joining operations of the ullage standoff post configuration. However, 3003 Aℓ brazing tends to anneal structural titanium alloys like 6Aℓ-4V. For effective installation of the Fruhof into the tank, the first assembly procedure after standoff post fabrication is joining the standoff post to the outlet fitting. Since the outlet fitting is a structural element of the propellant tank, use of 3003 Aℓ brazing in this joining step and in following steps appears undesirable because of the annealing problem. The thickness of the outlet fitting could be increased to reduce the effect of the loss of strength resulting from annealing; however, electron beam welding and fusion welding processes are also applicable and, therefore, were chosen as joining techniques for the Mission A_2 and B systems (Fig. V-18).

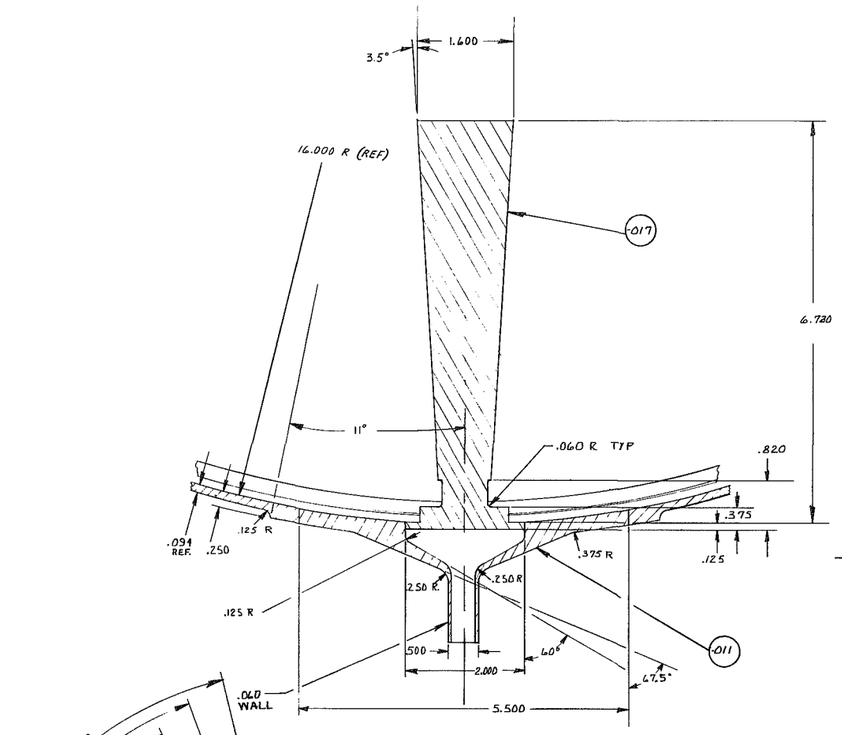

DETAIL D
ENLARGED PICTURE

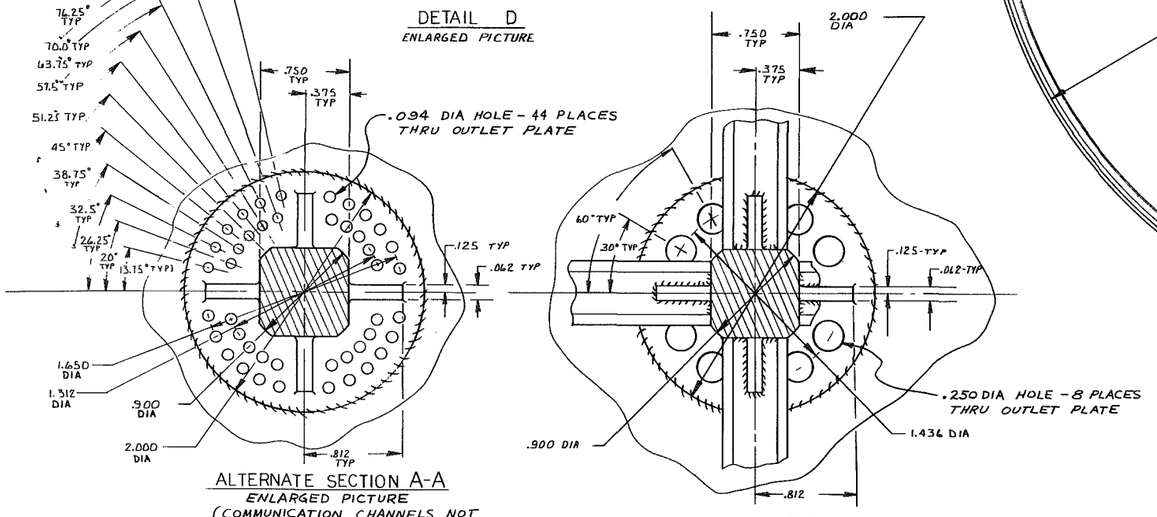

ALTERNATE SECTION A-A
ENLARGED PICTURE
(COMMUNICATION CHANNELS NOT SHOWN FOR CLARITY)

SECTION A-A
ENLARGED PICTURE

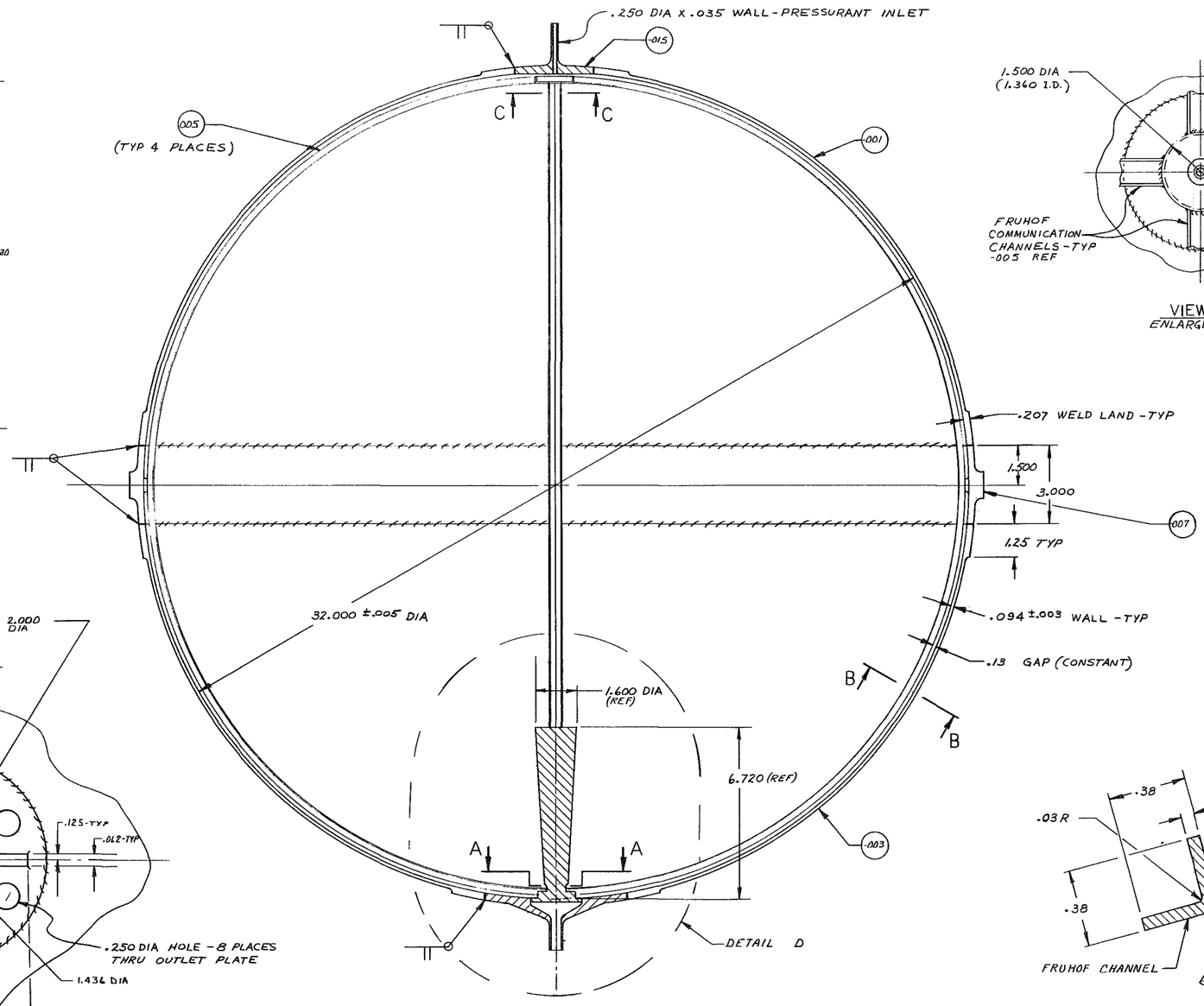

TANK ASSEMBLY
CROSS-SECTION VIEW

VIEW C-C
ENLARGED PICTURE

SECTION B-B
ENLARGED PICTURE

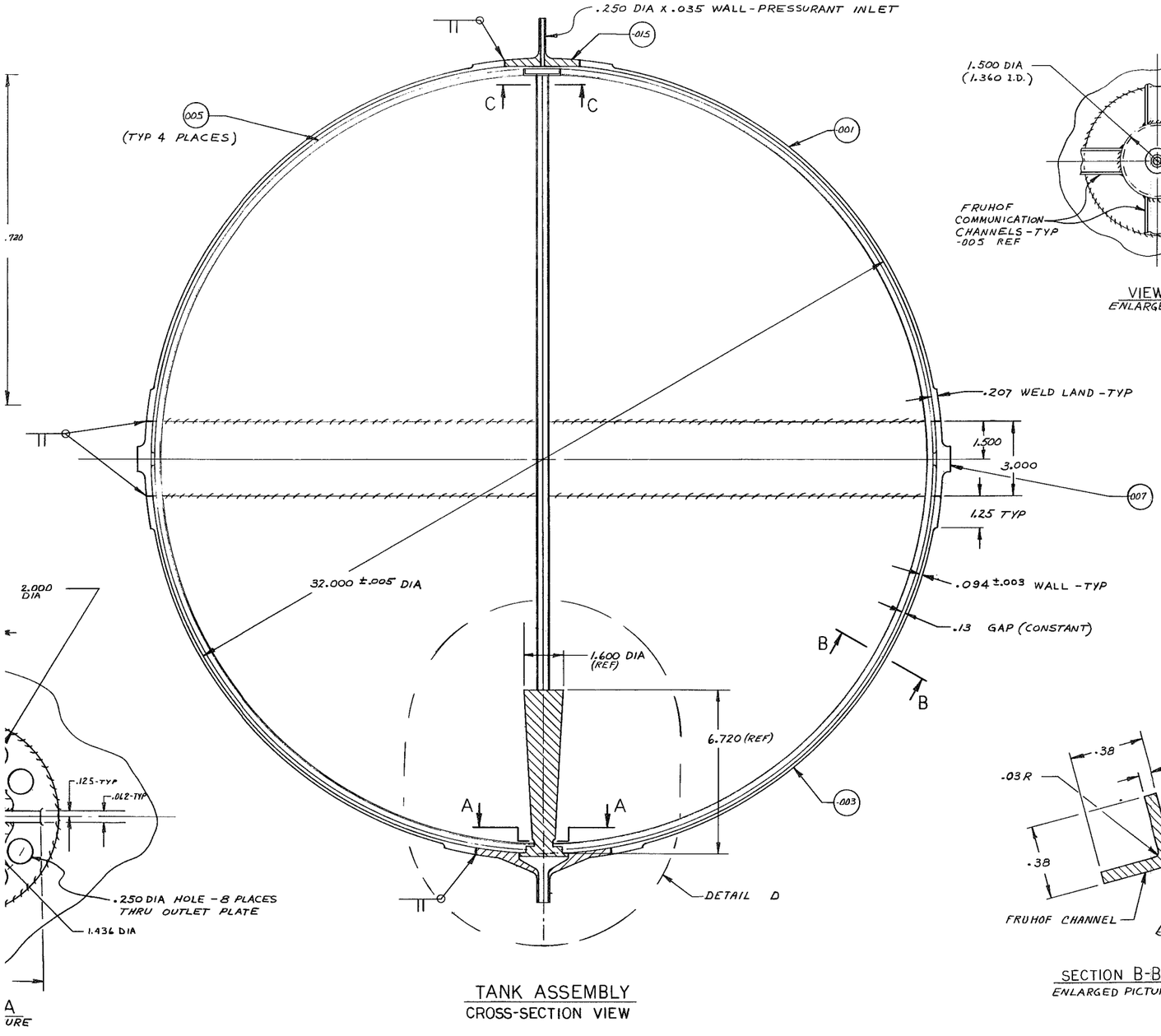

TANK ASSEMBLY
CROSS-SECTION VIEW

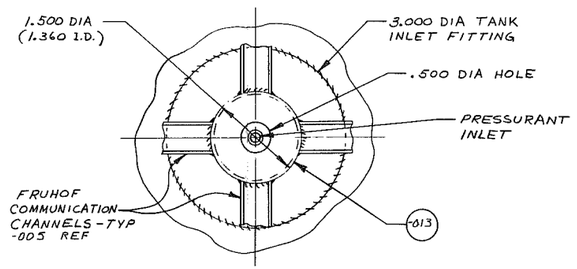

VIEW C-C
ENLARGED PICTURE

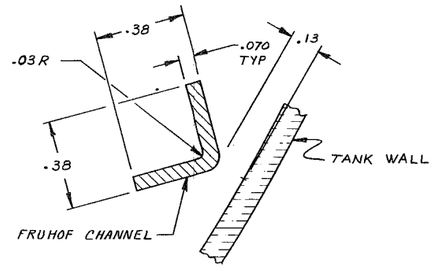

SECTION B-B
ENLARGED PICTURE

NOTES:

1. ALL TOLERANCES UNLESS OTHERWISE SPECIFIED .XX = ±.03 , .XXX = ±.010
2. ALL DETAILS TO BE JOINED BY FULL PENETRATION FUSION WELDS.

1	-017	PILLAR	ALUM 6061
1	-015	PRESSURANT INLET FITTING	ALUM 2219
1	-013	HUB FITTING	ALUM 6061
1	-011	PROPELLANT OUTLET FITTING	ALUM 2219
1	-007	SUPPORT RING	ALUM 2219
4	-005	CHANNEL	ALUM 6061
1	-003	TANK HEMISPHERE	ALUM 2219
1	-001	TANK HEMISPHERE	ALUM 2219
1	-009	TANK & EXPULSION ASSEMBLY	

T. Cassidy 0431 7/23/70

Figure V-17 Fruhof Low-g Design, Propellant Acquisition System for OF_2/B_2H_6 Mars Orbiter

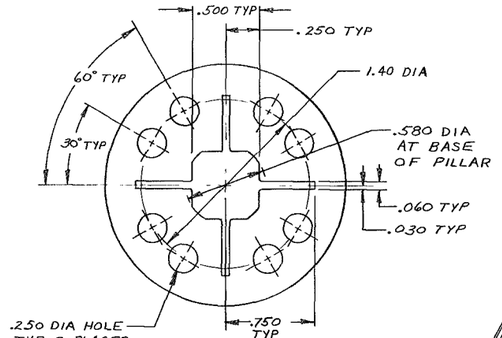

SECTION F-F

(COMMUNICATION CHANNELS NOT SHOWN FOR CLARITY)

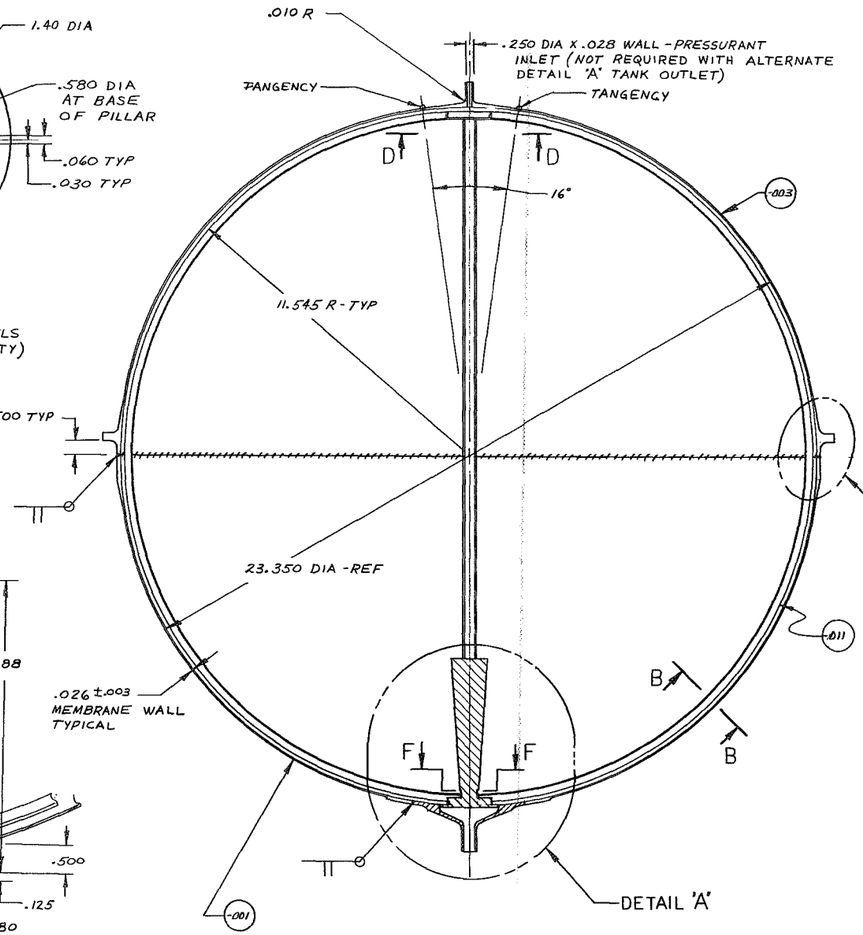

TANK ASSEMBLY

CROSS SECTION VIEW

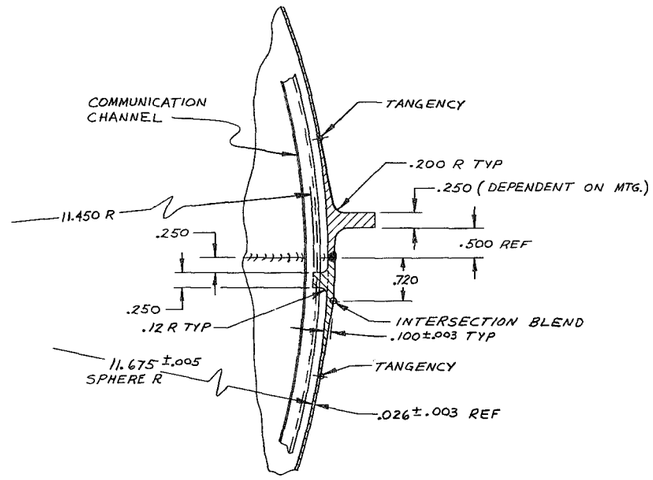

DETAIL "C"

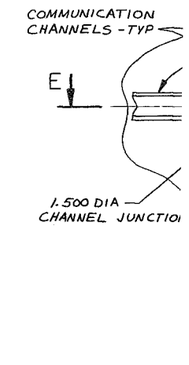

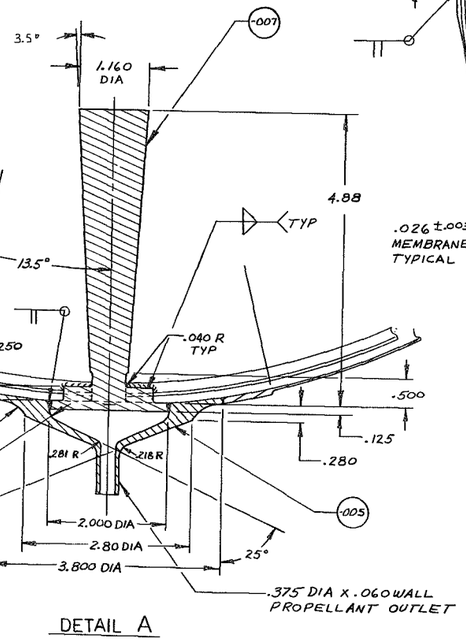

DETAIL A

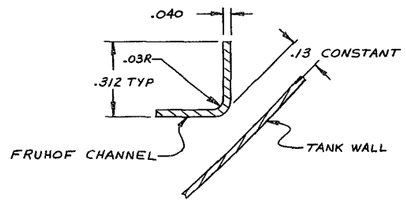

SECTION B-B

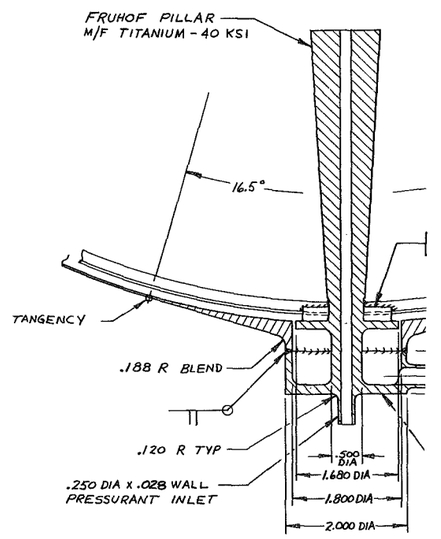

ALTERNATE DETAIL

(SAME AS DETAIL 'A' EXCEPT AS SHOWN)

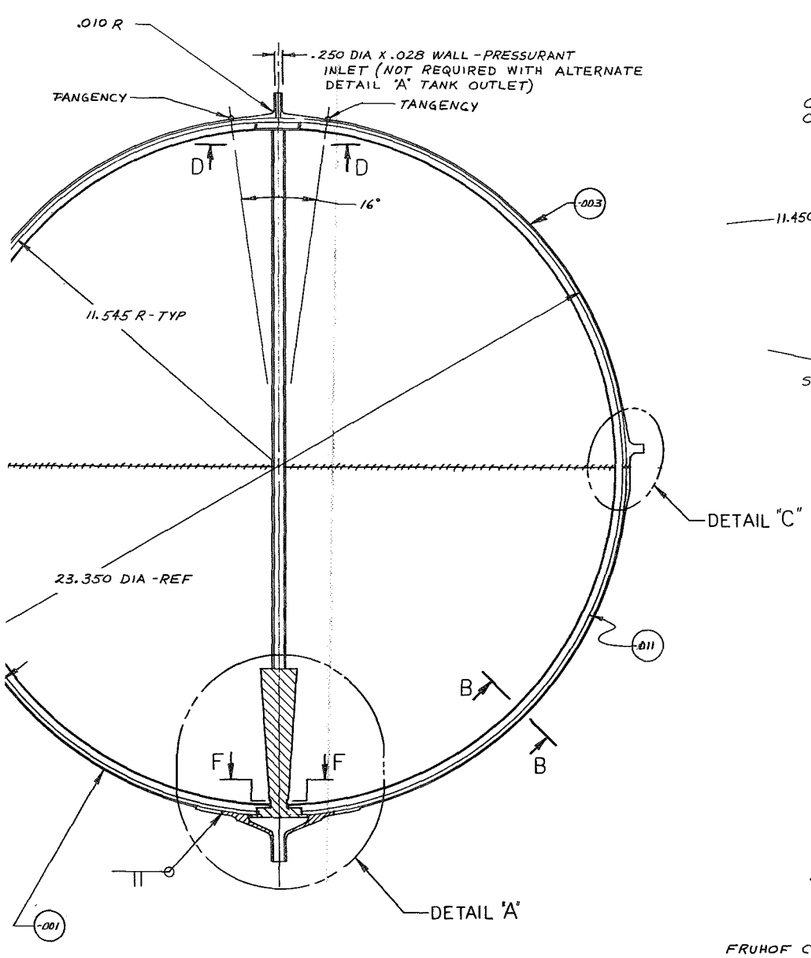

TANK ASSEMBLY

CROSS SECTION VIEW

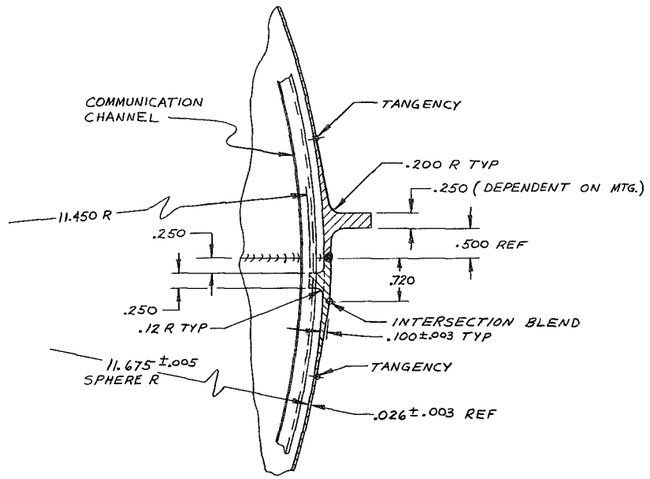

DETAIL "C"

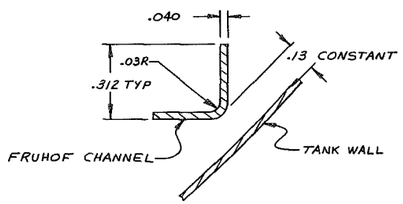

SECTION B-B

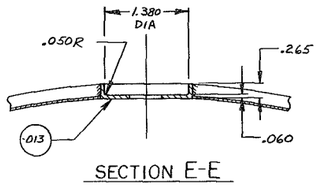

SECTION E-E

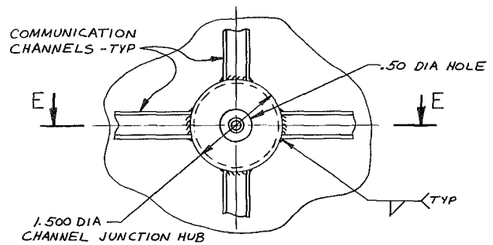

VIEW D-D

NOTES:

1. ALL TOLERANCES UNLESS OTHERWISE SPECIFIED: .XX = ± .03 , .XXX = ± .010
2. ALL DETAILS TO BE JOINED BY FULL PENETRATION FUSION WELDS.

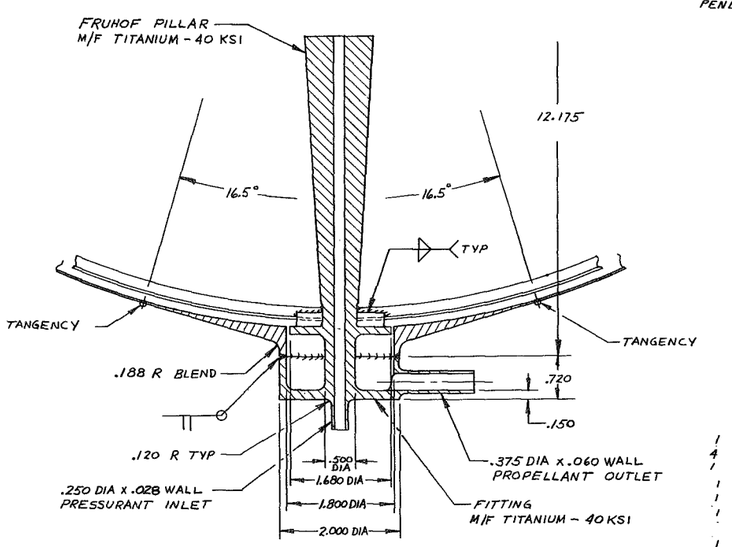

ALTERNATE DETAIL A

(SAME AS DETAIL "A" EXCEPT AS SHOWN)

1	-013	HUB FITTING	TITANIUM RMI-55 REACTIVE METALS INC.
4	-011	CHANNEL	TITANIUM RMI-55 REACTIVE METALS INC.
1	-007	PILLAR	TITANIUM RMI-40 REACTIVE METALS INC.
1	-005	PROPELLANT OUTLET FITTING	TITANIUM 6AL-4V
1	-003	TANK HEMISPHERE	TITANIUM 6AL-4V
1	-001	TANK HEMISPHERE	TITANIUM 6AL-4V
1	-009	TANK & EXPULSION ASSEMBLY	

T. Cassidy 0931 7/31/70

Figure V-18 Fruhof Low-g Design, Propellant Acquisition System for Grand Tour Mission

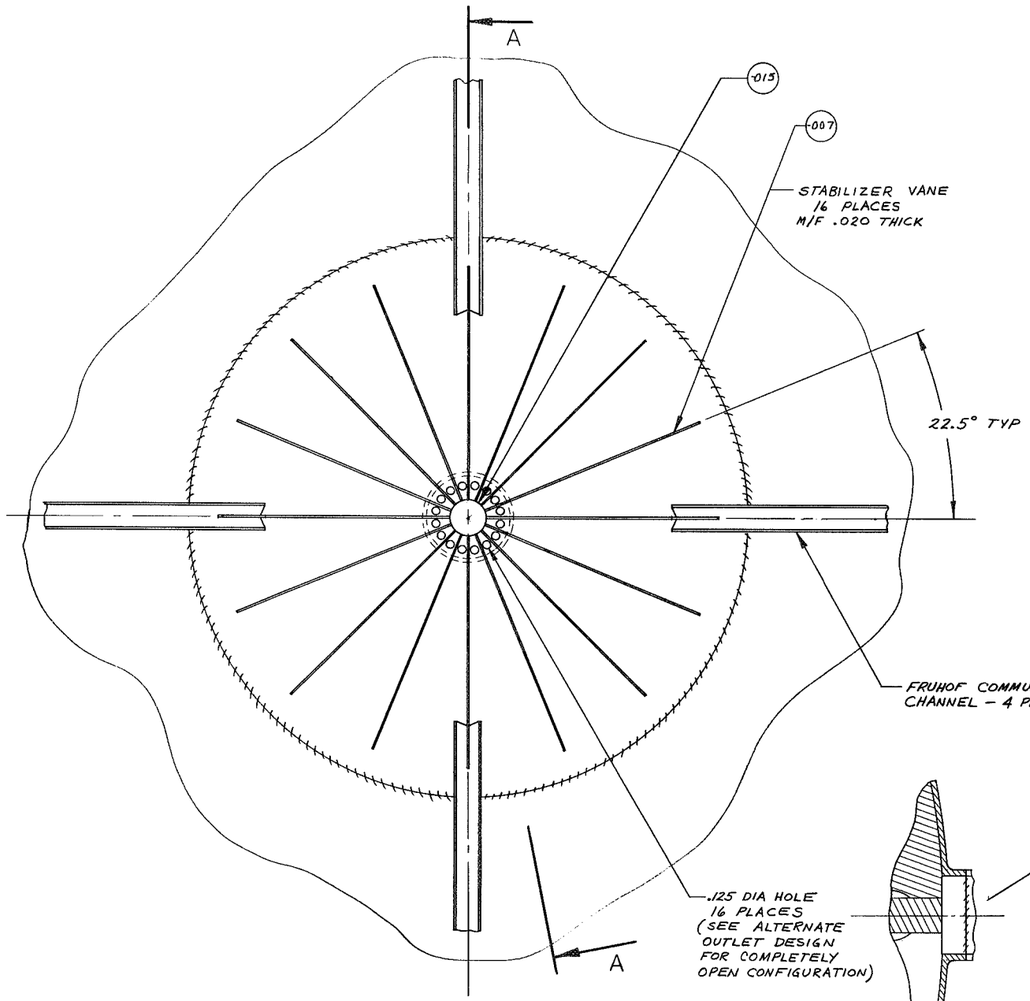

TANK BOTTOM VIEW

ALTERNATE
OUTLET

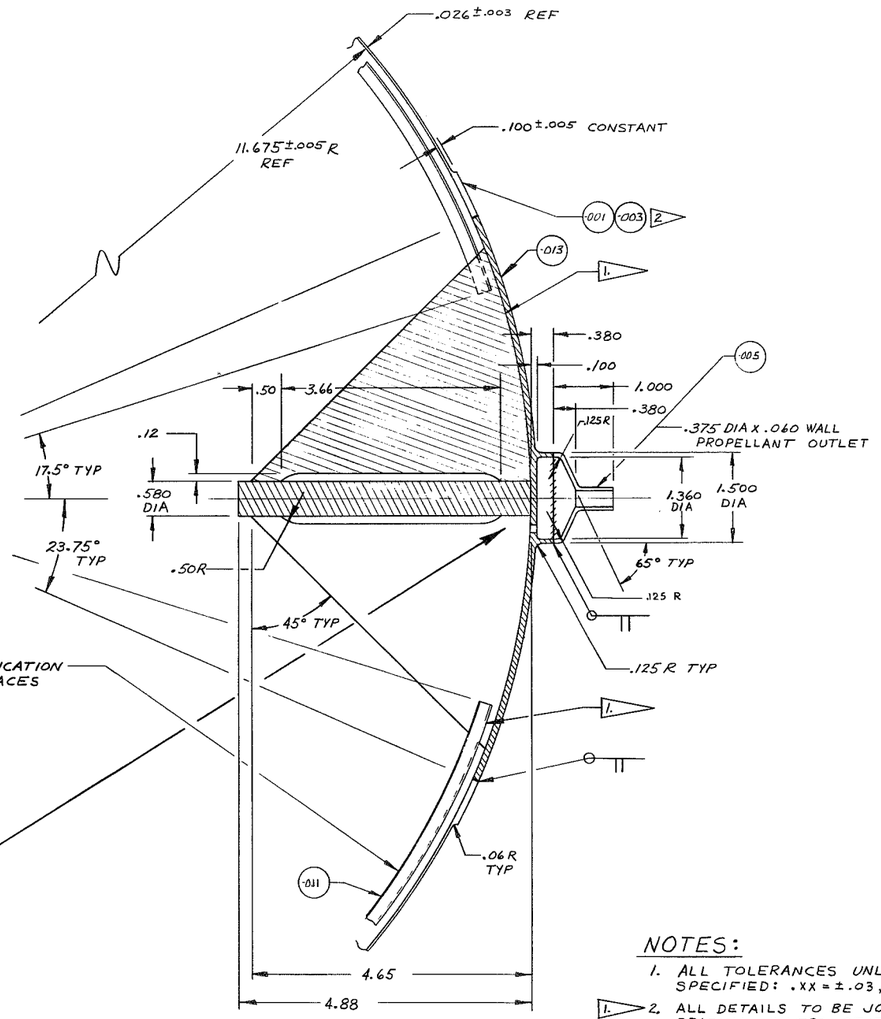

SECTION A-A

NOTES:

1. ALL TOLERANCES UNLESS OTHERWISE SPECIFIED: .XX = ±.03, .XXX = ±.010
1. 2. ALL DETAILS TO BE JOINED BY FURNACE BRAZING UNLESS OTHERWISE SPECIFIED (SEE FABRICATION AND ASSEMBLY DISCUSSION)
2. 3. HEMISPHERE NOT SHOWN

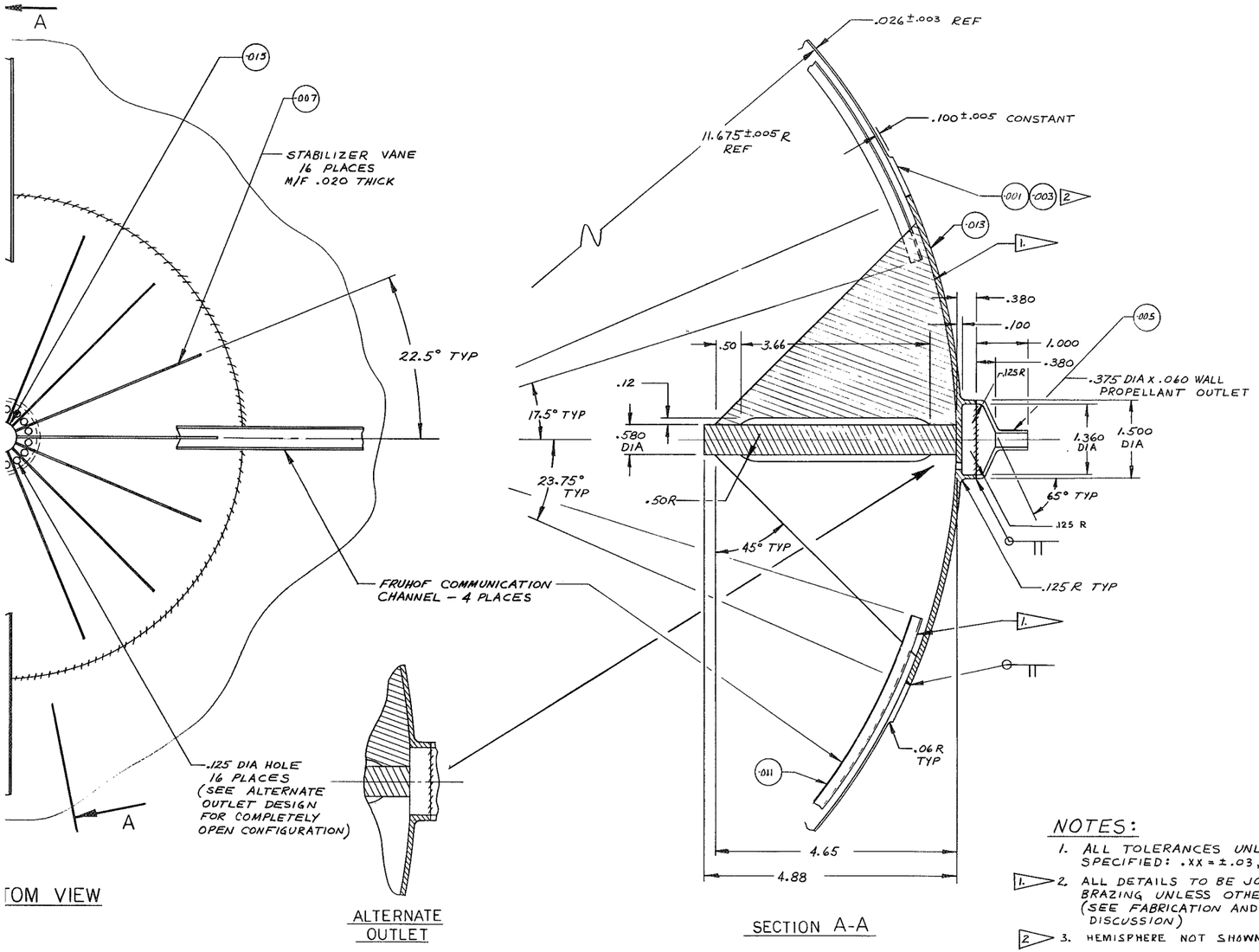

NOTES:

1. ALL TOLERANCES UNLESS OTHERWISE SPECIFIED: .XX = ±.03, .XXX = ±.010
2. ALL DETAILS TO BE JOINED BY FURNACE BRAZING UNLESS OTHERWISE SPECIFIED (SEE FABRICATION AND ASSEMBLY DISCUSSION)
3. HEMISPHERE NOT SHOWN

1	-015	PILLAR	TITANIUM RMI-55	REACTIVE METALS
1	-013	POLAR CAP	TITANIUM 6AL-4V	
4	-011	CHANNEL	TITANIUM RMI-55	REACTIVE METALS
16	-007	VANE	TITANIUM RMI-55	REACTIVE METALS
1	-005	PROPELLANT OUTLET FITTING	TITANIUM 6AL-4V	
1	-003	TANK HEMISPHERE	TITANIUM 6AL-4V	
1	-001	TANK HEMISPHERE	TITANIUM 6AL-4V	
1	-009	TANK & EXPULSION ASSEMBLY		

T. Cassidy 0431 8/11/70

Figure V-19 Fruhof Low-g Design, Propellant Acquisition System with Vanes for Grand Tour Mission

For the Mission A_1 aluminum tankage, electron beam or fusion welding appear to be the only joining processes available because of the incompatibility of all Aℓ brazing alloys with the propellant.

For the vaned post configurations, either one piece machining or brazing of the vanes to the post seem applicable. Welding the individual vanes to the post becomes impractical because of restricted space. For Mission A_1, one piece machining is recommended because of the unavailability of compatible braze alloys. For Missions A_2 and B, 3003 Aℓ brazing is recommended.

The steps of tank assembly and installation of the ullage standoff post are as follows:

Missions A_2 and B

1) Weld standoff post to outlet fitting;
2) Weld communication channels to junction hub;
3) Weld channel assembly to standoff post;
4) Weld outlet fitting to bottom spherical shell;
5) Weld channel assembly to bottom spherical shell;
6) Weld pressurant inlet fitting to top spherical shell (if required);
7) Closure weld top spherical shell to bottom shell.

Mission A_1

1) Same as above;
2) Same as above;
3) Same as above;
4) Weld bottom spherical shell to support ring;
5) Weld outlet fitting to bottom spherical shell;
6) Weld channel assembly to support ring;
7) Weld pressurant inlet fitting to top spherical shell (if required);
8) Closure weld top spherical shell to support ring.

Quality control checks by X-ray of each weld are essential. Checkout of the structural integrity under simulated launch loads, including slosh and vibration, is required. Verification of the structural compatibility with mission temperature extremes is necessary. A quality control check on the maintenance (within acceptable limits) of low contact angle over long periods of aging is needed to guarantee maximum surface tension orientation and control capability.

Unlike the 1-g testable designs, the reasons for precise cleaning of the designs presented here are, at least, two-fold: propellant-material compatibility; and nondegradation (increase) of propellant contact angle. If certain organic contaminants (stearic and oleic acids, paraffin oil, etc) are present in sufficient quantity, propellant contact angles may increase to a point where operation may be seriously compromised, as discussed. Cleaning procedures must, therefore, be selected and used so contaminants that degrade propellant or propellant/material compatibility like oxide coatings (the major cleaning concern for the 1-g designs) and contaminants that cause an increase in contact angle are minimized or eliminated.

Based on various cleaning procedures usually employed for aerospace tankage application (Ref V-8), the use of acid-type cleaning techniques as the sole cleaning process (Chapter IV) does not remove contaminants that affect contact angle. Pure alkaline cleaning procedures (Ref V-8) are satisfactory, although prior acid cleaning does degrade their effectiveness. A vacuum-annealing process removes the type of contaminants that affect contact angle and has the added advantage of being able to remove oxides, as does acid cleaning. Acid-type cleaning techniques, therefore, cannot be the sole cleaning process. Rather, acid cleaning must be followed by an alkaline cleaning technique or possibly a vacuum-anneal. For these reasons, the following cleaning procedures are recommended for the low-g design of Missions A_2 and B:

1) Prior to assembly, all parts (except the tank and outflow port assemblies) should be cleaned by vacuum annealing. Since the tank and outflow port assemblies cannot be vacuum-annealed and yet must be cleaned of all oxides, an acid cleaning process will be used;

2) An alkaline cleaning process should then follow for complete cleaning. As with the 1-g testable designs, all joining processes should be performed under strict cleanliness and inert atmospheres;

3) The last cleaning operation (acid cleaning, followed by an alkaline cleaning) should be performed after the final tank closure weld has been made.

Considering Mission A_1, the effect of contaminants on the OF_2 and B_2H_6 contact angles is practically nil, due to their very low surface tensions. No contaminant will survive when exposed to OF_2. Therefore, contaminants increasing contact angle are not a serious concern for Mission A_1. It is an academic consideration, however, since for fluorine service, no contaminant, whether it affects contact angle or not, can be tolerated. Therefore, the same cleaning procedures as recommended for Missions A_2 and B, should also be applied to Mission A_1. Also, as with the 1-g designs, use of GF_2 for passivation prior to propellant loading is recommended. The simplicity of the Fruhof design does allow it to be cleaned easily.

C. OPERATIONAL DISCUSSION

1. Prelaunch

A major attractiveness of the simple ullage standoff post design is that there are no special handling and loading requirements (except for the need for cleanliness). The design provides no place for ullage to be trapped during loading, and tilting after loading is of no concern. There is no special restriction on emptying and refilling cycles resulting from checkout procedures during prolonged holds on the launch pad.

2. Boost Phase

The high-g environment during boost, along with slosh and vibration, are structural considerations only. The design is rigid and can easily meet the launch loads.

Launch with the tank outlet pointed away from Earth, as with Mariner '71, presents a problem in that the ullage may be forced into the propellant feed line and trapped after insertion into the low-g space environment. If an inverted tank attitude is a launch requirement, one of several options could be incorporated in the design. For example, a fine mesh screen at the coverplate will prevent gas from entering the feed line. An overboard vent of the feed line in zero g could also be used to refill the line with liquid. Another option is a capillary pumping system to bring liquid back into the feed line while displacing ullage. Also, the tank could be initially pressurized at a low level with propellant vapor. Once in zero g, the tank pressure would then be raised with pressurant to collapse any vapor in the feed line. The choice of a given method will, of course, depend on particular mission requirements.

At boost-thrust termination and entrance into low g, the liquid free-surface relaxes from its nearly-flat, high-g configuration to a near-spherical shape. The addition of the vehicle structural relaxation and slosh kinetic energy may conceivably cause sufficient turbulence to produce a number of small ullage bubbles. Some might locate at the outlet coverplate and, at engine startup, may be drawn into the feed line, particularly if the thrust buildup is sufficiently slow. Drop tower studies (conducted at Martin Marietta, Ref V-21) of the slosh amplification at the step transition from 1 to zero g indicate that the fluid motion is not violent enough to break up the ullage into small bubbles. However, these data are qualitative. While the possibility of gas ingestion by this mechanism appears remote for the missions of interest, further verification is merited.

The transient motion associated with small ullages as in Missions A_1 and A_2, (nominally 10%) is illustrated in Figure V-8. The liquid motion created by the free surface reorientation carries the ullage bubble from the top of the tank to the bottom. With the Fruhof pillar, for Mission A_1 and A_2 the ullage bubble will be repulsed and kept away from the outlet. The drop tower tests of the Fruhof concept conducted under this study show that the boost termination phase of the A_1 and A_2 Missions presents no hydrodynamic problems.

3. Low-g Phase

Following the decay of propellant sloshing caused by stage separation, the spacecraft will reorient itself to a celestial reference, e.g., the sun on the Z-axis and a star, Canopus, on an off-axis (Ref V-22). The continuous thrusting levels of the attitude control system during roll, pitch, and yaw maneuvers to gain celestial reference may be sufficiently large to move ullage over the tank outlet (Table II-2 and II-4). However, the ullage will not enter the feed line because of the small drain holes in the outlet coverplate. Once celestial reference is attained, and the continuous thrusting ends, the communication channels will provide a path for liquid to reorient over the outlet in the designed maximum stability configuration. The periodic ACS thrusting to maintain celestial reference is of such short duration relative to the low-g liquid characteristic response time, $\sqrt{\rho r^3/\sigma}$, that disturbance of the liquid will be slight unless the ACS thrust period is near the natural slosh period of the liquid. Then the small slosh energy can accumulate, eventually yielding large amplitude liquid motion. Analysis of slosh effects has not been possible within the scope of this program.

Prior to all engine firings, the spacecraft must be aligned on the desired thrust axis. This requires switching to an inertial reference, then executing a roll motion to align the pitch plane, pitching to align the thrust axis as desired, and then executing a second roll to align the spacecraft antenna toward Earth. This continuous thrusting may cause ullage to be oriented over the outlet. The Bo associated with the roll maneuver thrust on Mission A_1 is about 20 for the oxidizer and about 4 for the fuel. These are sufficient to move the propellants to one side of their tanks, exposing the Fruhof pillars to ullage for the low liquid levels following orbit insertion. The acceleration is not large enough to break ullage into the outlet line, however (by 3 orders of magnitude). The roll coast required to align the pitch axis develops a centrifugal Bo of less than 0.7 for up to 500 sec, which is sufficient to orient all but a small amount of the liquid away from the outlet (Fig. V-10).

The roll-pitch-roll maneuvers to align the vehicle thrust axis on Mission A_1 will keep the liquid propellants against the tank walls and removed from the outlet. After completion of the maneuver and the return to the 10^{-7} g environment, the propellants will again reorient over the tank outlets. A period of time is needed between these maneuvers and the next engine firing to guarantee liquid reorientation over the outlet. An estimate of reorientation time can be made using the parameter, $\sqrt{\rho r^3/\sigma}$. For the missions and propellants of this study, the estimate ranges from 100 to 500 seconds.*

At the start of engine thrust, the curved zero-g free-surface, when held axisymmetric by the standoff post, will settle to a nearly-flat surface for each propellant and mission of this study. For Missions A_1 and A_2, the tanks are not necessarily on the thrust axis since a large gimbal cone angle (9 to 12°) is possible. The off-axis thrust can cause an asymmetric slosh wave during settling, as observed in drop tower experiments (Ref V-21). These effects on the attitude control system requirements are of concern and should be examined further.

Missions A_1 and A_2 expend 90%, or more, of the propellant load to enter the Mars orbit. A number of short burns is then required for orbit trims, maneuvers for the Mars/Lander separation, and possible orbit changes for mapping studies. The ullage standoff pillar with its communication channels is particularly suited to these mission requirements since it tends to keep propellant over the outlet, preventing any large accumulation of propellant at regions removed from the outlet area. In addition, there is no limitation on the number of burns that can be made in orbit.

The thermal environment and associated effects on the propellant and acquisition device were divided into two categories in this program. The first was the normal steady-state environment of the spacecraft as influenced by hardware, solar heating, radiant cooling, etc. The second was the transient environment due to heat soakback following an engine burn. The significance of heat soakback increases with the burn duration.

The thermal control system of the spacecraft will control the propellant temperature within the allowable range, tending to minimize any effects which the thermal environment may have on the propellant acquisition device. It is, however, desirable that the

*If the reorientation time were critical, programming of the desired thrust alignment would have to be planned and executed earlier to allow for liquid resettling over the tank outlet.

acquisition device operate efficiently in the worst probable thermal environment. Therefore, an investigation was conducted to evaluate and estimate the magnitude of these effects assuming an uncontrolled thermal environment. Two potential problem areas were recognized. The first is the establishment of a propellant vaporization-condensation cycle. The propellant located in the tank outlet would be heated, vaporized, and condensed at the cooler forward end of the tank. This cycle is similar to that for a heat pipe. The net result could lead to some loss of liquid from the reservoir of the Fruhof device (similar to the effect noted in Chapter IV for the minus 1-g device). A second potential problem is the drying of the liquid reservoir due to thermocapillary flow. Thermocapillary flow occurs when a temperature gradient exists along a gas/liquid interface and produces a gradient in surface tension. The surface tension gradients produce tangential shear forces which, if of sufficient magnitude, will pump the liquid from a hot to a cooler region. Temperature gradients along the gas/liquid interface are produced by relatively high heating rates at, or near, the location of the liquid, as discussed later.

The results of the propellant vaporization investigation (Chapter IV) conducted for Missions A_1 and A_2 showed that significant vaporization may occur only with the oxidizers (OF_2 and N_2O_4). This vaporization will occur at the gas/liquid interface. For the Fruhof, the estimated amounts of vaporization do not present a problem since the propellant remaining is adequate for engine restart. Also, any vaporized propellant condensed at the forward end of the tank (or other regions) would be pumped back into the reservoir.

The effect of thermocapillary flow is described by Larkin (Ref V-23), and its magnitude is measured by the Marangoni number. The Marangoni number must be on the order of 10^5 before thermocapillary flow is significant. The Marangoni number is a function of physical and thermodynamic fluid properties, heat flux, and bubble radius. Of the three missions, only A_2 may yield great enough heat fluxes, due to the engine heat soakback following the orbit insertion burn, for thermocapillary flow to be significant. Using available engine heat soakback data for Mission A_2, the heat fluxes were estimated to be approximately 3.7 Btu/ft^2-hr. Even for this possible case, in order for thermocapillarity to be significant, i.e., Marangoni number 10^5, the bubble radius would have to exceed the tank radius for the N_2O_4 and MMH Mission A_2 propellants.

VI. CONCLUSIONS AND RECOMMENDATIONS

A. CONCLUSIONS

The basic conclusion of the two-phased program is that passive devices are the best means to provide gas-free liquid propellant, as required, for the Mars and Grand Tour missions. Two kinds of propellant acquisition devices -- the simple Fruhof designs (Chapter V) and the more complicated screen trap systems (Chapter IV) -- were judged to be the most reliable and lightest for long duration (up to 10 yr) planetary flights. In addition, they are not explusion cycle limited, nor constrained to a particular tank geometry.

Volume I is recommended to the propulsion designer as a guide to understanding the basic operational principles and design criteria for the various propellant acquisition concepts developed or being developed. These concepts include dielectrophoresis, polymeric bladders and diaphragms, metallic bladders and diaphragms, bellows, surface tension systems, external settling rockets, capillary/bellows, and start tanks. Since each concept poses certain distinct advantages and disadvantages, a numerical rating technique was established to aid the designer in selecting the best acquisition system for the particular mission. This rating method, which considers availability, compatibility, reliability, testability, mass, and design versatility, was used to show that surface tension systems were clearly best for each of the three baseline missions considered.

The following conclusions also resulted from the Phase I comparative effort:

1) Propellant tank subsystem - The two-tank configuration is preferred for Missions A_1 and A_2; spherical tanks are best for all three missions; and all-metal tanks [2219 aluminum (Mission A_1) and 6Aℓ-4V titanium (Missions A_2 and B)] are recommended over composites;

2) Pressurization subsystem - Helium is preferred over nitrogen because of its weight savings for all three baseline missions. A single, spherical storage tank constructed of 6Aℓ-4V titanium is best. The storage spheres for Missions A_1 and A_2 should be loaded with helium to 4000 psia at nominal propellant temperature

(250°R for A_1 and 500°R for A_2). For the Mission B blowdown system the propellant tank with 50% initial ullage should be pressurized to 350 psia with helium (nominal propellant/pressurant temperature is 500°R);

3) Propellant acquisition subsystem - Surface tension systems were rated best for each mission; they are 28% better than the second-best system for Mission A_1, 26% better for Mission A_2, and 69% better for Mission B. The preferred materials are aluminum (Mission A_1) and titanium (Missions A_2 and B).

Based on the surface tension designs presented in this report, the Fruhof concept is preferred for each baseline mission because of its simplicity and inherent reliability. However, it is not testable under -1 g, as are the fine-mesh trap designs. The added complexity, with regard to fabrication, cleaning, and handling makes one question the 1-g test requirement, particularly because it doesn't, by itself, verify the operational capability of the device.

B. RECOMMENDATIONS

The following recommendations are presented separately for each of the two different surface tension designs.

1) Fine mesh screen designs (testable at -1 g) - The following fabrication and analysis areas are identified as requiring additional work: forming of titanium, twilled screen; compatibility of brazed aluminum joints; slosh analysis and coverplate structural analysis; and the overall thermal analysis. The fabrication considerations could be easily resolved as part of a prototype build program. The thermal analysis requires a better definition and refinement of the mission environment and engine heat soakback criteria (Chapter IV). This is particularly true for the space storable propellants, OF_2 and B_2H_6. An analytical model should be developed and modified, as required, by data obtained from engine firings;

2) Fruhof surface tension systems - This unique device is the more attractive of the two concepts analyzed and designed during this program (provided that the requirement for testing at minus 1 g is eliminated) It poses no hardware-type problems; however, because it cannot be demonstrated under 1 g, we recommend a program to further verify its performance. One effective means is to use numerical experimentation with a computer model of the low-g fluid dynamics. The numerical model should be broad enough to describe the performance of Fruhof designs during critical mission periods.

   This program would include an experimental effort to qualitatively evaluate critical mission phases (such as outflow initiation) and liquid response to perturbations (such as ACS thrusts). Variations in the value of contact angle due to contaminants and aging need further investigation, based upon our review (Ref VI-1 to VI-4). The aging effects are of particular importance because of the long mission durations of one to ten years. Acceptable cleaning techniques should be experimentally verified and documented. The testing, in addition to 1-g bench tests, should be done in the controlled acceleration environment of the drop tower and possibly in the KC-135 aircraft. The latter provides an order of magnitude increase over the two-second test interval of the drop tower. Even longer weightless periods are needed, however, to evaluate performance with full-scale tankage. An orbital experiment is recommended to accomplish this.

VII. REFERENCES

I-1 Gorman, D. N. and Paynter, H. L.: *Investigation of Space-Storable Propellant Acquisition Devices - Project Work Plan.* MCR-69-443, Martin Marietta Corporation, Denver, Colorado, August 1969.

I-2 Balzer, D. L., *et al.: Advanced Propellant Management System for Spacecraft Propulsion Systems, Phase I - Survey Study and Evaluation.* MCR-69-87, Martin Marietta Corporation, Denver, Colorado, February 1969.

I-3 Uney, P. E.: *Compatibility of Storage Materials with Various Rocket Propellants.* SR-1660-69-20, Martin Marietta Corporation, Denver, Colorado, November 1969.

I-4 Uney, P. E.: *Compatibility of Storage Materials with Various Rocket Propellants.* Addendum SR-1660-69-20A, Martin Marietta Corporation, Denver, Colorado, January 1970.

I-5 *Investigation of Space-Storable Propellant Acquisition Devices, Final Report, Volume I - Evaluation.* MCR-70-171 (Vol I), Martin Marietta Corporation, Denver, Colorado, October 1970.

III-1 Perry, J. H.: *Chemical Engineers' Handbook.* Third Edition. McGraw-Hill Book Company, Inc., 1950, p. 363

III-2 Lyerly, G. A. and Peper, H.: *Summary Report - Studies of Interfacial Surface Energies.* NASA CR-54175, Harris Research Laboratories, Inc., Washington, D.C., 31 December 1964.

III-3 *Contact Angle, Wettability and Adhesion.* Advances in Chemistry Series 43, American Chemical Society, Washington, D.C., 1964.

III-4 Bowman, T. E.: *Cryogenic Liquid Experiments in Orbit. Vol I. Liquid Settling and Interface Dynamics,* Contract NAS8-11328, Martin Marietta Corporation, Denver, Colorado, December 1966.

III-5 Paynter, H. L.: "The Martin Company's Low Gravity Experimental Facility." *Proceedings of the Symposium on Fluid Mechanics and Heat Transfer under Low Gravitational Conditions*, Palo Alto, California, June 1965.

III-6. Barksdale, T. R. and Paynter, H. L.: *Design, Fabrication, and Testing of Subscale Propellant Tanks with Capillary Traps - Final Report.* MCR-68-11, Contract NAS8-20837, Martin Marietta Corporation, Denver, Colorado, March 1968.

III-7 Paynter, H. L., *et al.: Experimental Investigation of Capillary Propellant Control Devices for Low Gravity Environments.* MCR-69-585, Contract NAS8-21259, Martin Marietta Corporation, Denver, Colorado, June 1970.

III-8 Petrash, D. A., *et al.: Effect of Surface Energy on the Liquid Vapor Interface Configuration during Weightlessness.* NASA TN D-1562, January 1963.

III-9 Abramson, H. N.: *The Dynamic Behavior of Fluids in Moving Containers.* NASA SP-106, 1966.

III-10 Salzman, J. A. and Masica, W. J.: *Experimental Investigation of Liquid Propellant Reorientation.* NASA TN 03789, January 1967.

III-11 McCarthy, J. F.: "Zero-g Propulsion Problems." *Jet, Rocket, Nuclear, Ion and Electric Propulsion-Theory and Design.* W. H. T. Loh (Editor). Springer-Verlag, New York, Chapter 17, pp. 644-727.

III-12 Bowman, T. E.: *The Literature of Low-g Propellant Behavior, 1966-1969.* MCR-69-438, Contract NAS9-8939, Martin Marietta Corporation, Denver, Colorado, September 1969.

III-13 Hastings, G. A. and Hill, D. W.: *The Literature of Low-g Propellant Behavior.* CR-92081, Contract NAS9-5174, Lockheed Missiles and Space Company, Sunnyvale, California, May 1967.

III-14 DeBrock, S. C., *et al.*: "A Survey of Current Developments in Surface Tension Devices for Propellant Acquisition." Paper No. 70-685, Presented at the AIAA 6th Propulsion Joint Specialiat Conference, San Diego, California, June 15-19, 1970.

III-15 *Advanced Maneuvering Propulsion Technology, Fourth Quarterly Report (U).* AFRPL-TR-68-221, Rocketdyne Division, North American Rockwell Corporation, Canoga Park, California, December 1968. (Confidential)

III-16 *Low-Gravity Propellant Control Using Capillary Devices in Large-Scale Cryogenic Vehicles, First Quarterly Progress Report.* 584-4-20B, Contract NAS8-21465, General Dynamics/Convair Division, San Diego, California, October 1968.

III-17 *Passive Retention/Expulsion Methods for Subcritical Storage of Cryogens.* MCR-70-85 (Issue 3), Contract NAS9-10480, Martin Marietta Corporation, Denver, Colorado, May 1970.

IV-1 *Investigation of Space-Storable Propellant Acquisition Devices, Final Report, Volume I - Evaluation.* MCR-70-171 (Vol I), Martin Marietta Corporation, Denver, Colorado, October 1970.

IV-2 Balzer, D. L., *et al.: Advanced Propellant Management System for Spacecraft Propulsion System, Phase II - Detail Design.* MCR-69-436, Martin Marietta Corporation, Denver, Colorado, September 1969.

IV-3 Paynter, H. L., *et al.: Experimental Investigation of Capillary Propellant Control Devices for Low-Gravity Environments.* MCR-69-585 (Vol II), Martin Marietta Corporation, Denver, Colorado, June 1970.

IV-4 Knop, L. H.: *Practical Applications of Explosive Welding.* Report 6710-69 (02)ER, Aerojet-General Corporation, Fullerton, California, August 1969.

IV-5 Fester, D. A. and Bingham, P. E.: *Evaluation of Fine-Mesh Screen Device in Liquid Fluorine.* R-70-48631-010, Martin Marietta Corporation, Denver, Colorado, June 1970.

IV-6 Personal Communication with H. Brown, Martin Marietta Corporation, Denver, Colorado, July 1970

IV-7 Personal Communication with Dr. Tolbert, Stanford Research Institute, Palo Alto, California, July 1970.

IV-8 *Fluorine Systems Handbook*. NASA CR-72064, Douglas Aircraft, Santa Monica, California, July 1967.

IV-9 Personal Communication with T. Hikido, Pyromet Industries, Los Altos, California, July 1970.

IV-10 Berry, W. E, *et al.: Compatibility of Materials with Rocket Propellants and Oxidizers*. Memo 201, Defense Metals Information Center, Columbus, Ohio, January 1965.

IV-11 Eberstein, I. J. and Glassman, I.: *Consideration of Hydrazine Decomposition*. Lab Report 490, Princeton University, Princeton, New Jersey, December 1969.

IV-12 Muraca, R. F., *et al.: The Results of Long-Term Storage Tests for Compatibility of Spacecraft Materials with Hydrazine and Hydrazine Mixtures*. Report 951581-6, Stanford Research Institute, Palo Alto, California, October 1967.

IV-13 Personal Communication with W. E. Berry, Defense Metals Information Center, Columbus, Ohio, July 1970.

IV-14 Personal Communication with D. Hurwertz, Boeing Company, Seattle, Washington, July 1970.

IV-15 Muraca, R. F., *et al.: The Results of Long-Term Storage Tests for Compatibility of N_2O_4 with Various Spacecraft Materials*. Special Report No. 2, Stanford Research Institute, Palo Alto, California, May 1967.

IV-16 Muraca, R. F., *et al.: Treatment of Metal Surfaces for Use with Space Storable Propellants: A Critical Survey*. Special Report No. 951581-8, Stanford Research Institute, Palo Alto, California, August 1968.

IV-17 Schmidt, H. W.: *Handling and Use of Fluorine and F_2O_2 Mixtures in Rocket Systems*. NASA SP-3037, Lewis Research Center, Cleveland, Ohio, 1967.

IV-18 English, W. D., *et al.: Halogen Passivation Procedural Guide*. AFRPL-TR-67-309, McDonnell Douglas Corporation, Newport Beach, California, December 1967.

IV-19 Fester, D. A.: *Fluorine Propellant System Requirements.* SR-1660-69-9, Martin Marietta Corporation, Denver, Colorado, March 1969.

IV-20 *Prelaunch Operations for a Space-Storable Propellant Module.* GDC-BNZ69-013-8, General Dynamics, San Diego, California, May 1970.

IV-21 *Thermal Conditioning, Annealing, and Joining Methods for Dutch-Twill Aluminum Screen.* Test Plan No. RW-70-P15, Martin Marietta Corporation, Denver, Colorado, July 21, 1970.

IV-22 Barksdale, T. R., *et al.: Liquid Outflow Tests of Surface Tension Systems under Minus One-G.* TM 1661-66-12, Martin Marietta Corporation, Denver, Colorado, December 1966.

IV-23 Doub, J. D.: *Viking Orbiter Capillary System Preliminary Analysis.* SR-1660-70-1, Martin Marietta Corporation, Denver, Colorado, January 1970.

IV-24 Abramson, N. H., *et al.:* "Liquid Surface Oscillations in Longitudinally Excited Rigid Cylindrical Containers." *AIAA Journal,* Vol 3, No. 4, April 1965.

IV-25 Abramson, N. H., *et al.: Some Studies of Nonlinear Lateral Sloshing in Rigid Containers.* NASA CR-375, January 1966.

IV-26 Abramson, N. H.: *The Dynamic Behavior of Liquids in Moving Containers.* NASA SP-106, Southwest Research Institute, 1966.

IV-27 Leonard, W. H. and Walton, W. C.: *An Investigation of the Natural Frequencies and Mode Shapes of Liquids in Oblate Spheroidal Tanks.* NASA TND-904, June 1961.

IV-28 Berliner, E.: *PSI Propellant Tank Test Report - Slosh Test.* Martin Marietta Corporation, Denver, Colorado, December 1969.

V-1 Paynter, H. L., *et al.: Experimental Investigation of Capillary Propellant Control Devices for Low-Gravity Environments, Volume II - Final Report.* MCR-69-585 (Vol II), Martin Marietta Corporation, Denver, Colorado, June 1970.

V-2 Landau, L. D. and Lifshitz, E. M.: *Fluid Mecahnics,* Pergamon Press, 1959, p 230.

V-3 Zisman, W. A.: "Relation of Equilibrium Contact Angle to Liquid and Solid Constitution." *Contact Angle, Wettability, and Adhesion,* Advances in Chemistry Series 43, American Chemical Society, Washington, D.C., 1964, p 1-51.

V-4 Bascom, W. D., Cottington, R. L., and Singleterry, C. R.: "Dynamic Surface Phenomena in the Spontaneous Spreading of Oils on Solids." *Contact Angle, Wettability, and Adhesion,* Advances in Chemistry Series 43, American Chemical Society, Washington, D.C., 1964, p 355-379.

V-5 Hise, R. E.: *The Statistics and Dynamics of a "Stuck" Liquid Index.* Ph.D. Dissertation, Northwestern University, 1968.

V-6 Fox, H. W. and Zisman, W. A.: *Journal of Colloid Sciences,* Vol 5, 1950, p 514.

V-7 Shafrin, E. G. and Zisman, W. A.: "Upper Limits to the Contact Angles of Liquids on Solids." *Contact Angle, Wettability and Adhesion,* Advances in Chemistry Series 43, American Chemical Society, Washington, D.C., 1964, p 145-157.

V-8 Schwartz, A. M. and Ellison, A. H.: *The Effect of Surface Contamination on Contact Angles and Surface Potentials.* NASA CR-54708, January 1966.

V-9 Laplace, P. S.: *Mécanique Céleste,* Supplement to Volume X, Paris, 1806.

V-10 Aris, R.: *Vectors, Tensors, and the Basic Equations of Fluid Mechanics.* Prentice Hall, Englewood Cliffs, New Jersey, 1962, p 218.

V-11 Buff, F. P.: "The Theory of Capillarity." *Encyclopedia of Physics*, Vol X, Springer-Verlag, Berlin, 1960, p 284.

V-12 Bond, W. N. and Newton, D. A.: "Bubbles, Drops and Stokes' Law." *Philosophical Magazine*, Vol 5, 1928, p 794.

V-13 Young, T.: "Cohesion of Fluids." *Philosophical Transactions, Royal Society (London)*, Vol 95, 1805, p 65.

V-14 Bashforth, R. and Adams, J. C.: *An Attempt to Test the Theory of Capillary Action*. Cambridge University Press, 1883.

V-15 Balzer, D. L., *et al.: Advanced Propellant Management System for Spacecraft Propulsion Systems, Phase II - Detail Design*. MCR-69-436, Martin Marietta Corporation Denver, Colorado, September 1969.

V-16 Gilmore, D. E. and Barksdale, T. R.: *Low-G Laboratory Annual Progress Report: 1965, Development Task 605*. TM-0444-66-2, Martin Marietta Corporation, Denver, Colorado, 1965.

V-17 Paynter, H. L: "Time for a Totally Wetting Liquid to Deform from a Gravity-Dominated to a Nulled-Gravity Equilibrium State." *AIAA Journal*, Vol 2, No. 9, September 1964, p 1627-1630.

V-18 *Advanced Propellant Management System for Spacecraft Propulsion Systems*. P-68-114 (Vol I), Martin Marietta Corporation, Denver, Colorado, June 1968, p IV-10.

Capillary Retention Device Study. P-69-142 (Vol I), Martin Marietta Corporation, Denver, Colorado, November 1969, p II-10.

V-19 Personal Communication with William Schaatz, JPL, and David Carter, NASA-Langley, July 14, 1970.

V-20. Adams, R. G., Bynum, B., James, A. L., and Hastings, L. J.: *Performance Characteristics of Liquid Vapor Sensors Operating in a Reduced Gravity Environment*. NASA-TMX-53840, May 1969.

V-21 Bowman, T. E.: *Response of Laterally Oscillating Liquid to a Change in "Gravity."* SR 1660-67-10, Martin Marietta Corporation, Denver, Colorado, 1967.

V-22 Gardner, J. A.: *Viking Baseline Orbiter Conceptual Design Description.* Project Document No. 611-2, Jet Propulsion Laboratory, Pasadena, California, March 1, 1969, p 8I-3.

V-23 Larkin, B. K.: "Thermocapillary Flow around a Hemispherical Bubble." *AIChE Journal,* Vol 16, 1970, p 101-107.

VI-1 Lyerly, G. A. and Peper, H.: *Summary Report-Studies of Interfacial Surface Energies.* NASA CR-54175, 1964.

VI-2 Schwartz, A. M. and Ellison, A. H.: *The Effect of Surface Contamination on Contact Angles and Surface Potentials.* NASA CR-54708, 1966.

VI-3 Dalzell, J. F.: "Physical Properties of Selected Liquids." *The Dynamic Behavior of Liquids in Moving Containers.* NASA SP-106, 1966.

VI-4 Personal Communication with Dr. W. A. Zisman, Naval Research Laboratory, June 1970.

DISTRIBUTION

Copies	Recipient	Designee
	Ames Research Center NASA Moffett Field, California 94035	
1	A. S. Hertzog, Director of Procurement	(X)
1	Patents and Contracts Management	(X)
	Jet Propulsion Laboratory 4800 Oak Grove Dr. Pasadena, California 91103	
5	Mr. Robert F. Lem (Technical Manager)	(X)
3	Chief, Liquid Propulsion Technology RPL Office of Advanced Research and Technology NASA Headquarters Washington, D.C. 20546	(X)
1	Director, Technology Utilization Division Office of Technology Utilization NASA Headquarters Washington, D.C. 20546	(X)
25	NASA Scientific and Technical Information Facility P.O. Box 33 College Park, Maryland 20740	(X)
1	Director, Launch Vehicles and Propulsion, SV Office of Space Science and Applications NASA Headquarters Washington, D.C. 20546	(X)
1	Director, Advanced Manned Missions, MT Office of Manned Space Flight NASA Headquarters Washington, D.C. 20546	(X)

1	Mission Analysis Division NASA Ames Research Center Moffett Field, California 94035	(X)

NASA FIELD CENTERS

2	Ames Research Center Moffett Field, California 94035	Hans M. Mark
1	Goddard Space Flight Center Greenbelt, Maryland 20771	Merland L. Moseson Code 620
2	Jet Propulsion Laboratory California Institute of Technology 4800 Oak Grove Drive Pasadena, California 91103	Henry Burlage, Jr. Propulsion Div. 38
2	Langley Research Center Langley Station Hampton, Virginia 23365	Ed Cortwright Director
2	Lewis Research Center 21000 Brookpark Road Cleveland, Ohio 44135	B. T. Lundin Director D. Nored
2	Marshall Space Flight Center Huntsville, Alabama 35812	Hans G. Paul, Code RP+VED L. Hastings, Code R-P+VE PTF
2	Manned Spacecraft Center Houston, Texas 77001	J. G. Thibodaux, Jr. L. Rhodes
2	John F. Kennedy Space Center, NASA Cocoa Beach, Florida 32931	Dr. Kurt H. Debus

GOVERNMENT INSTALLATIONS

1	Aeronautical Systems Division Air Force Systems Command Wright-Patterson Air Force Base Dayton, Ohio 45433	D. L. Schmidt Code ASRCNC-2

1	Air Force Missile Development Center Holloman Air Force Base New Mexico 88330	Maj. R. E. Bracken
1	Air Force Missile Test Center Patrick Air Force Base, Florida	L. J. Ullian
1	Space and Missile Systems Organization Air Force Unit Post Office Los Angeles, California 90045	Col. Clark Technical Data Center
1	Arnold Engineering Development Center Arnold Air Force Station Tullahoma, Tennessee 37388	Dr. H. K. Doetsch
1	Bureau of Naval Weapons Department of the Navy Washington, D.C. 20546	J. Kay RTMS-41
1	Defense Documentation Center Headquarters Cameron Station, Building 5 5010 Duke Street Alexandria, Virginia 22314 Attn: TISIA	
1	Headquarters, U.S. Air Force Washington 25, D.C. 20546	Col C. K. Stambaugh AFRST
1	Picatinny Arsenal Dover, New Jersey 07801	I. Forsten, Chief Liquid Propulsion Laboratory
2	Air Force Rocket Propulsion Lab. Research and Technology Division Air Force Systems Command Edwards, California 93523	RPRPD/MR. H. Main Robert Wiswell
1	U.S. Army Missile Command Redstone Arsenal Alabama 35809	Mr. Walter Wharton

1	U.S. Naval Ordnance Test Station China Lake California 93557	Code 4562 Chief, Missile Propulsion Div. R. A. Gould

CPIA

1	Chemical Propulsion Information Agency Applied Physics Laboratory 8621 Georgia Avenue Silver Spring, Maryland 20910	Tom Reedy

INDUSTRY CONTRACTORS

1	Aerojet-General Corporation P.O. Box 296 Azusa, California 91703	W. L. Rogers
1	Aerojet-General Corporation P.O. Box 1947 Technical Library, Bldg 2015, Dept. 2410 Sacramento, California 95809	R. Stiff R. W. Schwantes B. K. Scoggan
1	Space Division Aerojet-General Corporation 9200 East Flair Dr. El Monte, California 91734	S. Machlawski
1	Aerospace Corporation 2400 East El Segundo Boulevard P.O. Box 95085 Los Angeles, California 90045	John G. Wilder MS-2293
1	Atlantic Research Corporation Edsall Road and Shirley Highway Alexandria, Virginia 22314	Dr. Ray Friedman

1	AVCO Systems Division Wilmington, Massachusetts	Howard B. Winkler
1	Beech Aircraft Corporation Boulder Division Box 631 Boulder, Colorado	J. H. Rodgers
1	Bell Aerosystems Company P.O. Box 1 Buffalo, New York 14240	W. M. Smith L. Thompson M. J. O'Connell
1	Bellcomm 955 L-Enfant Plaza, S.W. Washington, D.C.	H. S. London
1	Bendix Systems Division Bendix Corporation 3300 Plymouth Road Ann Arbor, Michigan 48105	J. M. Brueger
1	Boeing Company P.O. Box 3707 Seattle, Washington 98124	J. D. Alexander L. Lofgren
1	Boeing Company 1625 K Street, N.W. Washington, D.C. 20006	Library
1	Boeing Company P.O. Box 1680 Huntsville, Alabama 35801	Ted Snow
1	Missile Division Chrysler Corporation P.O. Box 2628 Detroit, Michigan 48231	John Gates
1	Wright Aeronautical Division Curtiss-Wright Corporation Wood-Ridge, New Jersey 07075	G. Kelley
1	Research Center Fairchild Hiller Corporation Germantown, Maryland	Ralph Hall

1	Republic Aviation Corporation Fairchild Hiller Corporation Farmingdale, Long Island, New York	Library
1	General Dynamics, Convair Division Library + Information Services (128-00) P.O. Box 1128 San Diego, California 92112	Frank Dorf E. J. Hujsak
1	Missile and Space Systems Center General Electric Company Valley Forge Space Technology Center P.O. Box 8555 Philadelphia, Pa.	F. Mezger F. E. Schultz
1	Grumman Aircraft Engineering Corp. Bethpage, Long Island New York 11714	Joseph Gavin
1	Honeywell, Inc. Aerospace Div. 2600 Ridgway Rd Minneapolis, Minn.	Gordon Harms
1	Hughes Aircraft Co. Aerospace Group Centinela and Teale Streets Culver City, California 90230	F. H. Meier V.P. and Div. Mgr. Research + Dev. Div.
1	Walter Kidde and Company, Inc. Aerospace Operations 567 Main Street Belleville, New Jersey	R. J. Hanville Dir. of Research Engr.
1	Ling-Temco-Vought Corporation P.O. Box 5907 Dallas, Texas 75222	Warren G. Trent
1	Arthur D. Little, Inc. 20 Acorn Park Cambridge, Massachusetts 02140	Library

1	Lockheed Missiles and Space Co. Attn-Technical Information Center P.O. Box 504 Sunnyvale, California 94088	S. DeBrock
1	Lockheed Propulsion Company P.O. Box 111 Redlands, California 92374	H. L. Thackwell
1	The Marquardt Corporation 16555 Saticoy Street Van Nuys, California 91409	Library R. Y. Yoshida
1	Baltimore Division Martin Marietta Corporation Baltimore, Maryland 21203	John Calathes (3214)
1	Denver Division Martin Marietta Corporation P. O. Box 179 Denver, Colorado 80201	S. R. Sadin A. J. Kullas
1	Orlando Division Martin Marietta Corporation Box 5837 Orlando, Florida	J. Ferm
1	Astropower Laboratory McDonnell-Douglas Aircraft Company 2121 Paularino Newport Beach, California 92663	Dr. George Moc Director, Research
1	McDonnell-Douglas Aircraft Corp. P.O. Box 516 Municipal Airport St. Louis, Missouri 63166	R. A. Herzmark
1	McDonnell-Douglas Astronautics Co. Bolsa Chica Avenue Huntington Beach, California 92640	R. J. Hoffman D. E. Brown
1	Missile and Space Systems Division McDonnell-Douglas Aircraft Co. 3000 Ocean Park Boulevard Santa Monica, Calif. 90406	R. W. Hallet Chief Engineer Adv. Space Tech.

1	Space + Information Systems Div. North American Rockwell 12214 Lakewood Boulevard Downey, California 90241	Library I. M. Chen
1	Rocketdyne (Library 586-306) 6633 Canoga Avenue Canoga Park, Calif. 91304	Dr. R. J. Thompson S. F. Jacobellis
1	Northrop Space Laboratories 3401 West Broadway Hawthorne, California 90250	Dr. W. Howard
1	Aeronutronic Division Philco Corporation Ford Road Newport Beach, California 92663	D. A. Garrison
1	Astro-Electronics Division Radio Corporation of America Princeton, New Jersey 08540	Y. Brill D. Balzer
1	Rocket Research Corporation 520 South Portland Street Seattle, Washington 98108	Foy McCullough, Jr.
1	Sunstrand Aviation 2421 11th Street Rockford, Illinois 61101	R. W. Reynolds
1	Stanford Research Institute 333 Ravenswood Avenue Menlo Park, California 94025	Dr. Gerald Marksman
1	TRW Systems Group TRW Incorporated One Space Park Redondo Beach, California 90278	G. W. Elverum J. Bevans
1	Tapco Division TRW, Incorporated 23555 Euclid Avenue Cleveland, Ohio 44117	P. T. Angell

1	Thiokol Chemical Corporation Huntsville Division Huntsville, Alabama 35807	John Goodloe
1	Research Laboratories United Aircraft Corp. 400 Main St. East Hartford, Conn. 06108	Erle Martin
1	Hamilton Standard Division United Aircraft Corp. Windsor Locks, Conn. 06096	R. Hatch
1	United Technology Center 587 Methilda Avenue P.O. Box 358 Sunnyvale, California 94088	Dr. David Altman
1	Florida Research and Development Pratt and Whitney Aircraft United Aircraft Corporation P.O. Box 2691 West Palm Beach, Florida 33402	R. J. Coar
1	Vickers, Inc. Box 302 Troy, Michigan	
1	Heller Associates 418 S. Westgate Los Angeles, California 90049	Wm. Heller
1	Arde, Inc. 19 Industrial Avenue Mahwah, New Jersey	A. Cozewith
1	COMSAT 1835 "K" St., N.W. Washington, D.C. 20036	G. Huson
1	Dynatech Corporation 17 Tudor St. Cambridge, Massachusetts 02139	R. F. Johnson

1	Dilectrix Corporation 69 Allen Blvd. Farmingdale, New York 11735	J. V. Petriello
1	G. T. Schjeldahl Company Northfield, Minnesota 55057	M. J. Werkema
1	Aerojet-General Corporation 601 S. Placentia Ave. Fullerton, California 92631	W. D. Peters
1	Sealol, Inc. Warwick Industrial Park 100 Post Road Providence, Rhode Island 02905	Harold F. Greiner
1	Gardner Bellows Corporation P.O. Box 3328 Van Nuys, California 91407	Vern L. Orth
1	The Belfab Corporation P.O. Box 1881 Daytona Beach, Florida 32015	Elliot Thompson
1	Stainless Steel Products 2980 N. San Fernando Blvd. Burbank, California 91504	D. E. Williams
1	Metal Bellows Corporation 20977 Knapp St. Chatsworth, California 91311	H. W. Johnson